

**WASM: Minerals, Energy and Chemical Engineering**

**FAILURE PREDICTION IN UNDERGROUND MINE EXCAVATIONS USING  
THE COMBINATION OF CRITICAL STRAIN AND GROUND REACTION  
CURVE (GRC) FOR THE PURPOSE OF APPROPRIATE SUPPORT TYPE AND  
INSTALLATION TIME**

**Reza Masoudi**

**This thesis is presented for the Degree of**

**Doctor of Philosophy**

**of**

**Curtin University**

**August 2019**

## DECLARATION

To the best of my knowledge and belief, this thesis contains no material previously published by any other person except where due acknowledgement has been made.

This thesis contains no material which has been accepted for the award of any other degree or diploma in any university.

Signature: .....

Date: .....

## ACKNOWLEDGEMENTS

I gratefully appreciate **Associate Professor Mostafa Sharifzadeh** who supervised this thesis and provided numerous constructive comments and suggestions without which was not possible to finalise this research. I also would like to express my gratitude to **Prof. Ernesto Villaescusa**, who gave valuable comments at early stages of the research.

I appreciate the **New Concept Mining Company** that provided all facilities and equipment and utilities for the experiments in this research specifically **Mr Brendan Crompton**, the company representative in Australia who facilitate all requirements.

I am also very grateful to **Professor Charlie Chunlin Li** from **Norwegian University of Science and Technology (NTNU)** for providing some valuable data, while he was neither asked to endorse the conclusions or recommendations nor did he see the final draft of the report before it is released.

It is with great appreciation that we acknowledge the **Curtin International Postgraduate Scholarship (CIPRS)/Department of Mining and Metallurgy Scholarship** for their financial support during three and half years of the research time.

Further thanks to **MEA** that supported partially some emerged part of this research, which was a collaboration with **UNSW** for laboratory and field experiments. It is still ongoing and hopefully further results come out soon.

I appreciate **Mr M. R. Shahverdiloo** for providing the data of tensioning the multi-strand tendons and Monobars of underground PHC cavern and TRC cavern of **Masjed Soleiman Hydro Electric Power Plant** – Iran. Thanks to **Mr M. Ali Masoudi** for providing the data of tensioning the multi-strand tendons and Monobars of underground PHC cavern and TRC cavern of **Siyah Bisheh Hydro Electric Power Plant** – Iran. I also grateful to **Mr Mousa Hazrati** for providing the data of tensioning the multi-strand tendons of underground PHC cavern of **Uma Oya Hydropower Complex - Sri Lanka**.

## **ABSTRACT**

The near-surface resources gradually are going to be depleted, and underground mines progressively are going deeper. Therefore, rock support design, ground reaction, and failure prediction are more critical than before in the deep mining industry. In this condition, the occurrence of seismic events is escalating, and the ground energy demand (GED) becomes more complex to estimate. On the other hand, rock support performance factors in seismic conditions such as energy dissipation and deformation capacity became more critical. Expanding the knowledge of reinforcement behaviour and their capacity, precisely that of the rockbolt as the primary element in seismic conditions, would help to develop an applicable, safe and economic support design.

The first requirement to achieve a practical design is having an estimate of the ground energy demand (GED) that to be tolerated by a support system. There is no accurate calculation or determination of the GED, but there are some methods to estimate it. This research contains various attempts to estimate the GED including the intact rock properties approach, failure thickness and ejection velocity estimation, and rockburst damage potential method.

The second requirement is to have an evaluation of the ground support system energy dissipation capacities as an integrated system. As an important part of the system to determine the reinforcement energy absorption/dissipation capacity, some approaches including the drop test, the blasting simulation, the back-calculation and the momentum transfer measurement method were presented. Additionally, dynamic testing facilities such as large-scale dynamic test rig which constructed by Geobruigg Company and the latest one, New Concept Mining Dynamic Impact Tester (NCM-DIT) that some part of the experiments of this research have been examined with, were also described. Considering the rockbolts bond decoupling mechanism and seismic event demand, practical modifications on rebar rockbolt encapsulation have been proposed to utilise it as a yielding reinforcement in seismic conditions effectively. Applying a sufficient decoupled length in the shank and leaving

a collar bonding underneath the bearing pad and plate of this kind of rockbolts, improves the deformation capacity of them.

As above mentioned, rock support specifically rockbolt behaviour was at the centre of attention of this research. Additionally, some complementary experiments, which have been performed overseas, enriched the study. Therefore, due to a wide range of the topic and research priority in Western Australia, it is narrowed down and focused to the laboratory and field study of the static and dynamic behaviour of rockbolts in deep mining.

Based on the findings in this research, the applicable ranges of each type of rockbolts were presented. Suitable rockbolt types for various GED and deformation capacity range were categorised in the table and the graph. It has been found that the stiff bolts, such as expansion shell and fully encapsulated rockbolts, are mostly suitable for static loading conditions and low surface deformation, as well as controlling the bulking of a volume of stress fractured ground in dynamic loading conditions. Yielding rockbolts such as Split set, Swellex, Roofex, Yield-Lok and Conebolt are suitable for medium to high ground demand; Par1, Par1R, MP1, and Vulcan bolts which were also under investigation of this research stay in high to very high energy dissipation capacity category. Conebolt and Garford might be suitable for extremely high demand. It is noteworthy that, very significant damage to surface support would be happened along with the dynamic event with the surface deformation of greater than 30cm, therefore, the bolts with the extremely high deformation capacity would not effectively work in that condition.

To sum up, the results of the research introduced a support selection method that facilitates the selection of a suitable reinforcement system at the preliminary stages of design and guides the designer to adjust the reinforcement system based on observed ground and support reaction.

**Keywords:** high-stress tunnels, Support system, ground demand, reinforcement capacity, rockbolt, Tunnel support, Collar bonding, Seismic rock support, Deep mining

This page intentionally left blank

# TABLE OF CONTENTS

DECLARATION	2
ACKNOWLEDGEMENTS	3
ABSTRACT	4
TABLE OF CONTENTS	7
LIST OF FIGURES	11
LIST OF TABLES	15
LIST OF SYMBOLS AND ACRONYMS	17
1. INTRODUCTION TO PROJECT	19
<b>1.1. Background to Project</b>	<b>19</b>
<b>1.2. Project Problem Statement</b>	<b>19</b>
<b>1.3. Project Objectives</b>	<b>21</b>
<b>1.4. Project Activities and Project Scope</b>	<b>23</b>
2. STATE OF THE ART OF THE ROCKBOLTS DEFORMATION UNDER THE STATIC AND DYNAMIC CONDITION AND DEEP MINING	25
<b>2.1. Introduction</b>	<b>25</b>
<b>2.2 Reinforcement (Rockbolt) systems</b>	<b>26</b>
<b>2.2.1 Key factors in reinforcement system performance</b>	<b>26</b>
<b>2.2.2 Typical load-deformation behaviour of rockbolts</b>	<b>28</b>
<b>2.2.3 Load transfers mechanisms in rockbolts with different anchorage conditions</b>	<b>29</b>
<b>2.3. decoupling mechanisms of partially encapsulated rockbolts</b>	<b>43</b>
<b>2.3.1. Outer length</b>	<b>44</b>
<b>2.3.2. decoupled length</b>	<b>44</b>
<b>2.3.3. encapsulation length</b>	<b>45</b>

2.4. Minimum Required Encapsulation Length of cemented rockbolts	46
2.5. Deep Underground High-Stress Mining	48
2.5.1. Ground behaviour in seismic conditions	48
2.5.2. Ground seismic energy demand	49
2.6. Dynamic capacity of Rockbolts	58
2.6.1. Drop test	60
2.6.2. Blast Simulation	62
2.6.3. Momentum transfer method	63
2.6.4. Back-Calculation	65
2.6.5. Large-scale dynamic test rig of ground support	65
2.6.6. NCM Dynamic Impact Tester (NCM DIT)	67
2.7. Summary of Literature Review	71
3. MODIFICATION OF REBAR ROCKBOLTS AND FIELD TESTING	73
3.1 Introduction	73
3.2 Experiments Modifications	73
3.2.1. Rebar rockbolt modifications	73
3.2.2. Laboratory test results	78
3.2.3. Field test results	80
3.3. Discussion on modified rebar performance in seismic prone zones	87
3.4. Summary and Results	88
4. FIELD TESTING ON PROGRESSIVE DECOUPLING OF PARTIALLY ENCAPSULATED ROCKBOLTS AND MULTI-STRAND TENDON	91
4.1. Introduction	91
4.2. Decoupling Process Background	91
4.3. Field testing to assess the decoupling Process	93
4.3.1. Stressing procedure	94
4.3.2. Experiment results	97



<b>4.4. Summary and Results</b>	<b>109</b>
<b>5. ROCKBOLT BEHAVIOUR UNDER DYNAMIC (SEISMIC) CONDITION</b>	<b>111</b>
<b>5.1. Introduction</b>	<b>111</b>
<b>5.2. Experiments with New Concept Mining Dynamic Impact Tester</b>	<b>112</b>
<b>5.3. The behaviour of the rockbolts under different applied parameters</b>	<b>113</b>
<b>5.3.1. Introducing the rockbolt types</b>	<b>113</b>
<b>5.3.2. The behaviour of rebar under dynamic impact test</b>	<b>120</b>
<b>5.3.3. The behaviour of the Dynamic Bolts concerning the applied energy of the multiple drops and number of drops</b>	<b>123</b>
<b>5.3.4. Dynamic behaviour of the bolt with respect to the length of the bolt</b>	<b>133</b>
<b>5.3.5. The effect of encapsulation material on rockbolt capacity</b>	<b>135</b>
<b>5.3.6. The effect of the velocity of the impacts on rockbolt capacity</b>	<b>136</b>
<b>5.4. Summary</b>	<b>143</b>
<b>6. DISCUSSION ON RESULTS</b>	<b>145</b>
<b>6.1. Introduction</b>	<b>145</b>
<b>6.2. Discussion on Static Experiment Results</b>	<b>145</b>
<b>6.3. Discussion on Dynamic Test Results</b>	<b>150</b>
<b>6.4. Ground Support Selection Strategy</b>	<b>150</b>
<b>6.5. Considerations of linking and terminating arrangements of reinforcements</b>	<b>155</b>
<b>6.6. Modified rebar rockbolt performance in seismic conditions</b>	<b>155</b>
<b>6.7. Summary and Results</b>	<b>156</b>
<b>7. CONCLUSIONS, RECOMMENDATIONS AND CONTRIBUTIONS TO STATE OF KNOWLEDGE</b>	<b>159</b>
<b>7.1. Conclusions and Recommendations</b>	<b>159</b>
<b>7.2. Contributions to the state of knowledge</b>	<b>161</b>
<b>7.3. Recommendation for future research</b>	<b>164</b>

<b>REFERENCES</b>	<b>165</b>
<b>APPENDIX A</b>	<b>169</b>
<b>Attribution table for the published papers included in this thesis</b>	<b>169</b>
<b>APPENDIX B</b>	<b>177</b>
<b>Graphs of more results for free length variation</b>	<b>177</b>
<b>APPENDIX C</b>	<b>179</b>
<b>More results of DIT tests</b>	<b>179</b>

## LIST OF FIGURES

Figure 1.1. Dissertation structure showing the design methodology of dynamic reinforcement selection.....	24
Figure 2.1. Major factors in reinforcement system performance .....	27
Figure 2.2. Average load-displacement behaviours obtained in a laboratory setting (modified after Stillborg (1993), Hoek et al. (1995), Li et al. (2014)).....	29
Figure 2.3. Stress components in a small section of a bolt (Li and Stillborg, 1999) .....	29
Figure 2.4. Shear stress along a fully coupled rockbolt subjected to an axial load before decoupling occurs (redrawn and modified after Li and Stillborg (1999)) .....	30
Figure 2.5. Axial deformation (conclude to the loading) of rockbolts (modified and redrawn after Thompson et al. (2012)) .....	31
Figure 2.6. Load distribution in mechanically two-point anchored rockbolts after Masoudi et al. (2019) .....	32
Figure 2.7. Stress distribution along a frictional rockbolt (Split set) (after Masoudi et al. (2019)) .....	34
Figure 2.8. Stress distributions along the length of an inflatable frictional bolt when subjected to a pull-load at the bolt head.....	35
Figure 2.9. Load distribution in fully grouted bolts with bearing plate in uniform media (after Masoudi et al. (2019)) .....	36
Figure 2.10. Stress distribution in fully grouted bolts with bearing plate under the effect of a discontinuity after Masoudi et al. (2019) .....	37
Figure 2.11. Load distribution in partially grouted bolts with bearing plate in uniform media after Masoudi et al. (2019) .....	38
Figure 2.12. Realistic load distribution in partially encapsulated bolts with the bearing plate in uniform media after Masoudi et al. (2019) .....	39

Figure 2.13. Load distribution in partially grouted bolts with an active discontinuity in free length after Masoudi et al. (2019).....	40
Figure 2.14. Stress distribution in fully grouted bolts without bearing plate in uniform media after Masoudi et al. (2019) .....	41
Figure 2.15. Axial stress distributions along a D-Bolt (redrawn and modified after (C. C. Li et al., 2014)) .....	43
Figure 2.16. Load-Displacement behaviour of a rockbolt under overloading condition (after Masoudi et al. (2019)).....	46
Figure 2.17. Failure mechanisms for underground deep and high-stress excavations due to induced stress and seismic events .....	51
Figure 2.18. a) Analytic calculation of energy in the rock sample cyclic loading of (after Kwaśniewski et al. (1994) and b) Calculation of potential elastic strain energy (J. A. Wang & Park, 2001).....	53
Figure 2.19. Momentum transfer mechanism dynamic testing facility (after J. Player, Thompson, et al. (2008)) .....	64
Figure 2.20. The large-scale dynamic testing rig of Geobruigg (Roth et al., 2014)	66
Figure 2.21. The New Concept Mining (NCM) Dynamic Impact Tester (DIT) .....	69
Figure 2.22. The Concept of Impact test on a) Continuous tube and b) Split tube .....	70
Figure 3.1. Sample of modified rockbolt after Masoudi et al. (2019).....	74
Figure 3.2. Load distribution in modified rebar rockbolts under the effect of a discontinuity opening after Masoudi et al. (2019) .....	76
Figure 3.3. Different combination of embedment and loading condition of the rebar rockbolts (redrawn after (J. Player, Thompson, et al., 2009; Villaescusa, 2014)). .....	79
Figure 3.4. Different views of the cavern including the tunnel under study Masoudi et al. (2019) .....	81

Figure 3.5. Deformometre to measure the large deformation along a rockbolt a) Schematic view b) photo of installed set sample after Masoudi et al. (2019) .....	82
Figure 3.6. Displacements monitoring results at different distances from rockbolt head SB-07 Masoudi et al. (2019) .....	82
Figure 3.7. Load monitoring in the shank of rockbolt SB07 Masoudi et al. (2019) .....	83
Figure 3.8. Displacements monitoring results at different distances from rockbolt head SB-08 Masoudi et al. (2019) .....	83
Figure 3.9. Load monitoring in the shank of rockbolt SB-08 Masoudi et al. (2019) .....	84
Figure 3.10. Displacements monitoring results at different distances from rockbolt head SB-09 Masoudi et al. (2019) .....	84
Figure 3.11. Load monitoring in the shank of rockbolt SB-09 Masoudi et al. (2019) .....	85
Figure 3.12. Changes of load versus deformation of the modified rebar rockbolt Masoudi et al. (2019) .....	86
Figure 4.1. Change of the load distribution in partially encapsulated reinforcement element in uniform media .....	92
Figure 4.2. Schematic stressing steps and measured values during the second cycle of loading.....	96
Figure 4.3. Load-deformation of a multi-strand during the stressing process in the first experiment.....	98
Figure 4.4. Encapsulation length/Free length calculation of a multi-strand tendon under increasing load.....	99
Figure 4.5. Load-deformation profile during the stressing process of the second experiment.....	100
Figure 4.6. Creep results for the monobar tendon for the second experiment .	101

Figure 4.7. The free length - the encapsulation length variation under increasing loading in the second experiment .....	102
Figure 4.8. The profile of load-deformation of the monobar in the third experiment .....	104
Figure 4.9. Creep result for the monobar tendon in the third experiment .....	105
Figure 4.10. The free length and the encapsulation length under increasing loading on monobar tendon third experiment.....	106
Figure 4.11. The profile of load-deformation of a rockbolt in the fourth experiment .....	107
Figure 4.12. The free length and the encapsulation length under increasing loading condition on rock bolt fourth experiment .....	109
Figure 5.10. The total absorbed energy of the VB-D20-L2.0 bolt in respect to the applied energy of multiple Drops and number of Drops.....	125
Figure 5.11. Total deformation of the VB-D20-L2.0 bolt in respect to the applied energy of multiple Drops and number of Drops.....	125
Figure 5.12. Dynamic Capacity of the VB-D20-L2.0 bolt subjected to multiple Drops .....	126
Figure 5.13. Dynamic Capacity of the VB-D20-L2.0 bolt subjected to multiple Drops .....	127
Figure 5.21. Illustration of the MP1 Split Tube Instrumentation (Loadcell) .....	128
Figure 5.22. Dynamic capacity of the MP1 bolt subjected to multiple drops.....	129
Figure 5.23. Dynamic capacity of the MP1 bolt subjected to multiple drops.....	130
Figure 5.24. Dynamic capacity of the MP1 bolt subjected to multiple drops.....	131
Figure 5.25. Dynamic capacity of the MP1 bolt subjected to multiple drops.....	132
Figure 5.26. Deformation capacity of the MP1 bolt subjected to multiple drops .....	133

Figure 5.27. Deformation capacity of the MP1 bolt subjected to multiple drops .....	134
Figure 5.28. Dynamic energy absorption and deformation Capacity of the PAR1-D20-L2.1-2.5 bolt subjected to multiple Drops.....	135
Figure 5.29. Dynamic energy absorption and deformation Capacity of the PAR1-D20-L2.1-2.5 bolt subjected to multiple Drops.....	135
Figure 5.30. Effect of the impact velocity on the dynamic capacity of the bolts	138
Figure 5.31. Effect of the impact velocity on the average dynamic capacity of the bolts.....	139
Figure 5.32. Effect of the impact velocity on the dynamic capacity of the bolts and their total deformation capacity .....	140
Figure 5.33. Effect of the impact velocity on the average dynamic capacity of the bolts and their average total deformation capacity .....	141
Figure 5.34. Effect of the impact velocity on deformation capacity of the bolts	142
Figure 5.35. Effect of the impact velocity on average deformation capacity of the bolts.....	143
Figure 6.1. Trend of the free length - encapsulation length variation under increasing load in the second experiment.....	147
Figure 6.2. Trend of the free length - encapsulation length variation under increasing load in the third experiment.....	147
Figure 6.3. Non-Linear trend of the free length - encapsulation length variation under increasing load in the third experiment. ....	148
Figure 6.4. Non-Linear trend of the free length - encapsulation length variation under increasing load in the fourth experiment.....	149

## **LIST OF TABLES**

Table 2.1. Rockburst potential based on intact rock property .....	54
Table 2.2. Failure thickness estimation (after Daniel P. Heal (2010)).....	56

Table 2.3. Typical Rockmass Demand for Ground Support Design (Thompson et al., 2012) .....	58
Table 4.1. Properties of the monobars for the first experiment .....	97
Table 4.2. Loading steps of the monobars in the first experiment.....	98
Table 4.3. Properties of the monobars for the second experiment .....	99
Table 4.4. Loading steps of the monobars in the second experiment.....	100
Table 4.5. Properties of the monobars for the third experiment.....	103
Table 4.6. Loading steps of the monobars in the third experiment .....	103
Table 4.7. Properties of the monobars for the fourth experiment.....	106
Table 4.8. Loading steps of the monobars in the fourth experiment.....	107
Table 5.5. Par1 Bolt Performance specifications .....	114
Table 5.6. Par1 Resin Bolt Performance Specifications.....	116
Table 5.7. MP1 Performance Specifications.....	118
Table 5.8. Vulcan Bolt Performance Specifications.....	120
Table 6.1. Demand – Capacity based support selection modified after Masoudi and Sharifzadeh (2018). .....	153
Table 6.2. Energy dissipation capacity category of different types of reinforcement modified after Masoudi and Sharifzadeh (2018).....	154



## **LIST OF SYMBOLS AND ACRONYMS**

AED	Applied Energy of each Drop
CEL	Collar Encapsulated Length
DAQ	Data Acquisition System
DIT	Dynamic Impact Tester
EVP	Excavation Vulnerability Potential
HDPE	High-Density Polyethylene
IRPA	Intact Rock Property Approach
MEL	Main Encapsulation Length
MREL	Minimum Required Encapsulation Length
NCM	New Concept Mining
PPV	Peak Particle Velocity
RDP	Rockburst Damage Potential
TAE	Total Absorbed Energy
WASM	Western Australian School of Mines

This page intentionally left blank

# **1. INTRODUCTION TO PROJECT**

## **1.1. BACKGROUND TO PROJECT**

Rock support design in underground mining is more challenging than before because the depth of mines is going to be increased. In this condition having the knowledge of support element behaviour, ground reaction, and prediction of failure is unavoidable. Deep mining is increasing worldwide because near-surface mineral resources become gradually depleted. Higher in-situ stress is the main difference between deep mining compared to near-surface mining, and the dynamic events such as the rockburst are more likely in this condition. Rockburst might occur below 600-800 m depth and more likely passing 1000 m depth. Such phenomena are not limited only to deep mines; however, they could be experienced at less deep due to the presence of high horizontal to vertical stress ratios.

Finding a practical support design requires determining the rockmass demand and rock support energy dissipation capacity. Whilst numerous unknowns, uncertainties in geomechanical parameters and furthermore the randomness of seismic events, increase the ambiguity of the rock demand determination and consequently extend the complexity of efficient support design. On the other hand, the complicated performance of a rock support system under dynamic loading conditions increases the complexity of the designation as well. Though significant attempts to estimate energy dissipation capacity of support elements have been carried out, this subject still needs more effort. Additionally, the performance of rock support as an integrated system and the role played by other mechanisms of loading, like dynamic shear loading, in the support system is also not clearly understood.

## **1.2. PROJECT PROBLEM STATEMENT**

To achieve stability and safety at deep excavations and sudden failure-prone conditions, appropriate support and reinforcement design are necessary. The support system should not only be able to tolerate the static rock load and potential dynamic load due to induced stress, but it should also not lose strength over a wide range of deformation.

It could be concluded that the energy dissipation capacities of not only support elements individually but also the ground support as an integrated system need to be determined. Ground energy demand cannot accurately be determined or calculated, however, some estimation might be achieved to help the engineering design. Some of the methods have attempted to find a relationship between intact rock properties and their potential to burst, and the real condition of rockmass under stress (Kwaśniewski & Wang, 1999; J. A. Wang & Park, 2001). Some other methods are based on the estimation of probable failure volume, ejection velocity and the travelling distance of ejected material (Kaiser, McCreath, & Tannant, 1996). Another recent method relies on the definition of the effective parameters on the potential of rockburst and its likelihood of damage (Daniel P. Heal, 2010).

Along with estimation of the ground demand during dynamic events, a large amount of effort has been expended in determining the rock support energy dissipation capacity. Rockbolt as the primary element to transfer the energy of the displaced volume of the rock to the ground in depth has been under the focus. Several approaches including the drop test, blast simulation, back-calculation and momentum transfer method have been developed in order to examine rockbolt performance (Daniel P. Heal, 2010; D.P. Heal & Potvin, 2007; L. Li, Hagan, & Saydam, 2014; J. Player, Villaescusa, & Thompson, 2008; J. R. Player, E., & A., 2004; Plouffe, Anderson, & Judge, 2008). Another so-called large-scale dynamic test rig has been constructed in 2012 by the Geobruigg in Switzerland in order to investigate the whole support system as an integrated system (Morissette, 2015; Roth, Cala, Brändle, & Rorem, 2014). New concept Mining Company (NCM) is also constructed a Dynamic Impact tester (DIT) laboratory-based facility that is similar to original drop test equipment with more sophisticated instrumentation. The main part of this research including all dynamic drop tests have been carried out and interpreted using NCM testing facilities. Despite several research studies on different ground types, support systems in a wide range of loading, rockbolt types, etc., there are still requirements for further studies on this subject.

Additionally, it has been found that, in case of overloading in the shank of rockbolts, they often fail by decoupling either at the bolt–grout interface or less likely

at the grout–rock/soil interface. Since rockbolts are usually under tension, they need to be attached appropriately to the ground so that the applied tensile force can be successfully transferred into the surrounding mass. For a decoupling failure, the understanding of the distribution of the interface shear stress along the bonded length is critical for predicting the ultimate bearing capacity, estimating of the available axial load in the bolt shank, and for obtaining an optimal design. It has been found that the ultimate load rises with the rock-to-grout stiffness ratio, the grout strength, the friction coefficient between the grout and the bolt, and it decreases with the increase in borehole diameter.

Field monitoring is always required to ensure the correct bolting design or applying modification, but it can be challenging and expensive. Generally, the working environments of the rockbolt and the adjacent area are unknown. It is necessary to have a good understanding of the interaction behaviour of the rockbolt in the deformed rock mass to improve the bolting design. Thus, before entering this stage of the modification of the design, some criteria and methods are needed for a preliminary support system and reinforcement design.

### **1.3. PROJECT OBJECTIVES**

Various kinds of rockbolts including mechanical bolts, fully-grouted rebars, frictional bolts and energy-absorbing rockbolts are utilised currently for stabilising structures in dynamic and static loading conditions in underground mines. However, the interaction mechanism of the rock mass and the rockbolt is not understood clearly enough so far, and to some extent, the basis for the bolting design is still empirical or semi-empirical (M Cai, 2013; Jin-feng & Ming-yao, 2016; Kaiser & Cai, 2012; Kristjánsson, 2014; Mark, 2016; Sandbak & Rai, 2013).

Rock reinforcement in seismic conditions has to dissipate the released energy of dynamic events. Therefore it needs specific requirements, including large deformation capability and high ultimate load capacity. There are varieties of rockbolts in the industry developed for this purpose such as Split set, Swellex, Roofex, Yield-Lok, D-Bolt, Cone-Bolt, Garford, etc. but many of them are not available in all

countries, and they need well-trained operators, certain considerations, and special installation equipment.

Different mechanisms are involved in improving the dynamic performance of the yielding bolts. Frictional bolts start to slip when the force exceeds the frictional strength of the bolt-rock interface. Slipping continues and shows larger deformation with an almost constant load in the shank of the rockbolt or with a decreasing load if the interface friction strength is reduced. Generally, this type of bolts does not have a high ultimate load capacity and even less in dynamic conditions (Charlie C Li, Stjern, & Myrvang, 2014) but their advantage is the large deformability. Stretching the shank of the bolt is another mechanism to increase its deformability similar to what is happening in D-Bolts. The shank of the bolt between two adjacent anchors is allowed to detach from the surrounding grout and stretch plastically to its ultimate deformation and load capacity (Charlie Chunlin Li, 2010; C. C. Li et al., 2014). Ploughing of the anchor in the grout surrounding the bolt such as in Cone-Bolts can also increase its deformability, but grout quality and its implementation need further considerations while applying a high strength cementation grout can lead to strong anchorage of the cone and prevent it from ploughing through the cement, and result in early rupture of the bolt (C. C. Li et al., 2014).

The rebars and threadbars are usually employed as ordinary rockbolts in underground mines all over the world. This kind of bolt wholly or partially encapsulated in cement or resin grout depending on the difference in expected performance. They are mostly used completely encapsulated in cement grout in mines as primary reinforcement in combination with surface wire mesh and shotcrete. Discontinuities opening in rockmass or ejection of a mass of rock in the tunnel wall cause local deformation and concentrated loading in the shank of the rockbolt. This phenomenon results in rupture of the bolt at the overloaded section while the rest of the rockbolt has not reached its deformation or load capacity.

In this research, reinforcement is at the centre of interest and the measurement methods to estimate their dynamic capacity. For this purpose influencing factors in a seismic condition such as the effect of the magnitude of the seismic event or applied impact, the velocity of the impact, the number of recurrence or frequency of the

impact, and the effect of the length of the rockbolt on its performance are investigated.

#### **1.4. PROJECT ACTIVITIES AND PROJECT SCOPE**

In this research, at first, different mechanisms of rockburst and rock ejection, various methods of ground demand estimation, and rockbolt energy dissipation capacity measurement are illustrated (Figure 1.1). Then, suitable rockbolt type selection is recommended for different ground demand levels. The method is simply presented by table and graph which is easy for use in practice. The presented methods can assist the selection of appropriate rockbolt type at the preliminary stages of mine design. Additional to the rockbolt selection, some further considerations for the selection of other support elements are given as well.

Followingly, the axial load and shear load distribution profile along different types of rockbolts were discussed. A conceptual model for the partially or fully coupled rockbolt system, frictional bolts, inflatable bolts and D-bolt were presented. On this basis, the coupling and decoupling behaviour of the rockbolts in a continuously deformed rock mass were discussed. A proposed conceptual model for rockbolt in the condition of discontinuity deformed rock is also developed.

An applied method for using the ordinary rebar rockbolt to improve their capability in the seismic condition is introduced. Distribution of the concentrated deformation such as of a discontinuity opening along a longer length of the rockbolt (instead of a limited length) would assist in increasing the total deformation capacity of the rockbolt as well as to prevent the local load concentration and early failure of the bolt.

One of the main parts of this research is the rock bolt dynamic tests through New Concept Mining company (NCM). these experiments include 53 static and 335 multiple dynamic drop tests on Par1, Par1Resin, MP1, and Vulcan rockbolts utilising NCM Dynamic Impact Tester (DIT). These sets of dynamic tests, clearly show the effect of different factors on energy absorption/dissipation capacity of several types of rockbolts with different mechanisms of anchorage. They have been categorised and explained in graphs showing the effect of a number of the dynamic incidents, the

magnitude of the incidents, length of the bolt, the velocity of the implied incident, the effect of one significant incident or several small incidents on energy absorption/dissipation capacity of the rockbolts and their deformation capacity, and discussed. Results show that the deformation capacity of the different types of bolts has less affected by different applied loading mechanisms.

Different practices, both on-field and laboratory, have been discussed in chapter 6. The summary of findings is concluded in chapter 7.

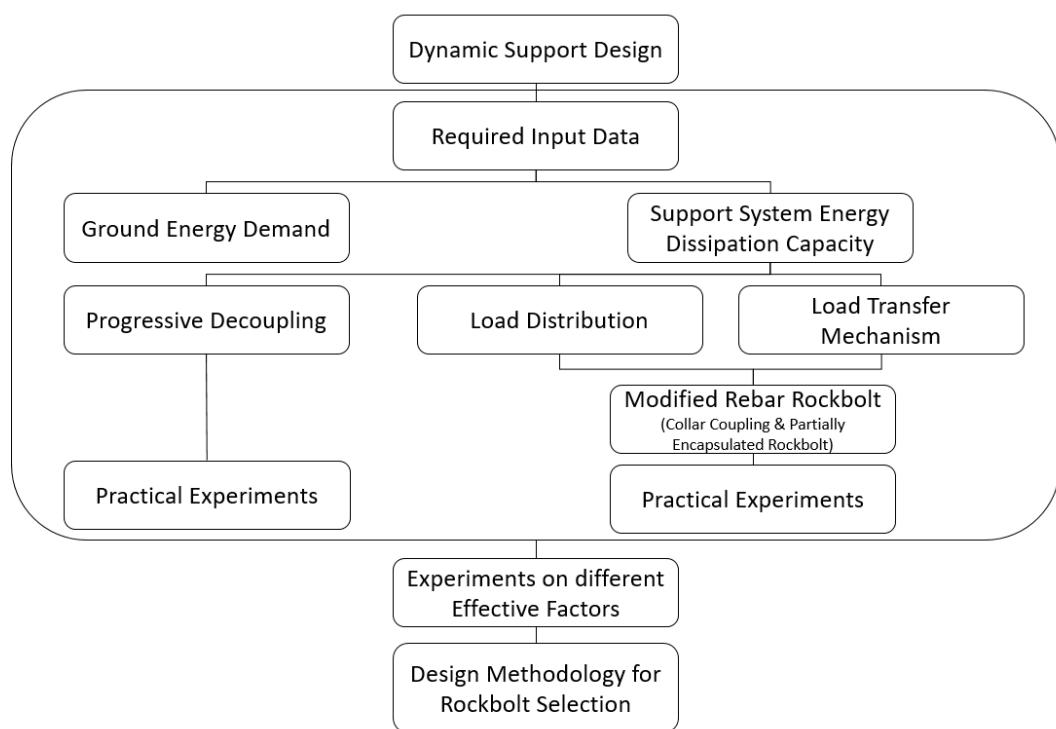


Figure 1.1. Dissertation structure showing the design methodology of dynamic reinforcement selection



## **2. STATE OF THE ART OF THE ROCKBOLTS DEFORMATION UNDER THE STATIC AND DYNAMIC CONDITION AND DEEP MINING**

### **2.1. INTRODUCTION**

Rockbolts (or reinforcement) plays a crucial role in ground support systems in underground mining with different mechanisms. It also shows different behaviour in static and dynamic condition depend on many parameters. On the other hand, the expected reaction and performance are altered in static and dynamic loading conditions. The static design of the rockbolt is well-known so that its maximum load capacity, length and spacing are the most influential design parameters while in a dynamic loading condition it inherent attribute such as elongation property also has a significant task. There are a great number of factors involving in the functioning of reinforcement element both in static and dynamic condition, some of which discussed in following sub-chapters.

In this chapter, a critical literature review by combining the state of arts of topics and the author industrial experiences and investigations were presented. Therefore, this chapter expresses the available body of knowledge with conceptualised figures and tables based on researcher understanding. For this purpose, at first key factors, load-deformation behaviour, and load transfer mechanisms in reinforcement system were reviewed and then decoupling mechanisms of partially encapsulated rockbolts and their Minimum Required Encapsulation Length (MREL) have been defined and explained. A new method of borehole rockbolt load monitoring was introduced and employed for parts of this research experiments. Followingly a review of deep underground high-stress mining including different methods of ground seismic energy demand estimation consisting of intact rock property approach, estimation of failure volume and ejection velocity, and rockburst damage potential were presented. Finally, different methods and facilities of dynamic capacity measurement of rockbolts were presented. The drop test, blast simulation, momentum transfer concept and back-calculation included in the final part as well as describing a large scale dynamic test rig of ground support and the New Concept Mining Dynamic

Impact Tester (NCM DIT) by which a significant portion of this research experiments have been carried out.

## **2.2 REINFORCEMENT (ROCKBOLT) SYSTEMS**

### **2.2.1 KEY FACTORS IN REINFORCEMENT SYSTEM PERFORMANCE**

There are various factors involving the performance of reinforcement in an underground stabilisation project. These factors vary from reinforcement material properties and manufacturing specification to the ground and loading condition and interface properties. As it is depicted in Figure 2.1, reinforcement performance can be affected by four groups of primary factors, including:

- Reinforcement Specification
- Ground condition
- Interface properties
- Loading condition

One of the main categories of reinforcement performance factors is its specifications which refer to those factors that are related to the properties of the material, fabrication of the reinforcement and its installation design. These factors contain material properties, diameter, length, stiffness, yielding properties, corrosion sensitivity and protection, loosening property, borehole diameter, head and faceplate designation, corrosion protection, and pre-tension.

The second main category of reinforcement performance factors is the ground condition. This group refers to those factors that are related to the active factors of the ground and geometry of structure which can change reinforcement performance containing the depth of installation, type of the ground, water condition, permeability, aggressiveness, discontinuity, geometry and location, distance from active faces, and installation sequence.

The third main category of reinforcement performance factors is the interface parameters between ground and reinforcement and mechanisms involving in

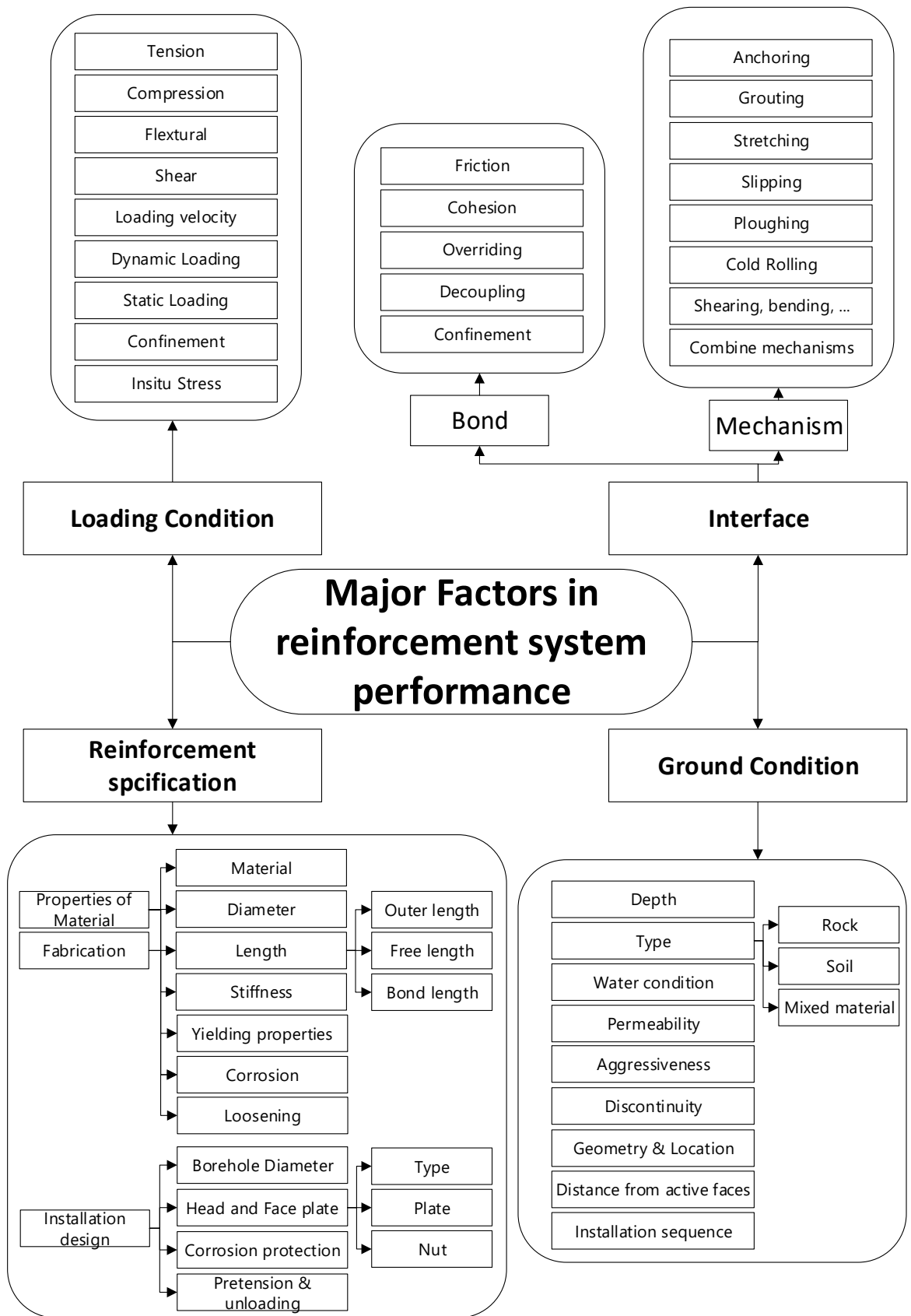


Figure 2.1. Major factors in reinforcement system performance

between. This category divided into two subdivision, bond factors and the factors related to different mechanisms of involving the reinforcement to the surrounding ground. Bond factors contain friction, cohesion, overriding, decoupling, and confinement. The friction is a physical resistance of the reinforcement against the movement, which is not an active force, but it is a passive force that is mobilised with the movement of the surrounded ground in any direction. The bonding mechanisms include the anchoring, grouting, stretching, slipping, ploughing, rolling, shearing, bending, torsion, deformation, and combined mechanism.

The fourth main category of reinforcement performance factors is the loading condition and their mechanisms, including static and dynamic loading, tension, compression, flexural, shear, confinement, in-situ stress, and loading velocity. All kind of loadings are dynamic but static loading state the kind of loading in which load transfer happens slowly and without a seismic event.

### **2.2.2 TYPICAL LOAD-DEFORMATION BEHAVIOUR OF ROCKBOLTS**

The behaviour of the rockbolt refers to changes that occur in the element under the loading condition. Load transfers to the shank of the bolt through the interface via a specific mechanism and rockbolt start to react. The most obvious alteration in reinforcement is its deformation, and therefore, generally, behaviour refers to the load-deformation property of the rockbolts.

Comparisons of the behaviours and capacities of various rockbolts subject to laboratory testing have been published previously (Hoek, Kaiser, & Bawden, 1995; C. C. Li et al., 2014; Stillborg, 1993). Figure 2.2 shows the results and is a widely used reference in the design of underground support systems. Some rockbolts are stiff and can tolerate a small amount of deformation while some others are more flexible with a large amount of deformation capacity. Another difference in this figure is the maximum amount of load that can be tolerated by a specific type of rockbolt. These diagrams are just some typical load-deformation behaviour of rockbolts, and every type of bolt can show different behaviour in different condition. In other words, maximum load and deformation capacity varies depending on a variety of parameters.

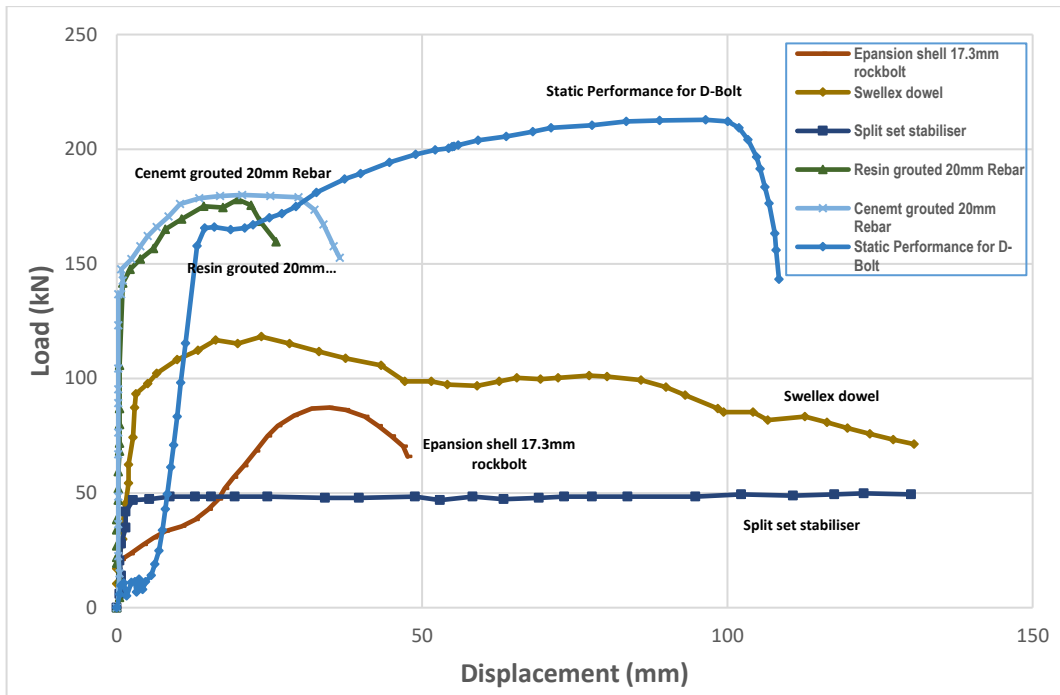


Figure 2.2. Average load-displacement behaviours obtained in a laboratory setting (modified after Stillborg (1993), Hoek et al. (1995), Li et al. (2014))

### 2.2.3 LOAD TRANSFERS MECHANISMS IN ROCKBOLTS WITH DIFFERENT ANCHORAGE CONDITIONS

When a bolt installed in rock is subjected to a tensile axial load, the relationship between the axial tensile stress of the bolt and the shear stress at the bolt interface can be established through considering a small section of the bolt as shown in Figure 2.3.

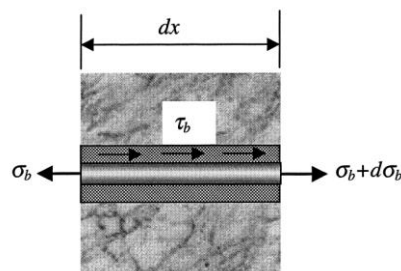


Figure 2.3. Stress components in a small section of a bolt (Li and Stillborg, 1999)

The force equilibrium in the axial direction leads to the following expression:

$$\tau_b = -\frac{A}{\pi d_b} \frac{d\sigma_b}{dx} \quad (2-1)$$

Where  $d_b$  is the diameter of the bolt, and  $A$  is the area of the cross-section of the bolt.

Primary studies on the behaviour and axial load distribution of the rockbolts under loading conditions have been started by Farmer (1975). According to literature, the axial and shear stress at the interface of the bolt – grout and the grout-rock decrease exponentially over a length of encapsulated rockbolt from the loading point to the distal end of the bolt as long as debonding has not occurred. As shown in Figure 2.4 the maximum shear stress is concentrated near the surface and then rapidly decreases with moving toward depth.

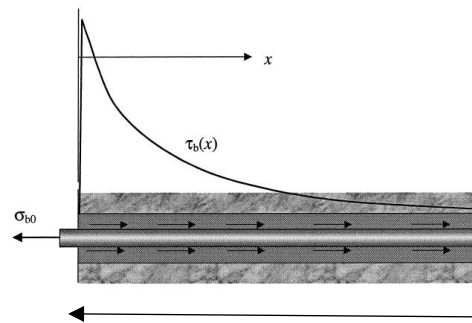


Figure 2.4. Shear stress along a fully coupled rockbolt subjected to an axial load before decoupling occurs (redrawn and modified after Li and Stillborg (1999))

Axial load at each point along the bolt could be calculated by the following expression

$$\sigma_b = -\frac{\pi d_b}{A} \int_0^l \tau_b dx \quad (2-2)$$

An encapsulated length of a rockbolt is coupled with the surrounding ground via cement or resin encapsulation material; therefore the rockbolt is loaded due to the deformation of the ground or surrounding material. As can be seen schematically in Figure 2.5, the relative axial deformation between the rockbolt and wall of the borehole is a result of ground deformation. The figure shows the deformation of massive rocks in the absence of discontinuities. However, the ground deformation and load distribution over the rockbolt are more complicated in such conditions (Thompson, Villaescusa, & Windsor, 2012).

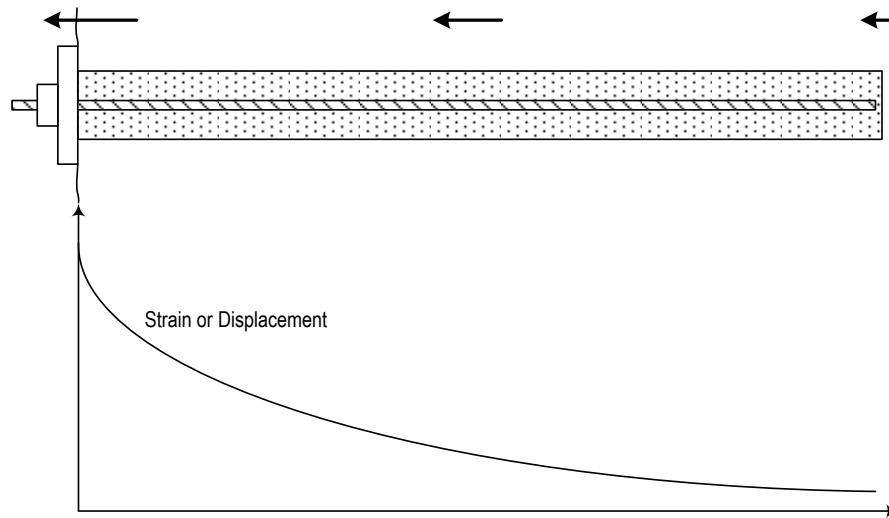


Figure 2.5. Axial deformation (conclude to the loading) of rockbolts (modified and redrawn after Thompson et al. (2012))

#### 2.2.3.1. Mechanically Two-point Anchored Rockbolts / End Anchored

A mechanically end anchored rockbolt is anchored in a borehole at both ends of the rockbolt so it can be called a two-point anchored bolt as shown in Figure 2.6. This kind of rockbolt must always have a bearing face plate on one end (head) and a mechanical anchor point such as an expansion shell on the other end of the rockbolt (Zou (2004)). In most cases, an initial pretension needs to be applied by tightening of the nut promptly after installation. The initial pretension helps to activate the rockbolt from the installation time. Then ground movements apply further tension in the shank of the rockbolt between the head (collar) and end (expansion shell) of it along with the loading of the support elements. The load distributes uniformly over the length of the rockbolt and all induced deformation due to ground movement or discontinuities openings cannot change the outline of the load distribution, and the load distributes over the whole length unless the rockbolt fails or is sheared off.

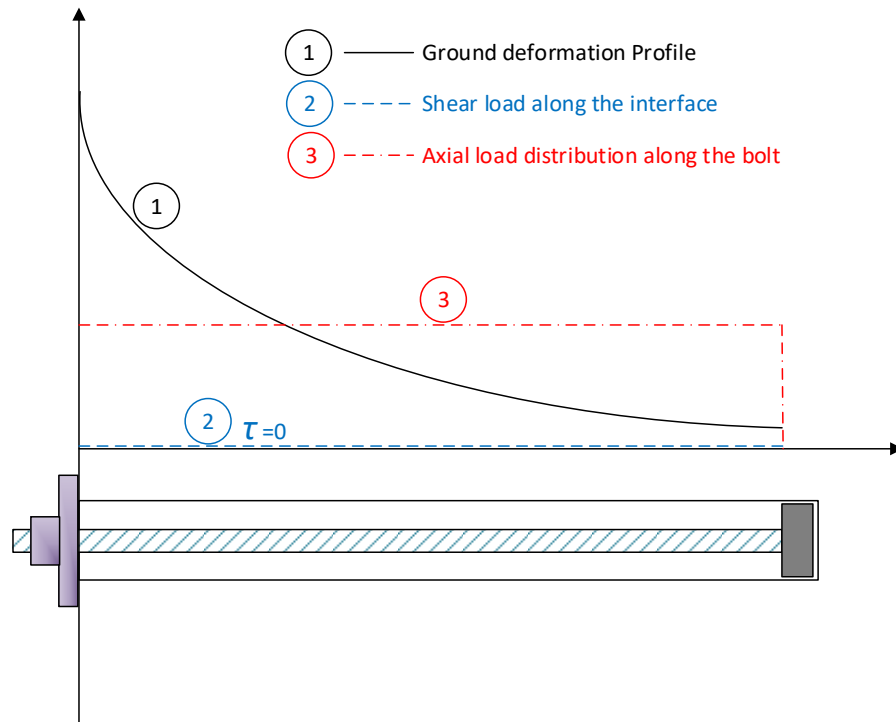


Figure 2.6. Load distribution in mechanically two-point anchored rockbolts after Masoudi et al. (2019)

The strength of the bearing faceplate, nut, thread, and the tightness of the end anchor, govern the load capacity of this kind of rockbolt while deformation capacity of the rockbolts depends on their material. Although these types of rebar rockbolts are produced in a broad range of load and deformation capacities, in comparison to fully grouted rockbolts, the two-point anchored rockbolts have much more deformation capacity because of distribution of the deformation over the whole length of the rockbolt.

Two-point anchored bolts have some weaknesses leading to a loss of their functionality for support the ground. Slippage of the expansion shell at the end of the bolt because of a small area of in-between contact would be a reason for releasing the load of the bolt. This phenomenon could be a result of failure due to stress concentration on an anchor point or creep of the rock under stress concentration. The other weaknesses of the mechanically end anchored rockbolts are nut and thread stripping and/or the failure of the bearing faceplate to retain the load and transfer it to the rockbolt. One of the main reasons for nut and thread stripping and the early failure of the bearing plate is the occurrence of dynamic events during which the nut



can expand laterally and strip off the threads and/or the bearing plate cannot tolerate its nominal resistance. Manufacturing and non-conformance of the bearing plate and the rockbolt could be another reason for early failure. Failure of screws of a threaded rockbolt in the threaded part of the head of the rockbolt often occurs because of the lower effective cross-sectional area of the rockbolt at the roots of the screw threads.

Local weaknesses, blasting and other methods of excavation can disturb the rock mass in the wall and roof where disturbance of the rock beneath the bearing plate is another reason for unwanted unloading of the rockbolt and ruin the functionality of a support system.

#### 2.2.3.2. *Frictionally Anchored*

Split set and inflatable bolts (e.g. Swellex and Omega) belong to the class of frictional bolts. A frictional bolt interacts with the rock via friction at the bolt-rock interface along with its entire or major part of the length. When it is subjected to a pull load at the bolt head (Figure 2.7), the shear resistance at the interface will be first mobilised at the loading point. The bolt starts to slip outward in the strength-mobilised section, with the length of the slipping section rising with the increase of the applied load (C. C. Li et al. (2014)). The shear stress on the slipping part of the bolt remains approximately same to the level of the shear strength during bolt deformation. Because of this characteristic, frictional bolts can tolerate large rock deformation without significant loss of their load-bearing capacity.

In theory, the ductile performance of this type of bolt can be achieved only when frictional slippage occurs along the entire length of the bolt. In reality, the slippage is only guaranteed for the Split set because of its particular installation procedure. At installation, Split set is pushed, for instance by a bolting rig, into the borehole. The push load has to be limited to a relatively low level to deter/prevent the Split set tube from buckling. In theory, the pull load capacity of a Split set is equal to the maximum push load in installation. Both field and laboratory tests show that the load capacity of a Split set is approximately 50 kN/m (Cheng & Feng, 1983; Myrvang & Hanssen, 1983; J. Player, Villaescusa, & Thompson, 2009). Therefore, Split set can accommodate large rock deformations but has a small load capacity.

Frictional bolts are anchored in the rock mass through the friction between bolt and rock, with a frictional resistance dependent upon the contact stress and the contact condition at the bolt-rock interface. The pull out the capacity of a Split set is low because of the low contact stress at the interface. The shear load capacity of a Split set is higher than its pull load capacity because of the mechanical locking of the tube.

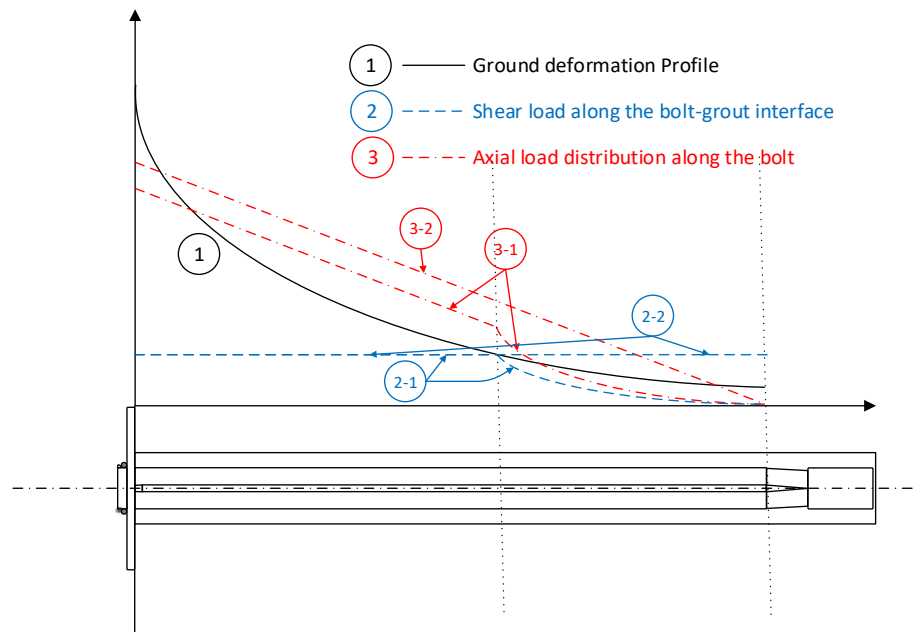


Figure 2.7. Stress distribution along a frictional rockbolt (Split set) (after Masoudi et al. (2019))

An inflatable bolt is installed by expanding the folded tube to match the size of the borehole. Its load capacity is not only related to the contact stress between the borehole wall and the bolt tube (resulting in frictional resistance) but also with the roughness of the borehole wall, which results in mechanical interlocking therefore in addition to frictional resistance, mechanical interlocking at the bolt-rock interface also contributes significantly to the pull-out capacity of this type of bolts. The pull out the capacity of an inflatable bolt is more significant than that of a Split set because of the superposition of the friction resistance and the mechanical locking at the bolt-rock interface. An inflatable bolt is maximum loaded in the bolt head when it subjected to a pressure applied to the bolt plate as illustrated in Figure 2.8. The bolt tube will slip if the bolt length is short enough and the load capacity is equal to the

unit frictional-and-interlocking force times the bolt length (C. C. Li et al. (2014)). The slippage will cause the mechanical interlocking to lessen as it can be seen in the load-displacement behaviour of rockbolts in Figure 2.8. therefore anchorage force or strength is reduced. Due to the mentioned fact, the axial load of this kind of rockbolts have a downward curvature to the bearing plate of the bolt; however, it would be maximised at that point. Slippage will not occur, and the tensile strength of the bolt tube will be mobilised if the bolt length is excessively long. In this case, the load capacity of the bolt is high, but its displacement capacity would only be limited to the stretch of the tube. In other words, inflatable bolt fails in the tube steel under shear loading, because its shear load capacity is larger than the pull-load capacity

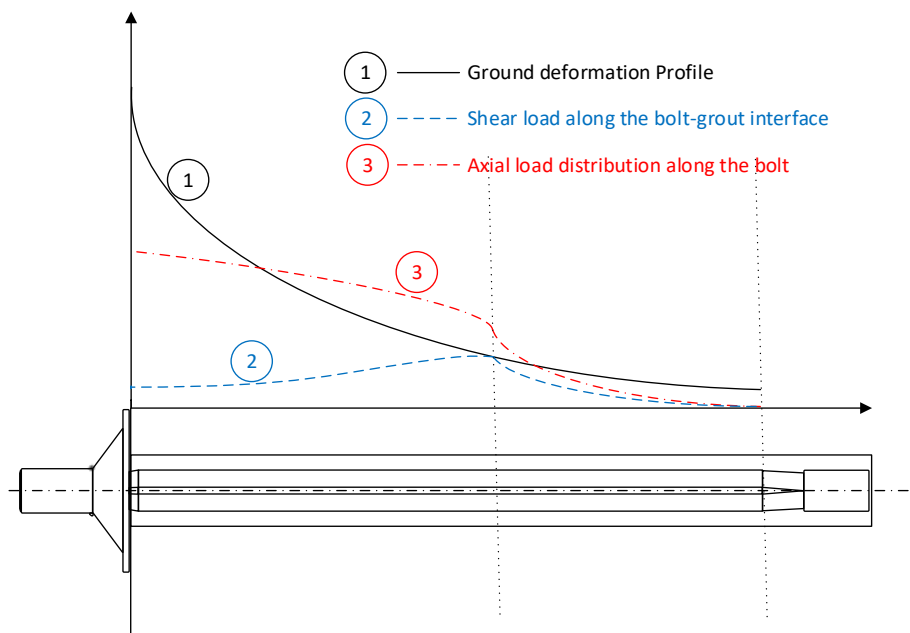


Figure 2.8. Stress distributions along the length of an inflatable frictional bolt when subjected to a pull-load at the bolt head

### 2.2.3.3. Cement/resin fully or partially encapsulated rockbolts

The length of the rebar rockbolts can be encapsulated partially or fully over their entire length. Pretension and deformation of the ground mobilise the anchorage strength, but the anchorage force and axial mobilised stress are not uniform over the encapsulated length of the rockbolt. Previous studies and experiments (Tadolini, 1990) show that when tension is applied to the head of the rockbolt, it is transferred to the initial anchorage point at the proximal end of the encapsulated length through the shank of the rockbolt. Anchorage resistance is mobilised in the first segment of

the encapsulation length and passes to the following segments by further deformation of the bolt until the anchorage strength is reached. Therefore, the maximum anchorage force (and axial induced load in the shank of the rockbolt) is on the first grouting point and decreases toward the end of the bolt (Figure 2.9).

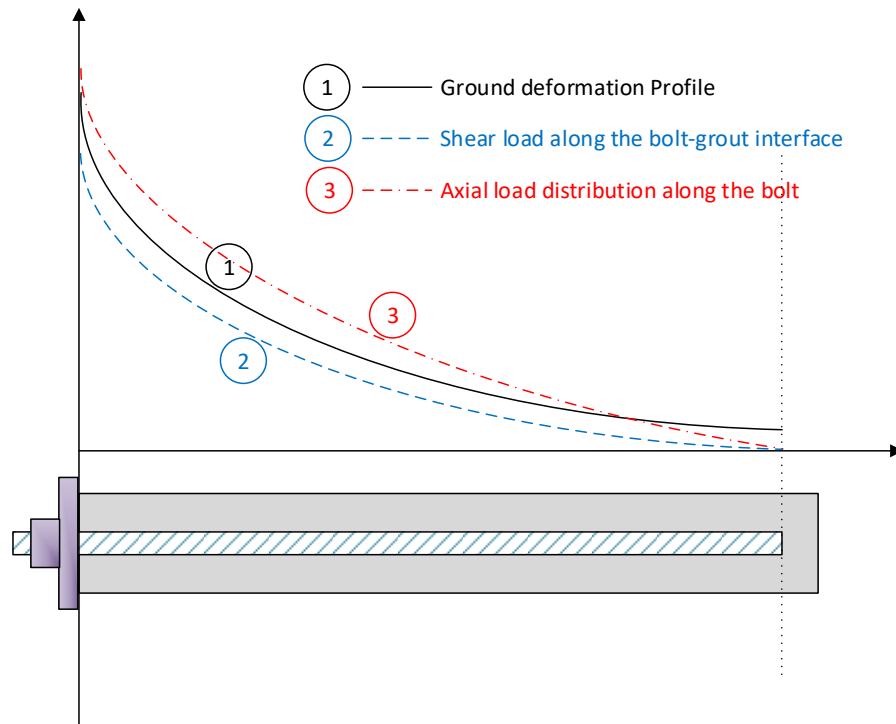


Figure 2.9. Load distribution in fully grouted bolts with bearing plate in uniform media (after Masoudi et al. (2019))

The summation of the mobilised anchorage strength over the segments (elements) of the encapsulated length of the rebar rockbolt determines the anchoring force. As mentioned before, the axial load distribution over the bond length is not uniform, and also it is governed by ground deformation to which it shows a similar pattern. Extending the ground deformation and increasing the induced load can result in stress above the strength of the rockbolt.

The presence of an active discontinuity in the surrounded ground causes a local change in loading around the discontinuity in the shank of the bolt because of the opening of the discontinuity. Due to the involvement of the bolt and surrounding encapsulation material, the displacement cannot distribute over the length of the bolt. Consequently, the axial load in the shank of the bolt rises (Figure 2.10). The load can increase at the location of the discontinuity gradually because of the progressive opening of it and lead it to local failure in the shank of the bolt, in the case of the bolt strength being exceeded.

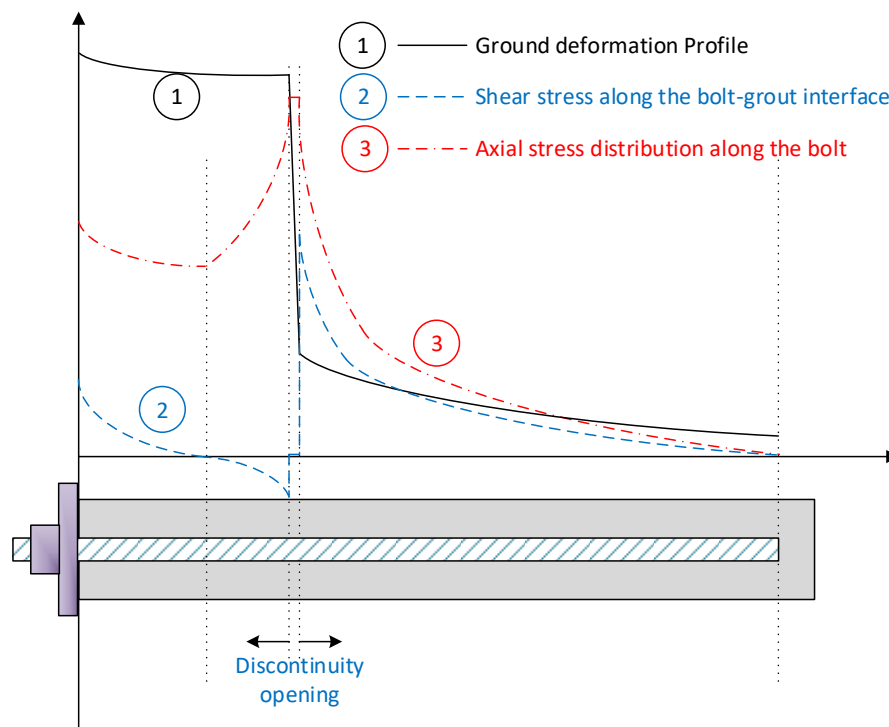


Figure 2.10. Stress distribution in fully grouted bolts with bearing plate under the effect of a discontinuity after Masoudi et al. (2019)

The partially encapsulated rebar rockbolts are those that have a bond length at the distal end of the rockbolts while the rest of the bolts are entirely decoupled from the surrounding grout or are free of the encapsulation material. The termination arrangement of this type is similar to mechanically end anchored type of rockbolts or fully grouted rebar rockbolts. This kind of rockbolt needs to have the termination elements to be able to contain the surface movement of the ground and transfer it to the shank of the bolt. The significant portion of induced deformation distributes

over the grout-free section of the bolt (decoupled length). Therefore, this kind of rockbolts can tolerate more deformation than the fully grouted type. The axial load distribution in the free length is constant as there is no shear stress at the interface to transfer the load to the bolt segments. The distribution of the load over the bond length is similar to that of the fully encapsulated rockbolts. The axial load in the bond length is the difference of applied load to the bolt and mobilised anchorage force, as shown in Figure 2.11.

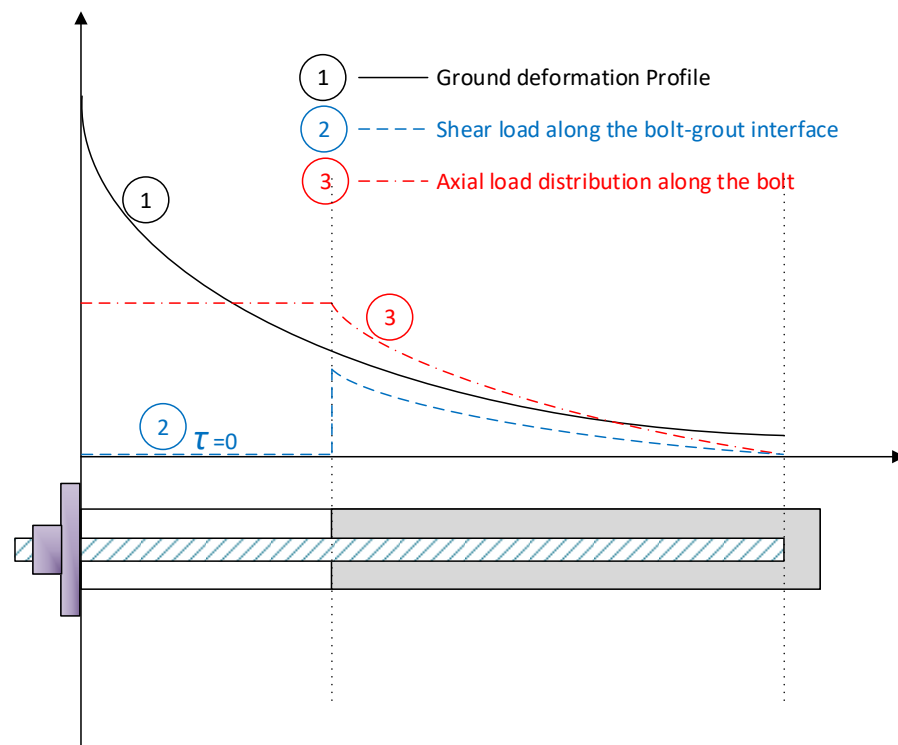


Figure 2.11. Load distribution in partially grouted bolts with bearing plate in uniform media after Masoudi et al. (2019)

It is worth mentioning that the real load/stress distribution along a partially encapsulated rockbolt has some differences over the bond length. Stress concentration at the beginning of the proximal end of the bonding length could locally overcome the strength of the anchorage resistance of the bolt-cement or cement-ground interface, and transfer the load to the following segments (Figure 2.12). As a matter of fact, if there was some friction along the shank of the rockbolt in the grout-free section, then the axial load in this part would not be horizontal and would have a small inclination toward the end of the bolt while the pattern of the

load distribution over the bond length would be the same. In this condition, the magnitude of the shear stress is the same as the friction.

Partially encapsulated resin/cement rockbolts should have enough bond length in the stable zone at depth to be able to secure the opening effectively. Due to the stress concentration on the proximal end of the encapsulated length, decoupling of the bolt-cement interface could occur so that under a load increasing condition, decoupling could develop progressively. Therefore, it has to be ensured in advance that the remaining part of the bond length is enough or has adequate strength to avoid failure.

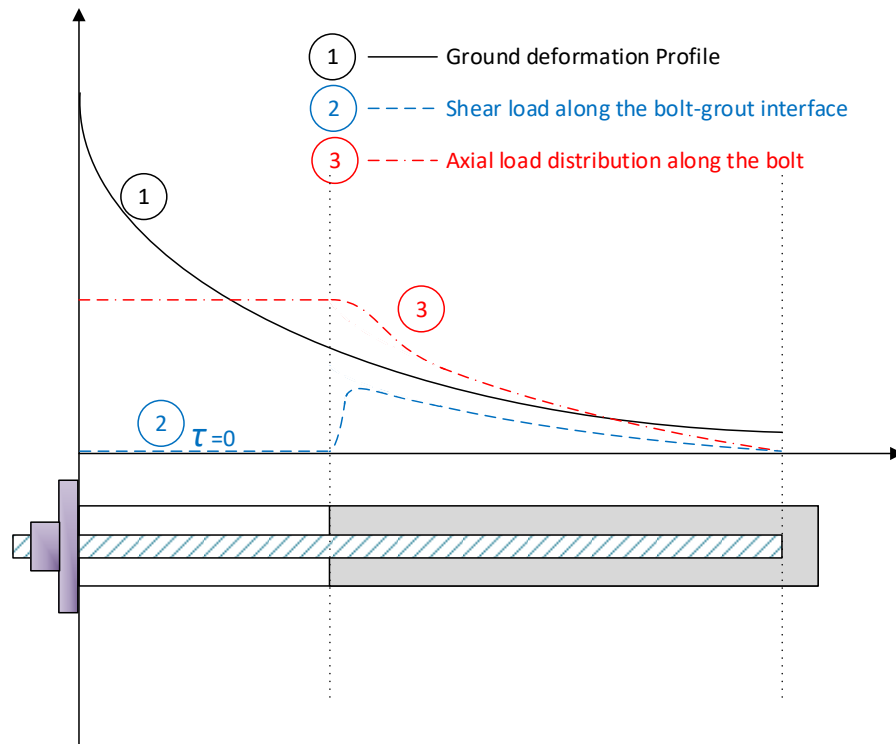


Figure 2.12. Realistic load distribution in partially encapsulated bolts with the bearing plate in uniform media after Masoudi et al. (2019)

If a ground movement such as concentrated deformation of the discontinuity opening or ejection of a mass of rock, locates in the decoupled length of the rockbolt (Figure 2.13), the imposed deformation is distributed over the whole of the free length, and just an increase in the load level occurs in the shank of the bolt. The exception is when the total deformation is large enough for the rebar to reach failure.

On the other hand, if the concentrated deformation locates in the encapsulated length of the rockbolt, the load distribution over the bond length is similar to what was explained for fully encapsulated rockbolts. It is worth mentioning that the initial pre-tension and induced tension of the ground movement are superimposed together (Zou, 2004).

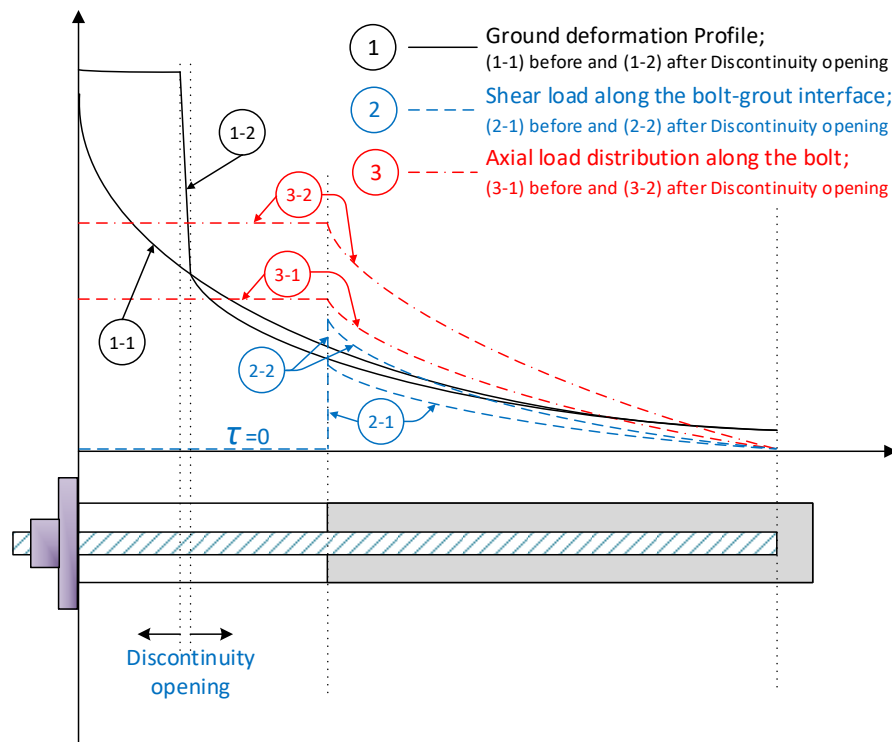


Figure 2.13. Load distribution in partially grouted bolts with an active discontinuity in free length after Masoudi et al. (2019)

For a partially encapsulated bolt, although the weakness of the two-point anchored rockbolts at the end anchoring part is removed, the other side termination arrangement (head) weaknesses, the early failure of bearing plate and nut, nut and thread stripping, or failure in the threaded part, especially in seismic conditions, still remain unsolved.

Fully encapsulated rockbolts sometimes can be utilised without a bearing faceplate; in this condition, the pattern of the load distribution will change to zero tension at the proximal end (head) of the rockbolt. Due to the lack of initial pretension, the rockbolt load is only induced by rockmass deformation. Depending on the ground movement and differential deformation, there is a separation line of



induced shear and consequently induced tension. The actual pattern of the induced tension is very complicated and challenging to determine. Stress adjustment induces more displacement near the collar in comparison to deeper parts in the borehole and this differential movement between two points induces shear stress over the bolt-grout interface then induced shear applies the axial load in the shank of the bolt. Shear stress near the head (collar) is in the opposite direction to that of the shear stress near the distal (far) end. Therefore, there is a separation line in-between which can be seen in Figure 2.14. The schematic profiles of the ground deformation, induced shear stress along with the bolt-grout (or grout-rock) interface, and the induced axial load along the shank of the bolt are illustrated in this figure. The tension in a rockbolt as well as mobilised anchorage achieves the maximum value at the separation line and go to zero at both ends. Shear force, as it has been mentioned, is zero at the separation line and they are in opposite direction on each side of it. Developing the deformation, the separation line moves normally toward the end of the borehole.

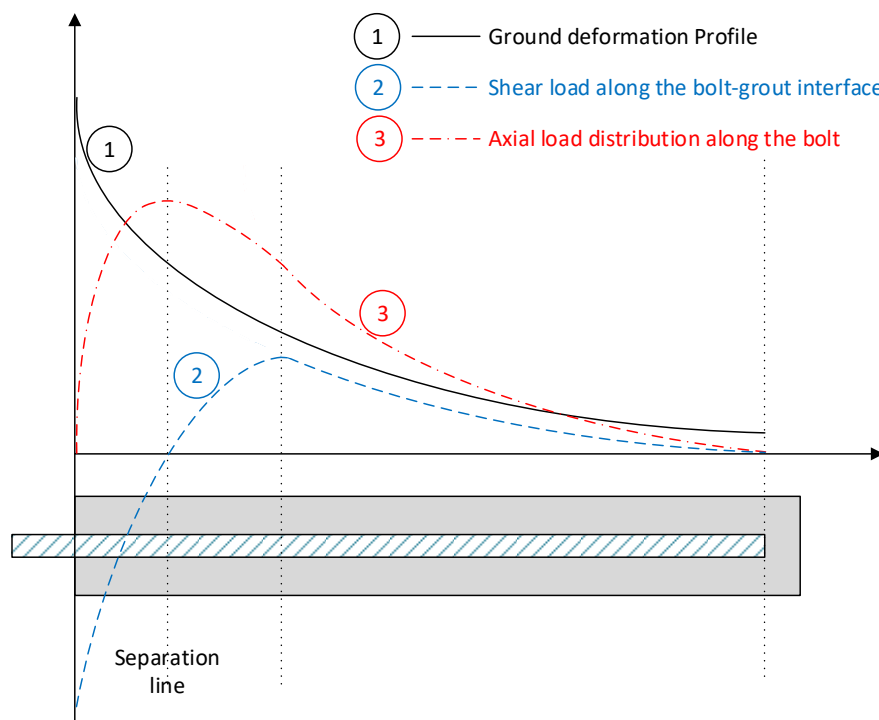


Figure 2.14. Stress distribution in fully grouted bolts without bearing plate in uniform media after Masoudi et al. (2019)

Fully-encapsulated rebar rockbolt shows the highest load-bearing capacity of the conventional rockbolts if the failure occurs in the shank of the bolt. The capacity is highest in shear and pull loading conditions, although it does not have much deformation capacity. In other words, the fully-grouted rebar rockbolts are characterised as strong but stiff rockbolts (C. C. Li et al., 2014) which may not suit in seismic prone zones.

#### *2.2.3.4. Multi-point anchored D-Bolts*

Energy-absorbing rockbolts are loaded in different ways when subjected to loading, depending on their anchoring mechanisms. The loading model for two-point anchored energy-absorbing rockbolts, such as the cone bolt, Garford bolt, Roofex and Yield-Lok is similar to that of conventional two-point anchored rockbolts, but the main difference being (is) that the energy-absorbing rockbolts yield at predefined load levels. The loading of multi-point anchored D-Bolts is different from that of other energy-absorbing rockbolts. In the case of a large deformation or opening of a rock discontinuity, load induces in the section of the D-Bolt that overrides the fracture or deformed section. The yield and ultimate loads of the bolt are equal to the corresponding strengths of the steel. The bolt absorbs deformation energy by fully mobilising the deformation capacity of the steel along the entire length of the bolt segment. The conceptual profile of the axial stress distribution along a D-Bolt is depicted in Figure 2.15

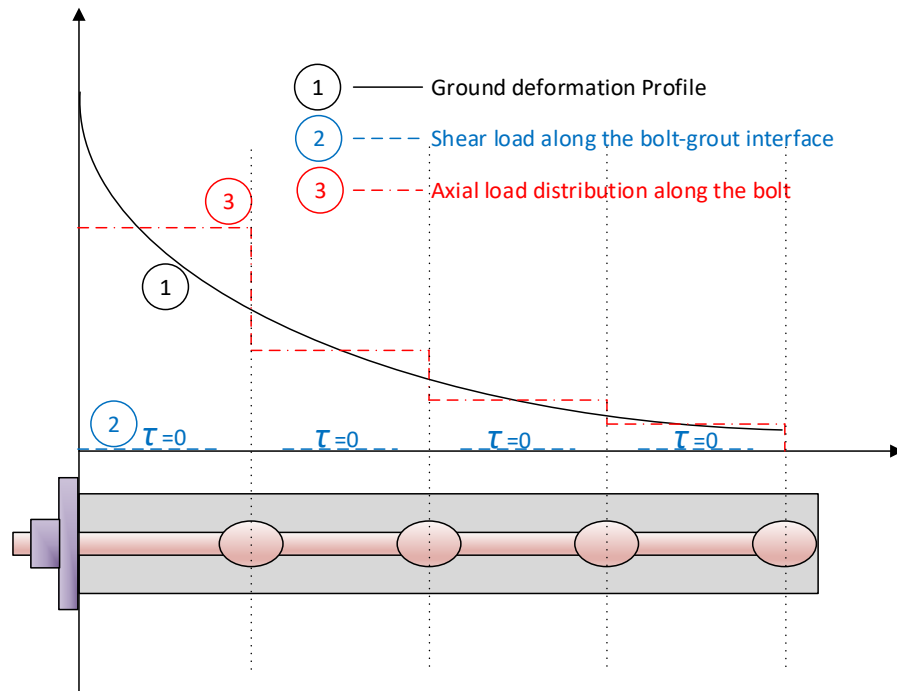


Figure 2.15. Axial stress distributions along a D-Bolt (redrawn and modified after (C. C. Li et al., 2014))

### 2.3. DECOUPLING MECHANISMS OF PARTIALLY ENCAPSULATED ROCKBOLTS

Partially encapsulated resin/cement rockbolts should have enough bond length in a stable zone in-depth to be able to effectively secure the opening. Due to stress concentration on the proximal end of bond length, decoupling of bolt-cement interface could happen. Under load increasing condition, decoupling could develop progressively; therefore, it has to be sure that the remaining part of bond length is enough or has adequate strength to avoid failure.

As it has been mentioned before, the length of reinforcements plays a crucial role in their performance. It has to be able to transfer the implied load to the stable ground in depth. Therefore the length should be adequate to contain the unstable zone's load and pass it to the far end of the bolt. Consequently, it has to have enough length in a stable zone to be able to transfer the load to the ground through its bonding or anchoring system. All types of rockbolts divide to three-part in their length including the outer/external length, the decoupled length and the encapsulated length. In following sections different part of a rockbolt are discussed with a more

focus on length, Minimum Required Encapsulation Length (MREL) and progressive decoupling of encapsulation length of a partially encapsulated rockbolt. The result of an experiment of the real behaviour of a partially encapsulated rock anchor under increasing load is presented.

### **2.3.1. OUTER LENGTH**

The outer or external length is that part of the rockbolt which stays out of the borehole. Bearing plate and underneath pad, Nut, probable centraliser and bevelling washers, probable load cell, and protection cap, place in this part of the rockbolt. This part should be long enough to contain all designed facilities with some extra length for the connecting element to extend the length of rockbolt. This extension is necessary for pretension equipment in case of applying pretension to the rockbolt and sometimes for releasing some part of the load when it is going to be overloaded. The longer outer length would be a problem due to reducing the effective span of the opening and extra cost. This length for normal rockbolts is about 30-40 cm and less than half a meter which is enough to put a bearing plate, nut, and make a concrete pad underneath of the bearing plate. For high capacity rockbolts, monobars, and multi-strand anchors this length should be designed. In this case, the bearing pad must have special requirement including, designed geometry (in order to distribute the implying load on a specific area of the ground), type (casting/pre-casted concrete, steel made pad with or without stiffener, etc.), internal reinforcement and probable spiral load distributor, trumpet and etc.

### **2.3.2. DECOUPLED LENGTH**

Free or Decoupled length is the part of rockbolt that typically begin precisely after the nut to the beginning of the encapsulated length. This length varies from a few centimetres to the whole length of the rockbolt. In case of fully encapsulated rockbolts, the decoupled length is limited to the thickness of the bearing plate and likely a few more uncoupled centimetres of the beginning of the borehole or bearing pad underneath the bearing plate. Conversely, in mechanically end anchored rockbolts, the decoupled length is almost the whole length of it apart from the outer length. An appropriate decoupled length for the reinforcement has to be designed in

different locations of a structure. Having expected total and local deformation, presence of discontinuities, general stiffness, group effect of reinforcement, etc. are factors involved with determining a specific length as decoupled length for a partially encapsulated rockbolt or a tendon.

### **2.3.3. ENCAPSULATION LENGTH**

Encapsulation length is the end part of the rockbolt in order to transfer the applied load to the ground. Applied load on the reinforcement comes from pretension or deformation of the ground due to face advance and change of geometry or from the dynamic seismic events. In all cases, encapsulated length has the role of transferring the load to the ground; therefore, it is necessary that a particular part of it lays in the stable ground. In case of partially encapsulated reinforcement, encapsulation length in the stable ground should be long enough to carry the total applied load and to be able to transfer it to the ground. If the bond length was not long enough, it could not tolerate the load, and probably the interface of the grout/resin-bolt or less likely the interface of the grout/resin-rock would be decoupled. The encapsulation length of rockbolt in the stable ground should be more than the Minimum Required Encapsulation Length (MREL). The Minimum Required Encapsulation Length (MREL) is the maximum length of embedment that failure can happen in the interface, and more embedment length causes the failure in the shank of the rockbolt in case of overloading (Charlie C Li, Kristjansson, & Høyen, 2016). If the encapsulation length were not enough (less than MREL), then the load-displacement behaviour of rockbolt would govern by the behaviour of cement grout. Therefore, in this case, if rockbolt fails, the failure diagram would be similar to the failure in the grout (grout failure behaviour). Otherwise, it governs by the behaviour of the material of the bolt (steel failure behaviour) itself and shows the adequacy of the bond length. Figure 2.16 compares these two behaviours and failure mode.

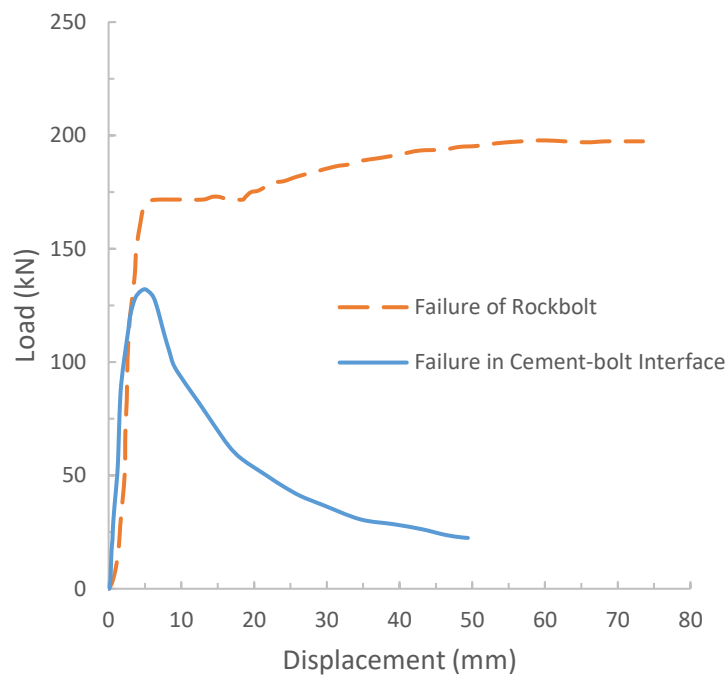


Figure 2.16. Load-Displacement behaviour of a rockbolt under overloading condition (after Masoudi et al. (2019))

The practical Minimum Required Encapsulation Length (MREL) have been defined and presented in subchapter 2.3.3 and design of it presented in 3.3.1 based on this research. Having such a practical encapsulation length results in avoiding any failure in the interface of the bolt-grout. In other words, however, the bounding length between rebar and rock will reduce, the ultimate strength of the shank of the rebar is lower than the total resistance of the interface of the bolt ground so that in the case of any overloading the failure happens in the shank of the bolt. Therefore it would not be a weak point in the design as long as the bounding length consider more than MREL. It is worth mentioning that the test plan can be conducted on-site for more reliable design, or in laboratory considering an appropriate factor of safety.

#### 2.4. MINIMUM REQUIRED ENCAPSULATION LENGTH OF CEMENTED ROCKBOLTS

The length of the encapsulation in rockbolt reinforcements plays a crucial role in bolt performance. The reinforcements have to be able to transfer the applied load to

the ground. The Bond length is the end part of the rockbolt, which has the function of transferring the applied load to the stable ground at depth. Loads increase after installation of a reinforcement element in parallel with the progress of the structure. Advances in faces or benches, change in geometry, time-dependent behaviour of the surrounding ground, the setting time or other property of the grout material if applicable, pretension or applying an external load, dynamic seismic events, failure of other elements, changes in underground water level, etc. are the main factors for increasing the load on the reinforcement element. In all cases, encapsulation length has the role of transferring the load to the ground, so it is necessary that a particular part of it lies in the stable ground. Therefore, the length should be adequate to sustain the load of the unstable ground and pass it to the far end of the bolt where its coupling or anchoring system is located.

In the case of partially encapsulated reinforcement, encapsulation length in the stable ground should be enough to carry the total applied load and to be able to transfer it to the ground. If the bond length was not long enough, it could not tolerate the load, and then the interface of the bolt - grout or the grout-rock would probably be decoupled. The encapsulation length of rockbolt in the stable ground should be more than the Minimum Required Encapsulation Length (MREL). The Minimum Required Encapsulation Length (MREL) is the maximum length of embedment for which the failure of the rockbolt will happen at the interface; greater embedment length causes the failure to occur in the shank (in the case of overloading). In other words, if the embedment length is less than the MREL, failure of the rockbolt will occur at the interface in the case of overloading. This indicates non-employment of the ultimate strength capacity of the rockbolt. If the embedment length is higher than the MREL, the failure will occur in the shank of the rockbolt (Charlie C Li et al., 2016). If the encapsulated length is less than MREL, then the load-displacement behaviour of the rockbolt failure would be similar to that of the cement grout. Otherwise, it is governed by the behaviour of the material of the bolt (steel) itself and shows the adequacy of the bond length.

Experiments on 20 mm diameter rebars show that the minimum required cement encapsulated length of between 25 cm to 36 cm for water to cement ratios of 0.40

to 0.50 (UCS of 37 to 28 MPa) would be enough as MREL in laboratory condition (Charlie C Li et al., 2016).

## **2.5. DEEP UNDERGROUND HIGH-STRESS MINING**

Seismically active underground mines are those that are prone to dynamic rockmass failure. As mining progresses, the natural stress equilibrium of the rockmass disturbed and re-distributes so that the stresses concentrate around the edges of an excavation or in pillars of rock between excavations left unmined for support, due to low grade or other reasons. These stress changes, cause the accumulation of potential energy in the unmined rock. This energy may be gradually dissipated, or it may be released suddenly during the process of inelastic deformation and radiates detectable seismic waves.

Stress may also be increased or relaxed on pre-existing planes of weakness such as faults, shears or lithological contacts. Accumulation of the energy over these weaknesses could conclude to a slip or further breakage of the mass of rock that could be another source of a seismic event.

A combination of both above-mentioned mechanisms are sometimes happened in practice and need to be predicted and controlled. As it has been mentioned before, the prediction of the seismic events with its exact location is not possible due to the nature of such events and randomness of them. However, there are some indexes to estimate the probability of a dynamic event, helping to consider appropriate countermeasure for them and maintaining a safe workplace. In the following subchapters, the mechanisms surrounding a tunnel opening are discussed.

### **2.5.1. GROUND BEHAVIOUR IN SEISMIC CONDITIONS**

Rockmass varies from massive, layered and jointed to heavily crushed conditions. Besides, dynamic loading has a broad range of frequency, amplitude, and wavelength. Therefore, ground behaviour varies widely considering the rockmass and dynamic loading conditions as well. The most common types of strain burst and seismic failure mechanisms in different ground types surrounding a tunnel opening



are categorised into four primary rockburst types based on various factors, as shown in Figure 2.17.

Figure 2.17-a shows the mechanism of strain burst during ejection of a volume of rock due to stress concentrations or induced stresses. In this condition, discontinuities have a minor effect on ejection, so it is difficult to predict the volume of rock to be ejected and even sometimes the likelihood of an ejection.

Figure 2.17-b shows the ejection of a volume of rock by the mechanism of sudden buckling or spalling of rock in the wall or even in the face due to induced or concentrated stress on the boundaries of the opening where foliation of the rockmass is nearby vertical. This mechanism applies to strong to extremely strong rocks.

Figure 2.17-c shows the ejection of a volume of rock in the wall due to a seismic event near the boundaries of a stope or a tunnel which is due to slip or energy transfer on an adjacent discontinuity. First or secondary discontinuities can bound the volume of ejection so it can be estimated if the location of such an event is known.

Figure 2.17-d depicts the mechanism of instability in the back due to a combination of the effect of loosening of discontinuous blocks, gravity, and/or a seismic event. Loosening of the blocks in the back could be a result of the lack of enough confining stress or previous blasting. The seismic event can accelerate the phenomenon under the effect of available gravity.

Therefore, considering the wide range of rockmass and dynamic load conditions, various types of failures such as spalling, rock ejection and block fall can be expected.

### **2.5.2. GROUND SEISMIC ENERGY DEMAND**

When a dynamic load propagates in the excavation, rock deformation occurs and cause an energy release. Estimating the magnitude of the released energy is important to design a suitable reinforcement system. Although several methods have been developed to estimate the ground energy demand, they can be categorised into three groups namely, Intact rock property approach (IRPA), Estimation of failure volume and ejection velocity, Rockburst damage potential. A brief illustration of each

method is given in the following subsections as well as a qualitative description of the ground demand.

#### *2.5.2.1. Intact Rock Property Approach (IRPA)*

When a significant amount of energy stored in the rockmass suddenly releases, it causes a rockburst. In other words, when the volume of energy which should be tolerated within the rockmass exceeds its capacity (Strength), sudden failure happens, and energy is quickly released. Although all factors like discontinuities and their infilling material properties and the presence of underground water and its effects are important, intact rock properties have significant roles in this phenomenon. As a matter of fact, the intact rock energy absorption capacity could determine the upper limit of energy absorption capacity or in other words, the

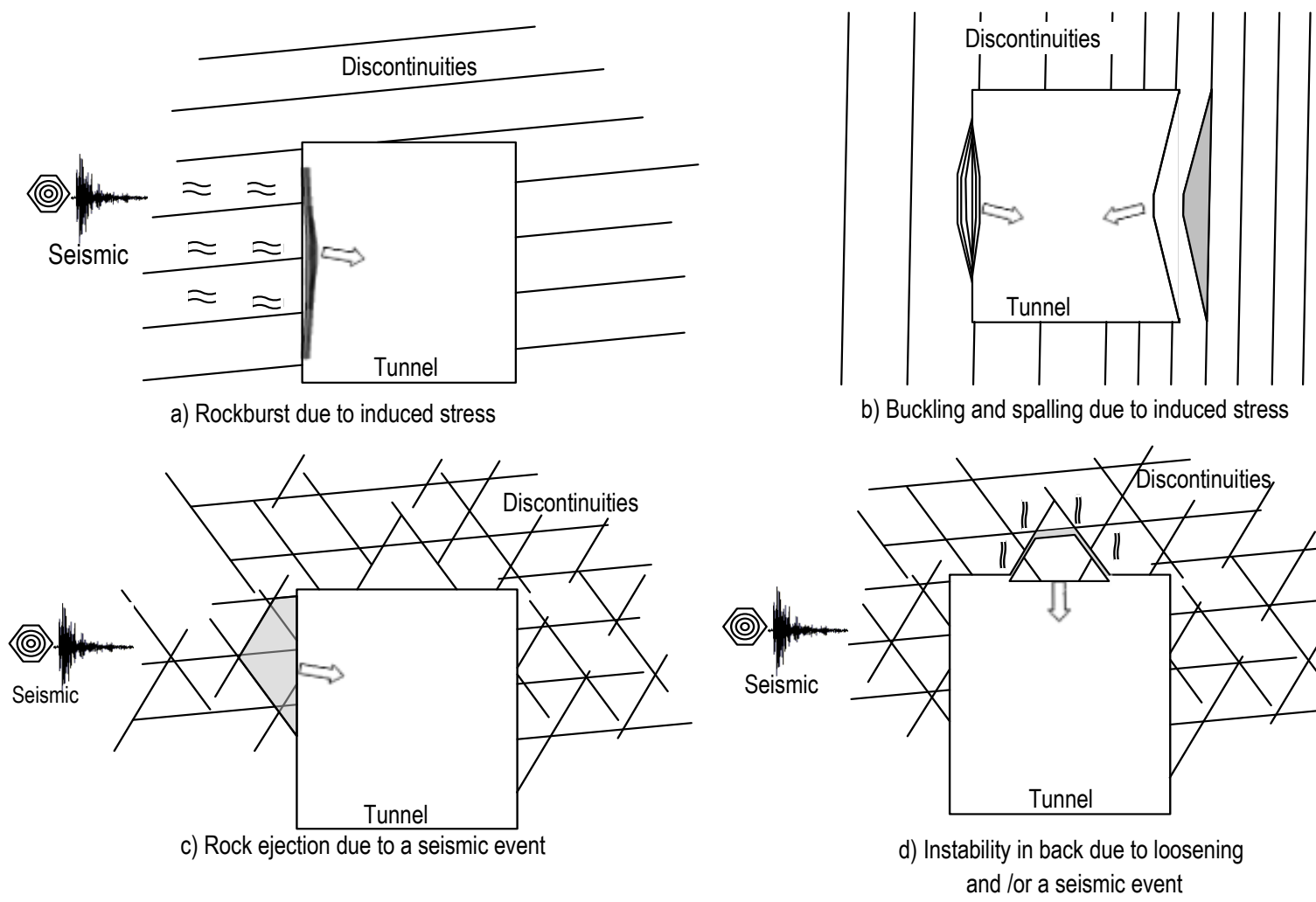


Figure 2.17. Failure mechanisms for underground deep and high-stress excavations due to induced stress and seismic events

potential releasable energy of the rockmass. Some criteria have been defined to estimate the potential of rockburst based on intact rock properties including Index of strain energy, Potential energy of elastic strain (Kwaśniewski, Szutkowski, & Wang, 1994; Kwaśniewski & Wang, 1999), Rock brittleness (Qiao & Tian, 1998), and Ratio of tangential stress to compressive strength (Y. H. Wang, Li, & Li, 1998).

An excess of energy during the post-peak deformation stage concludes in violent rock fracturing (Linkov, 1996). Energy release rate (ERR) has been developed as a basis for mining exploitation pattern design. Rock subjected to the compression process experiences elastic and plastic deformation. Elastic deformation (strain) of the rock can be recovered if unloading occurs before peak strength. At brittle failure, the elastic strain releases suddenly and causes a rockburst. Therefore, by applying a cyclic compressive strength test, the energy storage capacity of rock can be estimated. As it is shown in Figure 2.18-a,  $\Phi_{ds}$  is the portion of energy which is dissipated due to initiation and propagation of micro-cracks in the rock sample, or so-called plastic deformation.  $\Phi_{el}$  is the portion of energy which is consumed for elastic deformation and stored in the rock. This portion of the energy stored during the loading process up to point A could be released gradually by unloading or suddenly by failure. The ratio between elastic strain energy and dissipated energy (index of strain energy) could be used as a criterion or an indicator of rockburst potential.

$$F = \Phi_{el}/\Phi_{ds} \quad (2-3)$$

Investigations demonstrate that the potential energy of elastic strain (PES), in other words, the elastic strain energy which is stored in a unit volume of rockmass, is another criterion that could scale the shock and rockburst occurrence (Kwaśniewski et al., 1994). As it is depicted in Figure 2.18-b, the maximum elastic strain energy which could be stored in a sample of rock before the peak strength is given by:

$$PES = \Phi_{elm} = \sigma_c^2/2E_s \quad (2-4)$$

Where  $\sigma_c$  is the uniaxial compressive strength (MPa), and  $E_s$  is the unloading tangential modulus (MPa).

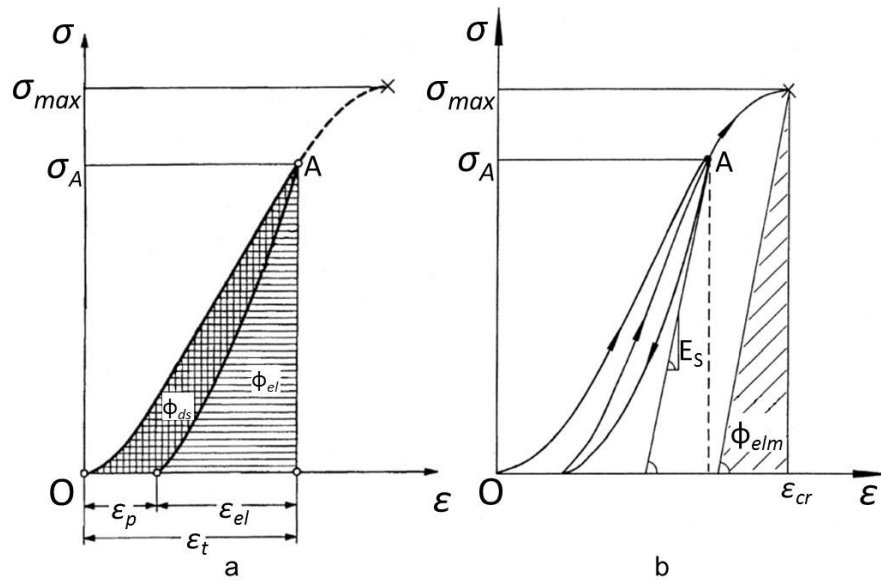


Figure 2.18. a) Analytic calculation of energy in the rock sample cyclic loading of (after Kwaśniewski et al. (1994) and b) Calculation of potential elastic strain energy (J. A. Wang & Park, 2001)

The third criterion is the index of Rock brittleness which is defined as follows:

$$B = \sigma_c / \sigma_T \quad (2-5)$$

In which  $\sigma_c$  is the uniaxial compressive strength (MPa), and  $\sigma_T$  is the tensile strength of the rock (MPa). Based on this criterion, the lesser index indicates the probability of the more violent rockburst.

The fourth criterion considers both the state of in-situ stress in the rockmass and the mechanical property of rock is expressed by:

$$T_s = \sigma_\theta / \sigma_c \quad (2-6)$$

In equation (2-6),  $\sigma_\theta$  is the tangential stress in the rockmass surrounding the openings or stopes (MPa), and  $\sigma_c$  is the uniaxial compressive strength of rock (MPa). A larger  $T_s$  indicates a more violent probable rockburst (Qiao & Tian, 1998).

A summary of these criteria is shown in Table 2.1.

Table 2.1. Rockburst potential based on intact rock property

Description	Index	Potential of Rockburst				
		Low	Strong			Violent
1 Index of strain energy* (Kwa'sniewski et al., 1994)	$F = \Phi_{el} / \Phi_{ds}$		2		5	
2 Potential energy of elastic strain (kJ/m <sup>3</sup> ) (Kwa'sniewski et al.)	$PES = \sigma^2_c / 2E_s$	50	100	150	200	250
3 Rock brittleness (Qiao & Tian, 1998)	$B = \sigma_c / \sigma_T$	40		26.7		14.5
4 Ratio of tangential to compressive strength (Y. H. Wang et al., 1998)	$T_s = \sigma_\theta / \sigma_c$	0.3		0.5		0.7

\* Based on tests on coal specimens to provide the intensity of shocks or coal bombs

Four indexes are available in this table indicating whether a rockburst event will be low, strong or violent based on estimated or calculated amount of each index. The indexes on the left side of the range indicate low potential, and on the right side of the range indicate the strong or violent potential of rockburst. It is worth mentioning that the table combined with the stress or loading system measurement can lead the designer to an appropriate engineering judgement and design.

#### 2.5.2.2. Estimation of Failure Volume and Ejection Velocity

Estimation of failure thickness and ejection velocity will allow the estimation of ground demand by calculating the potential energy release (stored energy in flying rock) by the prospective volume of ejected rock and the estimated velocity of ejection.

The energy demand on ground support due to a block ejected from the backs, wall or floor could be calculated by the following equation (Kaiser et al., 1996):

$$\text{Energy Demand} = \frac{1}{2} mV_e^2 + qmgd \quad (2-7)$$

Where in this equation:

- $m$  = the mass of the ejected block (kg);
- $V_e$  = the ejection velocity of the block (m/s);
- $g$  = acceleration due to gravity (m/s<sup>2</sup>);

- $d$  = distance the ejected block has travelled (m); and
- $q = 1, 0$  or  $-1$  for ejection from the backs, wall or floor respectively.

The second term in equation 2-7 contributing to the energy demand ( $qmgd$ ) represents the influence of the gravity that adds potential energy to rocks ejected from the backs and reduces the energy of a block ejected from the floor, while not contributing to ejection from the wall (Kaiser et al., 1996).

Considering the energy demand per square meter of excavation surface and substituting  $tp$  for  $m$ , the equation becomes (Kaiser et al., 1996):

$$\text{Energy Demand per } m^2 = \frac{1}{2}tpV_e^2 + qt\rho gd \quad (2-8)$$

In which:

- $t$  = thickness of failed rock at the excavation surface (m); and
- $\rho$  = rock density ( $\text{kg}/\text{m}^3$ ).

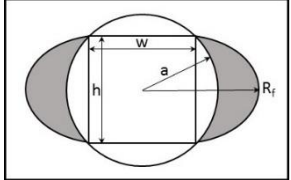
Therefore, the critical factors required for energy demand are:

- Peak particle velocity, which is assumed to equal the velocity of ejection ( $V_e$ );
- Excavation closure or ejection distance ( $d$ ), which can be estimated based on the displacement capacity of ground support elements in the backs; and
- The mass of ejected material, which is a function of the failure thickness ( $t$ ) and the rock density ( $\rho$ ).

The excavation closure (or ejection distance) “ $d$ ” is used in the gravity component of the energy demand equation and is only applicable when the design is being undertaken for the backs. It represents the work done by the support system to halt the downward movement of the rockmass. An approach is to use the displacement capacity of the ground support elements in the backs as a guide. In practice, the displacement capacities of the support element that fails first in a rockburst can be used for “ $d$ ”. The results of drop weight dynamic testing of support elements can be used to assist in determining appropriate “ $d$ ” values.

The fracturing due to induced stress, blast damage, geological structure or a combination of all these three factors can form the failure volume or mass of ejected rock which loads the support system.

Table 2.2. Failure thickness estimation (after Daniel P. Heal (2010))

Failure volume or thickness (t) can be estimated as the maximum of:	
1	The potential volume of instability or probable active discontinuities can be observed at intersections around the site of interest.
2	<p>The volume surrounding the excavation, based on a calibrated numerical model, where the strength factor (SF) is less than 1:</p> $SF = \frac{(UCS+q\sigma_3)}{\sigma_1} \quad (\text{Wiles, 2006}) \quad (2-9)$ <p>Where <math>q = \tan^2(45 + \phi/2)</math></p>
3	<p>Using the following empirical relationship to find the distance (<math>R_f</math>- a) (Haile, Grave, Sevume, &amp; Le Bron, 1998):</p> $a = \frac{h \text{ (or } w)}{\sqrt{2}} \quad (2-10)$ $\frac{R_f}{a} = 1.34 \frac{\sigma_{max}}{\sigma_c} + 0.43 \quad (2-11)$ <p>In which:</p> $\sigma_{max} = 3\sigma_1 - \sigma_3$ <p><math>\sigma_c</math> is the unconfined compressive strength of the host rock; and the other terms in the equation are represented in the diagram.</p> 
4	0.1 m for conventional blasting.
5	0.05 m for controlled blasting.
6	The volume of potential ejected mass based on pre-existing structural weaknesses in the rockmass up to h/2.

Failure volume can be estimated by various methods in an excavation. A borehole camera survey can help to find the potential discontinuities for ejection and hence the probable volume of rock. Numerical modelling also can be used for the estimation of the failure mass by measuring the overstressed zone surrounding an excavation, in other words, the zone around an excavation in which the stress exceeds the rock strength. Empirical estimation methods are also available. Table 2.2 summarises the methods for estimating the failure volume for use in design calculations. Based on



this table, the thickness should be calculated via as many possibilities as the previous six mentioned methods in the table, and the maximum thickness should be used in the calculation.

### 2.5.2.3. Rockburst Damage Potential

Daniel P. Heal (2010) has established a method to develop a tool for assessing the likelihood of rockburst damage occurring at particular excavations in seismically active underground mines. In this approach, five factors are combined into a single index for determining the potential for rockburst damage at a given location in an underground mine.

Excavation Vulnerability Potential (EVP) is proposed as an index to empirically quantify the effect of local site conditions on rockburst damage. It makes use of four of the five mentioned factors, those not related to the source of the seismic event:

- E1: The stress conditions ( $\sigma_{1T}$  / UCS);
- E2: The energy capacity of the installed ground support system (in kJ/m<sup>2</sup>);
- E3: The excavation span (in m); and
- E4: The presence or otherwise of seismically active major geological structure.

The empirical EVP index proposed makes use of these two components:

$$EVP = (\text{Damage Initiation Factor}) \times (\text{Depth of Failure Factor}) = (E1/E2) \times (E3/E4) \quad (2-12)$$

In order to consider the distance and magnitude of the seismic event involved in each case history, the EVP data was compared to the fifth factor, Peak Particle Velocity (PPV) to create a single index called Rockburst Damage Potential (RDP), as shown here:

$$\text{Rockburst Damage Potential (RDP)} = EVP \times PPV \quad (2-13)$$

The respective distributions of these factors show that, in general, an increasing level of rockburst damage is associated with:

- Increasing stress conditions (E1);

- Decreasing ground support system capacity (E2);
- Increasing excavation span (E3);
- Decreasing geology factor (E4); and
- Increasing peak particle velocity (PPV).

The above-explained procedure can be used to predict the level of rockburst potential. This method is almost the newest method which needs more experiments and practical feedback to prove or modify.

In most cases, it is difficult to carry out a specific design because the rockmass factors that define demand cannot be dependably evaluated. Therefore, the rockmass demand can be described qualitatively. As explained in Table 2.3, qualitative demand categories of rockmass could be defined in terms of Low, Medium, High, Very High, and Extremely high energy demand per square meter as well as the surface displacement and reaction pressure. Similarly, such a rating can classify the reinforcement system in order to satisfy the rock demand (Thompson et al., 2012).

Table 2.3. Typical Rockmass Demand for Ground Support Design (Thompson et al., 2012)

Demand Category	Reaction Pressure (kPa)	Surface Displacement (mm)	Energy (kJ/m <sup>2</sup> )
Low	<100	<50	<5
Medium	100–150	50–100	5–15
High	150–200	100–200	15–25
Very high	200–400	200–300	25–35
Extremely high	>400	>300	>35

## 2.6. DYNAMIC CAPACITY OF ROCKBOLTS

The reinforcement and support system is a critical measure to prepare a safe workplace as well as increasing the longevity of a stable opening. An effective support

system influences the safety of workforces and equipment along with the economical mine extraction. Different sorts of reinforcement and support systems required for a particular application rely on a few elements including, the geometry of the excavation, the strength of the rockmass, stresses present in the rock, corrosion and weathering processes, and blasting practices.

The primary method in order to lighten the impacts of mine seismicity is the design of practical geometry and appropriate mining sequence. A rock support plan would be a complementary step intending to mitigate the rockburst impact. The method based on the available stress in the ground around the opening and strength of the rockmass as the conventional method is suitable just for the static loading condition. However, such a method is not appropriate for dynamic loading conditions in a seismic or rockburst prone area anymore. A ground demand-energy dissipation capacity approach (GDEDCA) is a vital step in such circumstances. Therefore, acquiring the knowledge of energy dissipation capabilities of elements of a support system including the reinforcement, surface support, connecting elements and faceplates is necessary as well as a whole support system as an integrated system.

Implementation of a dynamic resistance support system is the most common method of stabilising an underground opening in mines. Rockbolts along with surface support comprised of mesh and shotcrete, play a crucial role as one of the main elements of a support scheme. A mine which experiences seismic activities like a rockburst needs to be supported by appropriate elements, capable of tolerating dynamic loading. This area in geotechnical engineering is still under development. In other words, the dynamic capacity or energy dissipation capacity of the rock support is under investigation by researchers (Potvin, Wesseloo, & Heal, 2010). The primary challenge in measuring the dynamic capacity of the ground support including the rockbolt is to prepare repeatable loading conditions similar to what is experienced at a supported face during a seismic event. Providing a sound monitoring system and qualified data acquisition apparatus along with well-controlled equipment are requirements of a dynamic testing facility in order to acquire reliable data and meaningful analysis.

“Drop testing” has been under the attention of a group of researchers to convey kinematic energy to ground support elements in order to measure energy dissipation capacity (Gaudreau, Aubertin, & Simon, 2004; Kaiser et al., 1996; W. Ortlepp & Stacey, 1998; W. Ortlepp & Swart, 2002; W.D. Ortlepp, 1997; W. D. Ortlepp, Stacey, & Kirsten, 1999; Plouffe et al., 2008; T. R. Stacey & Ortlepp, 1999; Yi & Kaiser, 1994) while the momentum transfer process to decelerate a sample which is supported and attached to a mass has been utilised by some other researchers (J. R. Player et al., 2004). Employing a simulated controlled blasting process as the dynamic load applied on a completely supported area along with a well-instrumented system is another category of measurement of the dynamic performance of a support system as an integrated system (D.P. Heal & Potvin, 2007; Tannant, Brummer, & Yi, 1995). Besides, back-calculation of support capacity has also been performed by Daniel P. Heal (2010) which can be assumed as the fourth method to estimate the dynamic support capacity.

The bearing plate and nut or terminating element plays a vital role to transfer the load which is contained by the surface support to the rockbolt and eventually to the ground. Therefore, the load which is produced by a seismic event could not be transmitted to the rockbolt or the ground if either the surface support, bearing plate or terminating element failed (Potvin et al., 2010).

As mentioned above, there are four methodologies for investigating the dynamic capacity of ground support elements. The ‘drop test’, ‘blast simulation’, the ‘momentum transfer concept’, and ‘back analyses’. These methodologies are discussed in the following sections.

### **2.6.1. DROP TEST**

The drop test rig is a controlled laboratory facility to investigate the dynamic behaviour of ground support elements submitted to a seismic event simulated by sudden loading of a dropping mass from a predetermined height (Yi and Kaiser, 1994, Kaiser et al., 1996, Ortlepp, 1997, Ortlepp and Stacey, 1998, Ortlepp et al., 1999, Stacey and Ortlepp, 1999, Ortlepp and Swart, 2002, Gaudreau et al., 2004, Plouffe et al., 2008, Li, 2010, Li et al., 2014a). This test has experienced numerous amendments

and has turned into a standard testing technique for laboratory assurance of rockbolt energy absorption or dissipation capacity. There are also various difficulties required with this test including slow instrumentation reaction, uncontrolled vibrations in the loading system, and other sources of unmeasured energy losses (Soleimani and Banthia, 2014). The advantage of this test facility is its repeatability and cost-effectiveness as soon as it is assembled. A number of drop testing equipment has been constructed during the last twenty years in Canada, South Africa and recently in Australia to be able to perform dynamic performance assessment of ground support elements. Although a standard method of testing has been available, these rigs have been constructed with considerable dissimilarities which make the examination of their outcomes to some degree complicated or not comparable (Potvin et al., 2010).

A rockbolt or cable bolt, cement or resin encapsulated in the thick-wall steel pipe to replicate the rock mass, is frequently used in the drop testing experiments. Despite the fact that a specific thickness and measurement of steel tube were given to provide similar confinement of the in-situ rockmass with the same magnitude, the steel pipe cannot completely replicate the rock mass which may introduce an error of some degree into the estimation (Li et al., 2014b).

In spite of the fact that there have been critical enhancements made to the drop testing mechanical assembly, it is still not illustrative of in-situ conditions. The drop test technique has numerous presumptions that would influence the performance of the support elements contrasted with their genuine performance in the field. Moreover, the drop tests deliver results of individual support elements that need to be compiled and consolidated to design the support system. It is helpful to take the outcomes from the different reinforcement elements and the surface support and assemble them together. However, providing a cost-effective, controlled and repeatable procedure for estimating the support elements' properties in a laboratory is its outstanding advantage.

### **2.6.2. BLAST SIMULATION**

Blast simulation experiments have been performed in-situ trying to recreate the seismic event that happens in a blasting to measure the consequences on most common ground support systems (Archibald et al., 2003, Espley et al., 2002, Hagan et al., 2001, Heal and Potvin, 2007, Hildyard and Milev, 2001b, Hildyard and Milev, 2001a, Reddy and Spottiswoode, 2001). In-situ simulated blasting testing to investigate the rock support behaviour and performance was innovated by Ortlepp (1969). In comparison to drop testing, the simulation of rockbursts by blasting has a large level of difficulty. Performing such a destructive test in the active mines during operation of other activities needs sophisticated coordination with operative units while the logistic of setting up and carrying out the tests is not straightforward, and the cost is also high. The positive points of the method are the testing of the support system as an integrated system which is completely installed in place as opposed to individual support elements. Issues, for example, installation procedures and the interaction with the rockmass were also investigated, and shortcomings of the whole system were underscored (Potvin et al., 2010).

It is worth mentioning that the movement of the ground in blasting is not similar to that of a rockburst because of seismic events. The gas pressure is not available in the rockburst condition while in blasting it is accompanied by the shock wave, as sometimes the generated gases quickly expand and may conclude to unpredictable results at the test location. On the other hand, the wave characteristics, including wavelength, amplitude and frequency created by blasting are different from those produced by large seismic events. Normally, the wavelengths in the seismic events are longer and frequencies are lower in comparison to those in blasting.

Obviously, to investigate and understand the behaviour of rock mass and ground support elements, a reproducible or repeatable simulated dynamic event would be a great success. Many researchers have tried to employ the blasting method for simulation of a rockburst, but there are few or small numbers of successful experiments. Distortion by gases and not enough generated energy to produce premeditated destruction have been the main reasons for ineffective experiments.

Nevertheless, the behaviour of the whole support system as an integrated system can be investigated with this method.

### **2.6.3. MOMENTUM TRANSFER METHOD**

The momentum transfer concept has been employed by the Western Australian School of Mines (WASM) via building a dynamic loading system in order to find out the energy dissipation capability of the ground support elements or system. This equipment utilises a mass to apply a dynamic impact to the sample by dropping it from a certain height and measurement of deceleration after impact. The testing facility is capable of testing different types of rockbolts, cable bolts, or reinforcement systems, prepared sample of surface support or a mixture of both to be able to assess the mechanism of dissipation of the energy by a ground support system and interaction of the surface support and reinforcement and transferring the dynamic load (J. R. Player et al., 2004).

The concept of this facility is illustrated in Figure 2.19. Using a dropped mass of 2000 kg as the simulated ejected rock with an impact velocity of 6 m/s is a standard arrangement for testing of rock reinforcement. This arrangement provides a kinetic energy of 36 kJ applied to the test sample and must be dissipated by the support element. The buffers have to absorb the energy of the beam as well as a portion of the energy of the dropping mass. The excess of energy is applied to the test sample following the impact because of the changing in potential energy of the dropping mass. An artificially radial cut in steel pipe simulates the discontinuity in rock mass typically situated 1.0 m from the beneath of the bearing plate. (J. Player, Thompson, & Villaescusa, 2008).

Characteristically, the investigation of a sample of reinforcement or support system has to be based on first impact loading that can be a single large dynamic impact. Therefore the testing equipment has to have sufficient energy or enough capacity to be able to exceed the strength of the sample not depend on more than one impacts. Base on previous experiments it has been proved that the multiple loading misleads the results to a greater measured capacity in comparison to the

results of a single large impact. The WASM testing equipment is capable to apply 120kJ of kinetic energy to the sample (J. Player, Thompson, et al., 2008).

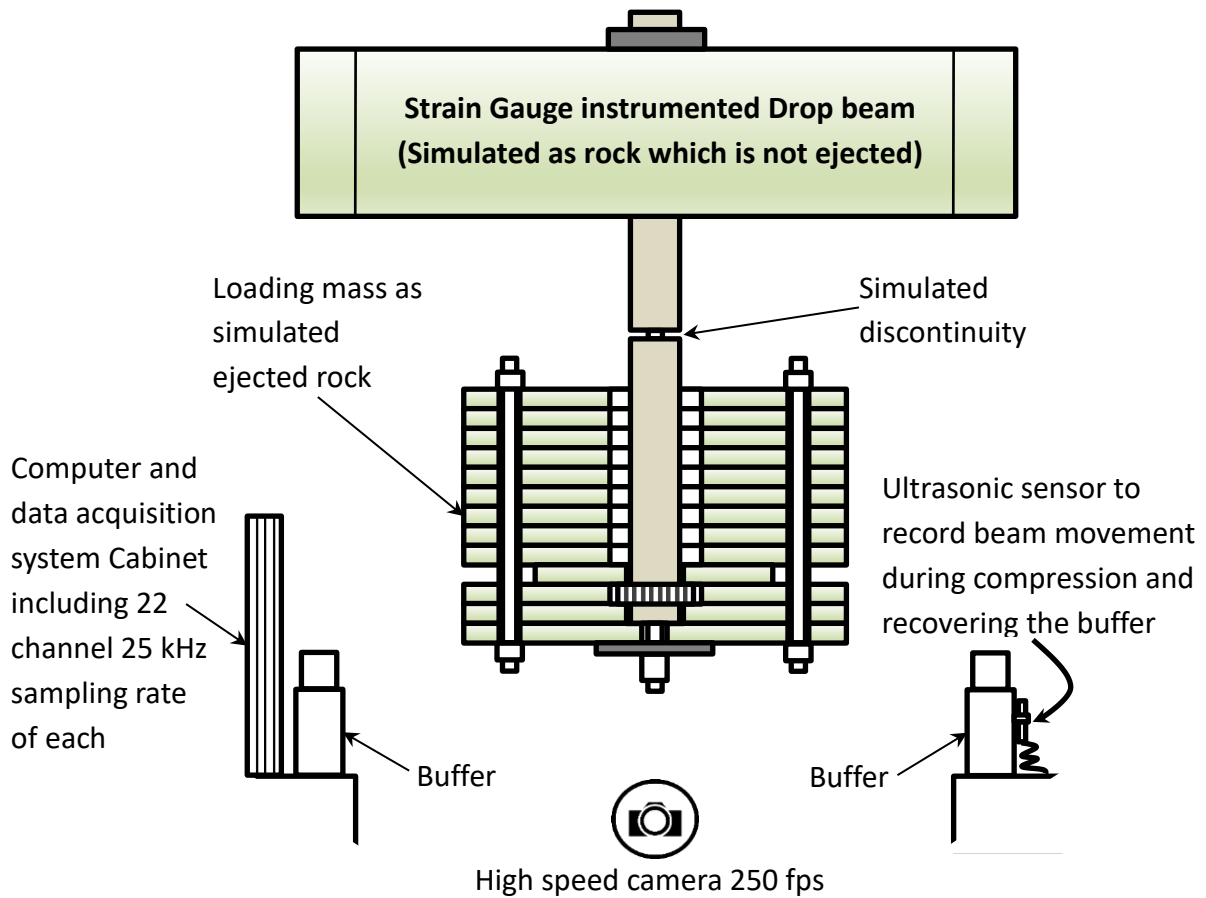


Figure 2.19. Momentum transfer mechanism dynamic testing facility (after J. Player, Thompson, et al. (2008))

The dynamic force-displacement diagram of the support element is practicable to be calculated via having a well-instrumented and monitored system. The portion of the applied kinetic energy which is dissipated by a prepared sample of support would be calculated by calculation of the area under the force-displacement graph. Another portion of energy which is absorbed by buffers can be calculated separately for every test. The accelerometers assist in evaluating and computing the deceleration response of the system. Alternatively, it can be calculated by a fast computerised video camera, measuring the relative displacement of a target by object tracking software.



Finally, the underground ejection velocity considered as the relative velocity between the loading mass and the dropping beam. The ejection phenomenon happens and a block of rock which was at rest or stationary under the stress at the wall or vault of the tunnel quickly accelerates and reaches to a pick velocity. The velocity returns to zero if the ground support system tolerates the dynamic impact. In compared to a strong ground support system a weak or soft support system would be a reason for larger displacement and greater ejection velocity. The most important aspects of the ground support design that has to be considered in a mining operation are the maximum permissible deformation of reinforcement system and being sure that the surface support has enough toughness to tolerate the displacement (J. Player, Thompson, et al., 2008).

#### **2.6.4. BACK-CALCULATION**

Back analyses of the happened real rock ejection and the associated support system potentially is a way of estimation of the dynamic capacity of the ground support. The problem is predicting the location of ejection due to its randomness and other uncertainties and consequently lack of sufficient monitoring to collect enough data regarding the event for example velocity of the ejected mass. Therefore back analyses of driven events like blasting would be an appropriate method to use back calculation for this issue.

A comparison between the test results of simulated rockbursts with back analyses of absorbed energy in some case studies has been performed by Daniel P. Heal (2010). A correlation has been found between the back-calculation of case studies and the simulated rockburst results, but it has not been proved yet nor used by other researchers. It seems that this method with some modification can be an approach to calculating rock support dynamic dissipation capacity in real scale.

#### **2.6.5. LARGE-SCALE DYNAMIC TEST RIG OF GROUND SUPPORT**

In order to examine the ground support as an integrated system, Geobruigg has been constructed a dynamic test rig. By using this rig, it is possible to apply a dynamic load to a sample of whole support containing a 3.6 × 3.6 m sample of surface support

combined with four dynamic rockbolts. Because the large sample includes all support elements, it is capable of demonstrating the performance of the surface support and the reinforcement in combination together as well as the connecting and terminating elements (Morissette, 2015; Roth et al., 2014). Figure 2.20 shows the test setup.

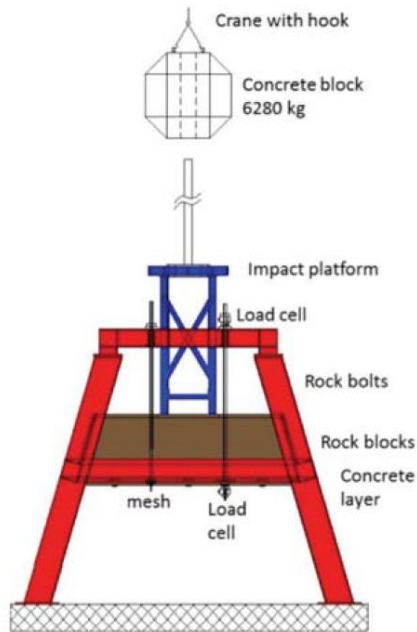


Figure 2.20. The large-scale dynamic testing rig of Geobruigg (Roth et al., 2014)

As it can be seen in the figure, a horizontal chain link mesh is connected to the main steel frame using lacing wire ropes while the mesh has been holding by four dynamic rockbolts. Surface support simulated by shotcrete or concrete slab could be poured over the wire mesh engaged with the four rockbolts via terminating and connecting elements. Some natural rock boulders and gravel are placed on top of the slab sample to simulate broken rocks during a rockburst event contained by surface support. Steel made impact platform places over the gravel to distribute and transfer the impact of a dropped block to the gravel layer, natural rock boulders, and simulated surface support. The mass of the dropped block is 6,280 kg and it can be lifted and dropped from a maximum height of 3.25 m limited by a guiding rail. One of the four bolts is instrumented by two load cells in both ends. Two high-speed cameras are installed in front of the mainframe, the upper one for the filming of the test block

movement and impact and the lower one to monitor the support with several measuring targets on the mesh and bolts with a computer tracking program to evaluate the displacement, velocity and acceleration of the targets. Dissipated energy can be calculated by the difference in potential energy of the test block before and after the impact (Morissette, 2015; Roth et al., 2014).

Testing a large scale of the support sample as an integrated system submitted to a dynamic impact is the powerpoint of this testing rig. Engineers, to some extent, can evaluate the energy dissipation capability of a ground support scheme exposed to dynamic impact and compare the compatibility of the elements in the prepared sample. The result would help the designer to avoid leaving a weak link in the support system because the weakest link in a support system affects and limits the maximum capacity of the whole system.

One weak point of the system is that a single drop would not fail the support system under test and multiple drops can conclude to overestimate the energy dissipation capacity of the rockbolts or even the whole support system.

There are not much-published results of this testing facility or a limited number of tested support system. Therefore the performance of it can be evaluated after publishing more testing result with comparison to real case studies. On the other hand, it seems that the monitoring data is not enough to calculate the portion of energy dissipated by support sample because the steel frame absorbs a part of the potential energy of testing block by deflection and vibration that cannot be measured or calculated by the predicted monitoring system. It is also worth mentioning that the testing facility does not completely replicate the seismic phenomenon that happens in the ground.

#### ***2.6.6. NCM DYNAMIC IMPACT TESTER (NCM DIT)***

The New Concept Mining (NCM) developed a dynamic testing facility called Dynamic Impact Tester (DIT) in South Africa. The Dynamic Impact Tester (DIT) (Figure 2.21) is used to transfer an impulse of energy to the sample, that would be expected during a rockburst. The dynamic testing machine that NCM has developed has been

designed in accordance with ASTM D7401-08 (Standard Test Methods for Laboratory Determination of Rock Anchor Capabilities by Pull and Drop Tests). The machine is designed to perform dynamic testing on the rock bolts by raising a known mass to a known height and then releasing the mass so that the mass will impact onto the sample either directly (continuous tube test) or indirectly (split tube test).

In the case of a continuous tube test, the mass impacts directly on the bolt simulating loading on the faceplate. In a split tube test, the impact plate and load cells are attached to the lower split tube. The impulse is transferred through the medium to the anchor points on the bolt, simulating a fracture between the anchor points. Figure 2.22 depicted the schematic concept of each type of test.

The input energy and velocity are calculated using the following two equations;

$$\text{Input Energy (J)} = m_{\text{trolley}} \times g \times h_{\text{drop}} \quad (2.14)$$

$$\text{Impact Velocity (m.s}^{-1}\text{)} = \sqrt{2 \times g \times h} \quad (2.15)$$

During each test the drop height, impact forces, and displacements are determined using the following sensors and data capturing hardware;

- **String Pot**: A PT9150 encoded string pot is used to measure the drop height and calculate the kinetic energy.

- **Load Cells**: The force of the impact is measured in three different locations during a split tube test and two locations during a continuous tube test. Each load cell is comprised of four individual PCB205C piezoelectric load cells, between two plates, allowing for a maximum force measurement of 800 kN. The piezoelectric load cells are connected to two eight-channel model 483C05 signal conditioners before the signals are captured at a rate of 10 kHz.

- **Line Scan Cameras**: A black and white striped flag is attached to the toe and impact plate of the test specimen; these flags are used as reference points, which are tracked by the cameras. The displacements of the specimen and the impact plate are captured at a rate of 10,000 lines per second, using two Basler Racer GigE line scan

cameras. Using the known width of the black and white lines on the flag, the pixel displacement is converted into a displacement in meters using the LabVIEW software.



Figure 2.21. The New Concept Mining (NCM) Dynamic Impact Tester (DIT)

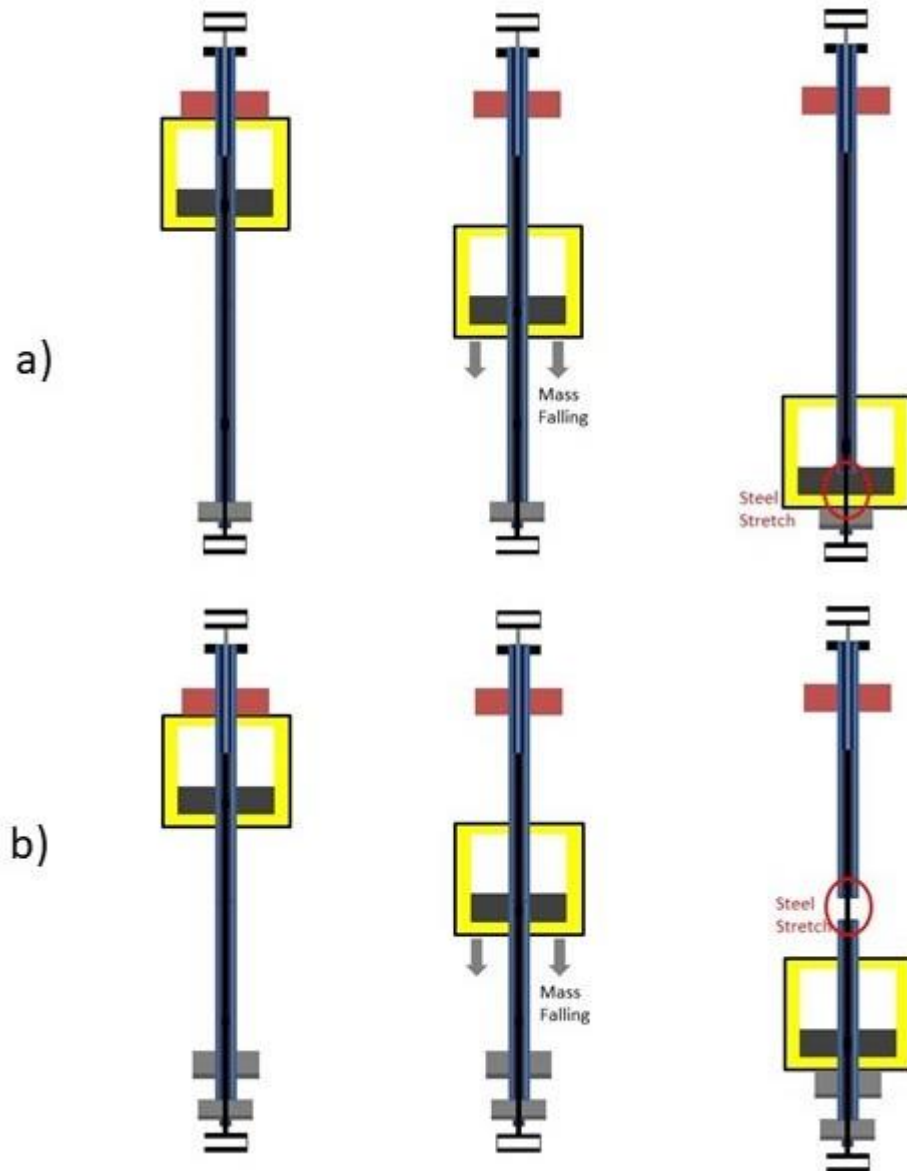


Figure 2.22. The Concept of Impact test on a) Continuous tube and b) Split tube

- **Data Capturing & Processing:** The analogue and digital signals are captured and generated by a National Instruments PCIe DAQ card (NI 6434). The load cell signals are converted and captured at a rate of 10 kHz, while the lines from the line scan cameras are captured as frames at a rate of 10000 lines per second using a PCIe GigE frame grabber (NI8233). To align the data, the analogue sample clock is output from the DAQ to the pair of line scan cameras and used as a line trigger. The data is not filtered by either the hardware or in software. More detail about this facility including some part of the thesis experiments explained in chapter 5.

## **2.7. SUMMARY OF LITERATURE REVIEW**

Rockbolt is an unavoidable element of a rock support system in underground mining. Rockbolts tolerate the contained load by surface support and have to have enough length to be able to transfer it to the stable ground in-depth, while they have not to be so long because of economical reasons and executive limitations. The bond length in a stable zone has the role of load transferring to the ground, therefore, uncertainty on this part should be minimised. Different experiments show that there is a minimum required embedment length for a rockbolt in every single situation that designer has to take into consideration. Experiments show that decoupling in bolt-cement interface varies depending on many factors and can affect the performance of the rockbolts under a load increasing condition. A sequential excavation of a large underground opening can produce such a condition of load increasing in the reinforcement system.

In this chapter key factors of the rockbolts have been discussed as well as their load vs deformation behaviour and load transfer mechanism to the ground through the anchorage system using the definition of Minimum Required Encapsulation Length (MREL) and decoupling process of encapsulation length. Failure mechanisms for underground deep and high-stress excavations due to induced stress and seismic events categorised and different methods of ground seismic energy demand estimation consisting of intact rock property approach, estimation of failure volume and ejection velocity, and rockburst damage potential were presented.

In the last part of the chapter different methods of dynamic capacity measurement of rockbolts and available facilities were explained. The drop test, blast simulation, momentum transfer concept and back-calculation were described while some of the other facilities such as the large scale dynamic test rig of ground support and the New Concept Mining Dynamic Impact Tester (NCM DIT) were presented in detail. As it will be seen in chapter 5 a large portion of this research experiments has been carried out by NCM DIT.

In the light of previous experience, some modification on ordinary rebar has been investigated by introducing a new method of borehole load monitoring of rockbolt. Although some laboratory work has already done for testing of the rebars subjected to dynamic impact, the practical monitoring and investigation of that still were unknown. The investigation on this issue is at the centre of the interest in chapter 3 of this research.

The concept of progressive decoupling of the encapsulation part of the rockbolt need to be investigated deeply to have a better understanding of a failure mechanism in anchorage system of reinforcement, therefore, some experiments have been considered for this purpose that will be discussed in chapter 4.

Although there is a lot of effort to determine energy absorption/dissipation capacity of different kind of rockbolts, the effects of dynamic events on rockbolts reaction still are not clearly known. Therefore, a large number of tests need to be done to find the different impressive factors on rockbolts response under seismic impacts. Some of this effective factors that need to be investigated are the amount of applied impact, the dimension of the rockbolts, material, geometry, velocity of the applied impact, etc. some of these factors are investigated in this research and presented in chapter 5.



### **3. MODIFICATION OF REBAR ROCKBOLTS AND FIELD TESTING**

#### **3.1 INTRODUCTION**

Fully encapsulated rebar rockbolt is the most common type of reinforcement elements in civil and mining projects. Due to extensive use of this type of rebar rockbolt, its installation technology significantly developed. The low deformation capacity of fully encapsulated rebar rockbolts is their main shortcoming for efficient use in seismic conditions. To resolve this issue, it is recommended to apply a decoupling length along the area of the largest probable concentrated deformation. In other words, the rockbolt is grouted in the whole length except along a small portion of its length between the anchorage length and the collar. Coupling of the rockbolts in both ends causes them to perform similar to fully encapsulated rockbolts loading wise and the decoupled part in the shank of the bolts helps them to tolerate the deformation much more than ordinary fully encapsulated ones. Following chapter explained more detail about this issue supported by some practical experiments and the actual performance of the modified rebar rockbolts.

#### **3.2 EXPERIMENTS MODIFICATIONS**

##### ***3.2.1. REBAR ROCKBOLT MODIFICATIONS***

Decoupling a part of the shank of a rockbolt from coupling to the hole's wall or surrounding ground prevents it to be coupled with the surrounding rock point-to-point so that it concludes to avoid tolerating any local deformation in a short length. Any local deformation such as discontinuity opening that occurs in the targeted length is not concentrated locally on rockbolt, but it can distribute along the decoupled length of the bolt. Making a free length part at the middle of rockbolt could be carried out by considering a section of the rockbolt covered by high-density polyethylene (HDPE) or PVC smooth pipe in the middle part as shown in Figure 3.1. The proposed modifications increase the total deformation capacity of the rebar rockbolts.

A sample of the proposed rockbolt can be found in Figure 3.1. The rockbolt is divided into four parts: “a) Main encapsulation length” which is different to conventional length in ordinary partially encapsulated rockbolts, “b) Free length” which is one of the modifications that discussed in the following subchapter, “c) Collar encapsulated length” which is another modification that will be discussed later, and “d) Outer length” which is not the main concern of this research and explained in 2.3.1.

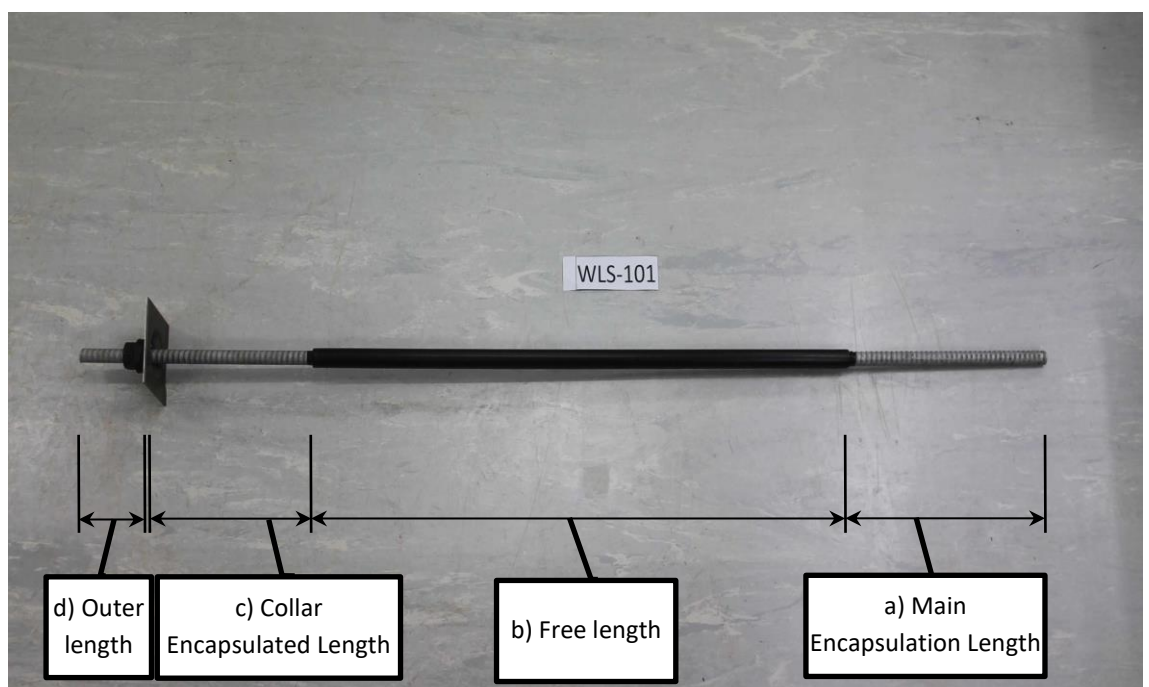


Figure 3.1. Sample of modified rockbolt after Masoudi et al. (2019)

#### 3.2.1.1. *Main Encapsulation Length (MEL)*

A particular length at the distal end of the rockbolt can be considered as the “Main Encapsulation Length”. Determination of the MEL needs some prerequisites because this part has the function of transferring the induced load to the ground. Therefore the length MEL should be at least as long as the MREL (as explained in 2.3.3). A large number of critical factors are involved with the performance of the rockbolts and its effectiveness so that considering a certain length of the bolt for MEL is not straightforward and needs its requirement.

Because of uncertainties in the ground, an extra length has to be considered to increase the factor of safety. As a rule of thumb, the additional length could be considered as 50%-100% of the MREL as shown in Equation 3.1.

$$\text{MEL} = \text{SF} \times \text{MREL} \quad (3.1)$$

$$\text{SF} = \text{Safety Factor} \approx (1.50 \text{ to } 2.00) \quad (3.2)$$

At the first stage, the MREL has to be evaluated by some laboratory-based or more efficiently on-site tests. In addition to MREL, the extra length should be considered for increasing the factor of safety that has to be determined by engineering procedures. Obviously, on-site testing for evaluation of the MREL is more reliable than the laboratory testing, and in the latter case, the factor of safety should be considered higher.

#### 3.2.1.2. *Free length*

Decoupling a particular length of a rockbolt by covering it with a piece of HDPE or PVC smooth pipe, with an appropriate inside allowance restrains the surrounding grout engaging the bolt and preventing it from them so that the rockbolt can freely move axially inside the smooth pipe. Therefore, this part can be considered as free length, and with this modification, it can tolerate more deformation. In other words, the free length on the middle of the rockbolt plays a influential role to distribute any applied axial deformation on the rockbolt because of discontinuity opening, wedge movement, ejection of a volume of rock due to seismic activity, etc., over the free length, instead of a concentrated deformation which can cause a failure.

The smooth pipe can be installed with sealing material like heat shrink sleeve or crimp fitting on two ends. In most cases, complete sealing is not necessary, because limited intrusion of the cement grout into the decoupling smooth pipe cannot couples the rockbolt with the surrounding grout or the ground. The cement grout might bleed into the pipe or at worst, there might be a small amount of grout intrusion, but this will not bind the rockbolt to the surrounding encapsulation material. Therefore, the pipe acts as an element for decoupling the rockbolt from the surrounding material and allows the applied deformation to be distributed over the

free length (Figure 3.2). It should be ensured that the dislocation of the pipe does not occur during the installation of the rockbolt in the borehole otherwise the designation decoupled part of the rockbolt is not the same as the design.

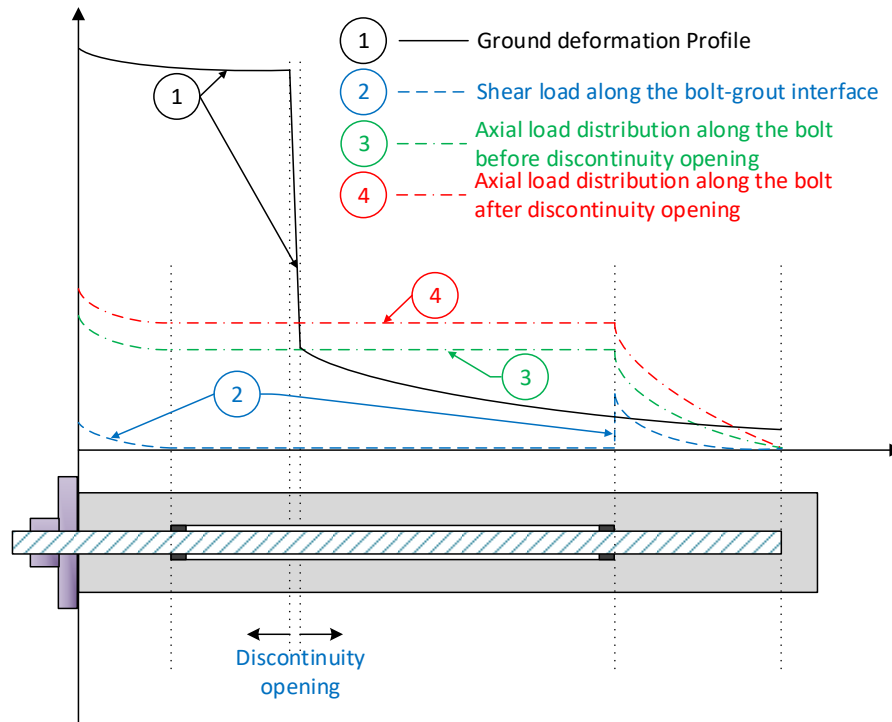


Figure 3.2. Load distribution in modified rebar rockbolts under the effect of a discontinuity opening after Masoudi et al. (2019)

### 3.2.1.3. Collar Encapsulated Length (CEL)

A rockbolt sometimes fails from the termination arrangement, specifically when a seismic event occurs. Weaknesses in bearing plate, nut, threading, bearing pad, or the fractured rock underneath the bearing plate or pad, lead the rockbolt to a malfunction or early failure. Even local failure of a rockbolt can be a reason for the failure of neighbouring bolts and gradual development of the support failure to a considerable portion of the support system.

For the best performance, bearing plates should be perpendicular to the corresponding rockbolts as well as being parallel to the ground surface, but due to the unevenness of the surface, operational difficulties, and human errors, most of

the times the holes are not precisely drilled perpendicular to the wall. They need concrete pads to fill between the bearing plates and the rock, in addition, to make it in an appropriate condition in order to transfer and distribute the concentrated load on the nut to the ground through the bearing plate and pad. Sometimes additional accessories such as Shim plates or bevelled washer are needed for this issue as well. The concrete pad thickness of a rockbolt is not uniform underneath the bearing plate so that it has not the same strength around the rockbolt and under a dynamic impact load cannot act its function, distribute and tolerate the load conclude to an early failure while the bearing plate itself deflects easily under the dynamic impacts and do not perform its function appropriately.

Nuts also sometimes stripped off the threads of the rockbolts under the seismic loading. Experiments on threadbars show that the surface elements have not strengthened as the threadbar; therefore the released energy of the impact cannot transfer to the ground in depth through the shank of the bolt and anchorage system in depth (Player et al., 2009).

In addition to above-mentioned facts, the rockmass beneath the bearing pad is not rigid enough as the undisturbed rock in depth because of blasting, stress release, unconfined structural weaknesses and proximity to the wet weather. Therefore, when a seismic load occurs, it can fail ahead of expectation in comparison to unperturbed rockmass.

All of the discussed facts, conclude to dysfunctioning of the reinforcement system to transfer the released energy to the ground and could drive the surrounded ground to a failure. Conventional practices such as making the bearing pad perpendicular to the rockbolt, using an extra bearing plate and nut, etc. not only result in additional costs and complexity of the application but also they cannot remove all of these weaknesses. A practical way to overcome these shortcomings is viable by the application of a collar bonding. Collar bonding is the coupling of rockbolt to the surrounding rock and can also couple to surface support. Mobilising the anchorage force in this part in addition to the resistance of the bearing plate and nut can form an appropriate terminating arrangement and involved with the surface

support and rock to contain the surface movement of the rock and transfer the load to the rockbolt at depth. Then, the main bond length can transfer the load to the ground.

#### *3.2.1.4. Outer length*

The outer or external length is a part of the rockbolt which stays out of the borehole. Bearing plate and underneath pad, nut, possibly centraliser and bevelling washers, and protection cap, are placed in this part of the rockbolt. The outer length should be long enough to contain all designed facilities. This length for conventional rockbolts is about 15-50 cm. It is worth mentioning that longer outer length reduces the effective span of the opening and this problem could result in extra costs.

### **3.2.2. LABORATORY TEST RESULTS**

Laboratory experiments have been performed by the Western Australian School of Mines via a dynamic testing facility on 20 mm threadbars (J. Player, Thompson, & Villasescusa, 2009). The results were compared with previous attempts on similar rebars under static loading condition. Dynamic tests have been carried out by dropping rockbolts, cast in grout within thick wall steel pipe attached to a loading mass, into a pit. The rockbolts were assembled with the proposed configuration ( $a = 1$  m Main bond length,  $b = 1.6$  m Free length, and  $c = 25$  cm Collar bond length) and compared with the fully grouted configuration. The mechanical properties of this type of rebar rockbolts are average yield force = 165 kN, average tensile strength = 191 kN, and average elongation capacity = 21%.

Typical results of three combinations of embedment and loading conditions of the rebar rockbolts are illustrated in Figure 3.3 for comparison. The fully grouted rockbolts are stiff and take up the load quickly, but they do not have much deformation capacity. As can be seen, they can tolerate about 30 mm deformation in the static loading condition. Under dynamic conditions, the fully grouted rockbolts showed higher strength, higher energy dissipation capacity (about 10-15 kJ), and higher deformation capacity (60-70 mm). As it was predicted, the proposed

configuration increases the deformation capacity of this type of rockbolt to more than 100 mm as well as their energy dissipation capacity to more than 20 kJ.

Additionally, it has been found that the rebar rockbolts show higher strength under the dynamic impact. Although the ultimate strength of the rebar rockbolts in the static loading condition is about 191 kN, the strength increases up to 250 kN under dynamic impact so that the higher strength increases the energy dissipation capacity of rebar rockbolts. The results show that both deformation capacity and energy dissipation capacity of rebar rockbolts would be improved by applying the suggested modifications.

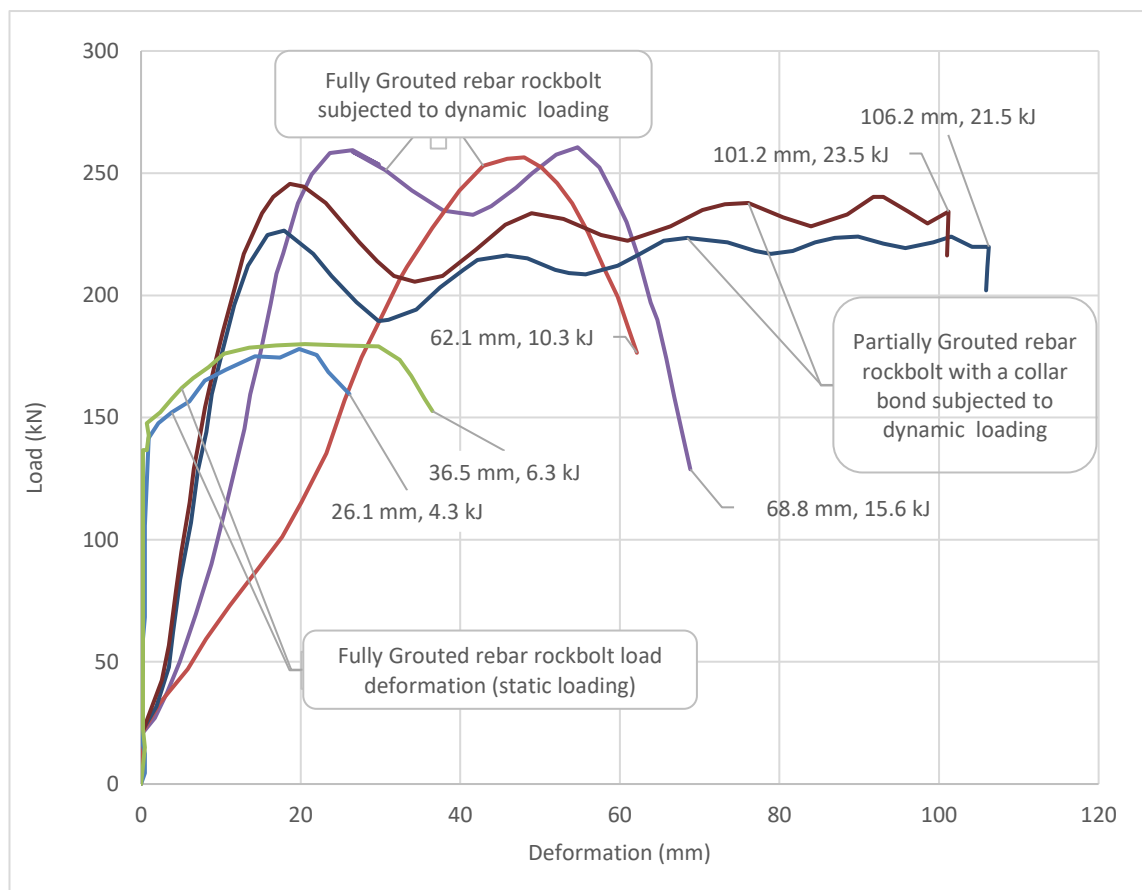


Figure 3.3. Different combination of embedment and loading condition of the rebar rockbolts (redrawn after (J. Player, Thompson, et al., 2009; Villaescusa, 2014)).

### **3.2.3. FIELD TEST RESULTS**

Field experiments have been carried out in order to evaluate the rebar rockbolts' behaviour under seismic condition produced by blasting. The experiment has been carried out in the access pilot of a transformer cavern a Pumped Storage Power Plant during the excavation in Iran located in the Alborz mountain range. The region of the project lies in the alpine Alborz mountain chain, the southern part of the Palaeozoic-Mesozoic Central Range. The rock sequences in the project area consist of massive limestones, detrital series (sandstones, shales) and volcanic rocks of Permian formations, Triassic dolomites and Jurassic (Lias) formations with black shales and sandstones. Several tectonic faults are crossing the project alignment. Due to uncertainty in location and time of natural seismic events, blasting is used to produce the seismic wave. Nine rockbolts installed in a pilot tunnel as shown in Figure 3.4. which was completely removed by backward excavation.

The rebar rockbolts behaviour in the 6 m×6 m pilot tunnel of a 16 m×27 m×161 m cavern is illustrated here. The pilot excavated to the roof level of the cavern by 12.5% upward inclination as an access tunnel. The top heading of the cavern horizontally excavated by 6 m height and 16 m span in two stages of a horizontal pilot and enlargement to the final span. Excavation in bench was continued in every 3 m depth. The support system of the roof and wall has been installed simultaneously. As shown in Figure 3.4. three arrays of monitoring have been carried out in chainages of 15.0m (array 1), 30.0m (array 2), and 45.0m (array 3). In each array three rebar rockbolt with the length of 4 m equipped with a deformometre to monitor the deformation over different segments of each rockbolts. The borehole loadcells installed on the bolt to measure the load along the shank of the rebars.

Each rockbolt was hot-rolled steel rebar that shows an extension in length at yield under constant load followed by strain hardening. Rebar specification consists: Yield strength/Ultimate strength = 400/600 MPa, Diameter = 20 mm, average yield force of the bolt = 130 kN, average ultimate strength = 190 kN, average elongation capacity = 6%, Length = 4 m. The suggested modification have done with: a) main bond length



=1.50 m, b) free length = 1.70 m, c) collar bond length = 0.50 m, and d) outer length = 0.30 m.

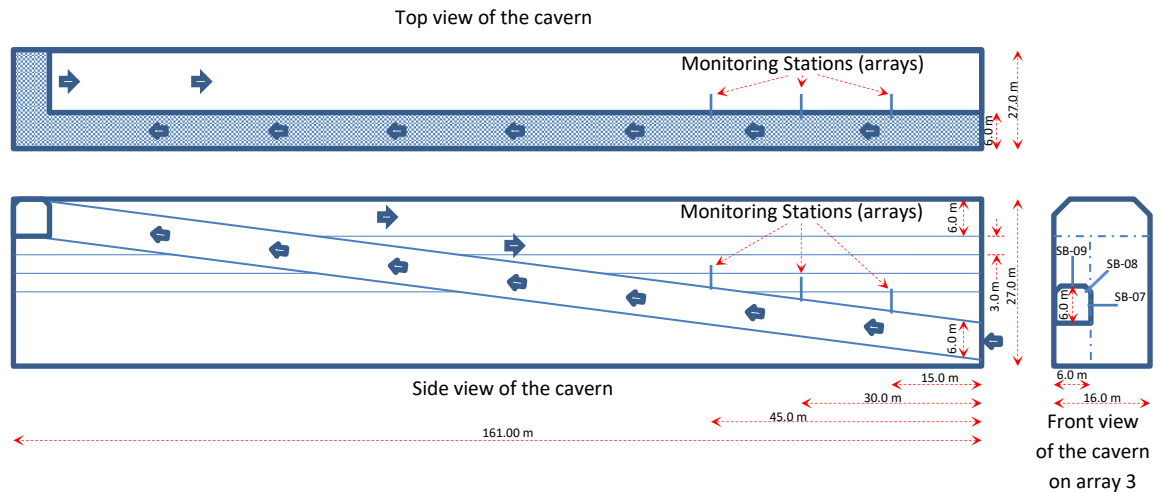


Figure 3.4. Different views of the cavern including the tunnel under study  
Masoudi et al. (2019)

The instrumentation has been carried through Folowrd Industrial Projects (FIP) Geotechnical Instrumentation Company. The load in the shank of the rockbolt was measured with a borehole load cell at the proximal end of the free length and deformation was measured in borehole and surrounding rock by multiple borehole deformometres in sections of the surface to the depth of 0.50 m (0.0 m to 0.5 m), 0.5 m to 2.2 m, and 2.2 m to 3.7 m. The outer length of 0.3 m for each bolt stayed out of the borehole for bearing pad, plate, nut, and initial tightening of the bolt. The proposed deformometre as sketched in Figure 3.5 is a wire strain gauges like material. Increase in length of wire leads in the change of its electrical resistance and output voltage of the readout unit calibrated for the instrument. The wire was covered by a smooth pipe to protect it from encapsulation material.

A geodetic target was also installed adjacent to the head of each rockbolt to monitor the surface movement of the bolt head. Results of the geodetic point data were used for calculation of absolute displacement of each point in the borehole. The instruments recordings were carried out on a daily basis plus recording after each blasting. The recorded results of the monitoring for three of the rockbolts (array No.

3 ch: 45 m), including displacement and load variation over a period of 100 days are depicted in Figure 3.6 to 3.11 and illustrated herewith.

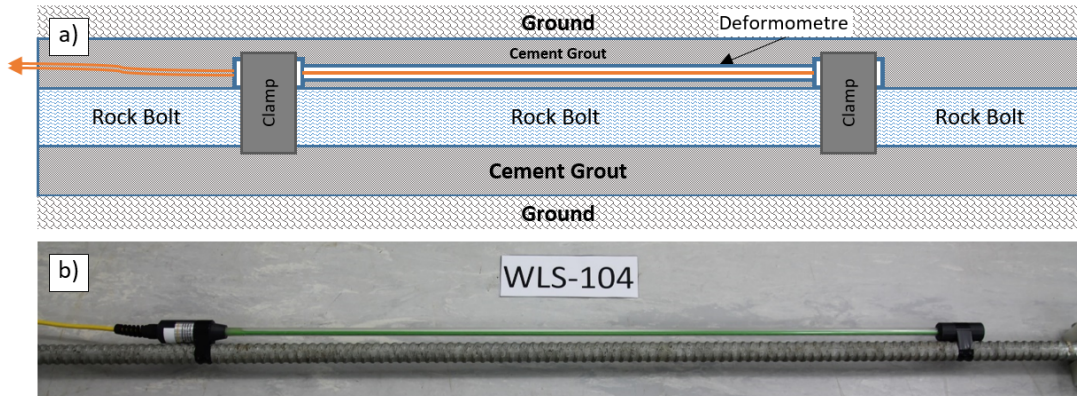


Figure 3.5. Deformometre to measure the large deformation along a rockbolt  
a) Schematic view b) photo of installed set sample after Masoudi et al. (2019)

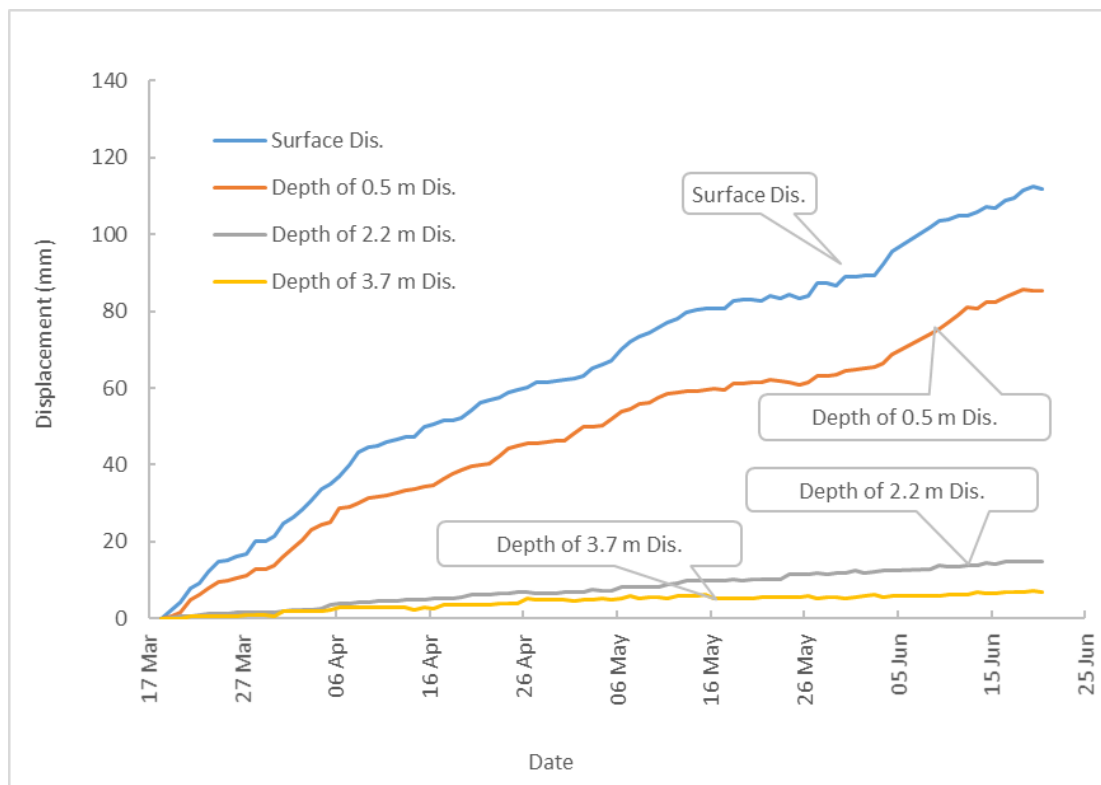


Figure 3.6. Displacements monitoring results at different distances from rockbolt head SB-07 Masoudi et al. (2019)

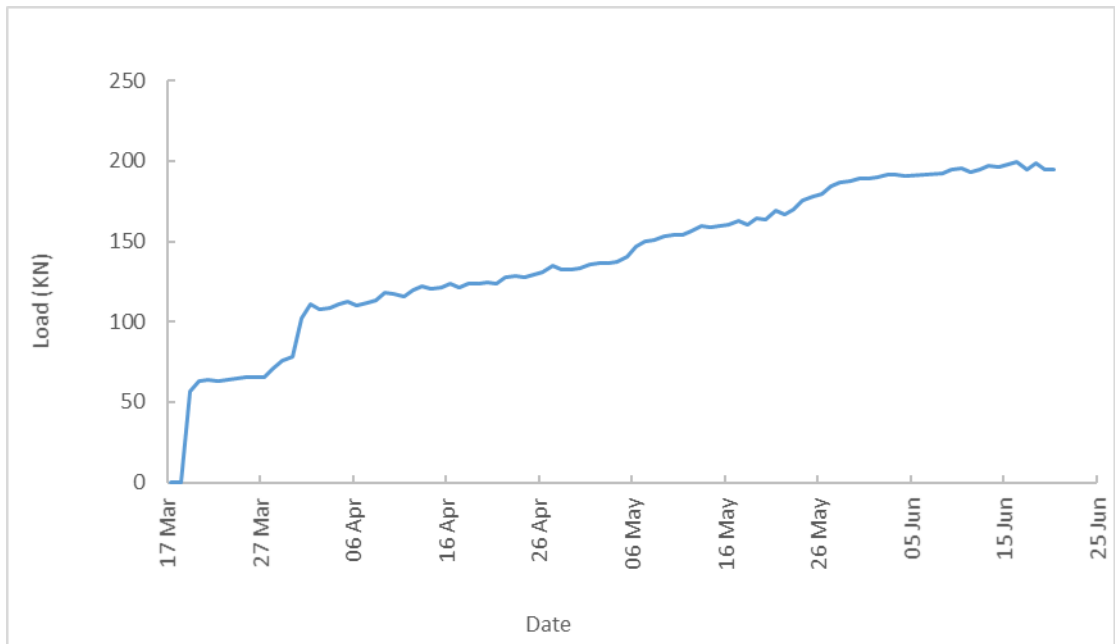


Figure 3.7. Load monitoring in the shank of rockbolt SB07 Masoudi et al. (2019)

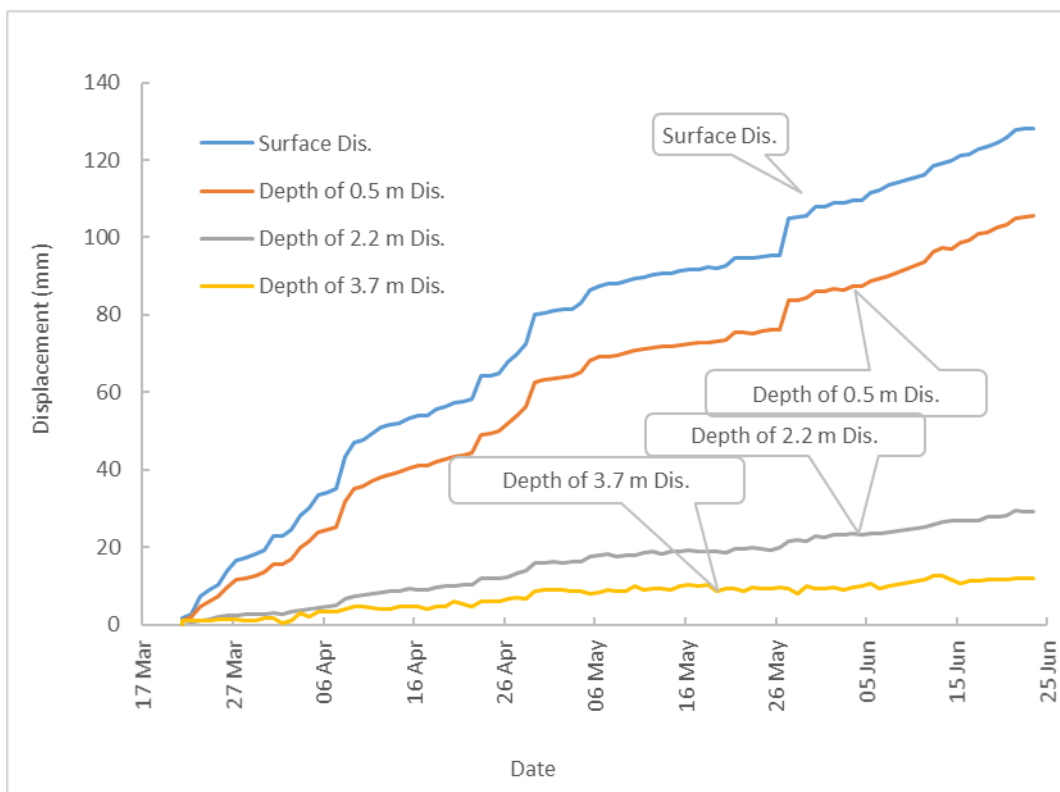


Figure 3.8. Displacements monitoring results at different distances from rockbolt head SB-08 Masoudi et al. (2019)

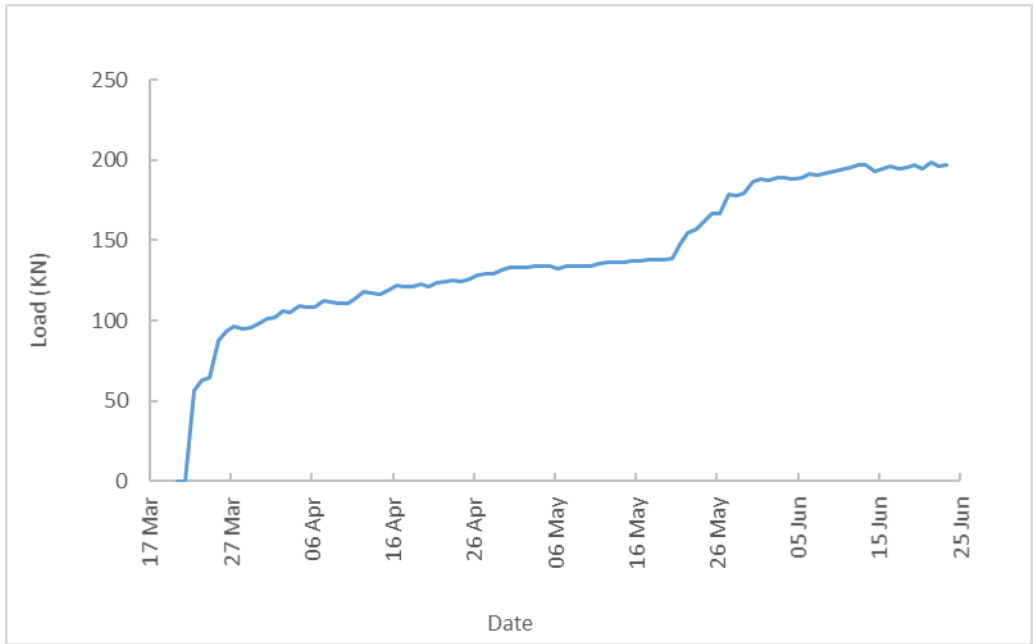


Figure 3.9. Load monitoring in the shank of rockbolt SB-08 Masoudi et al. (2019)

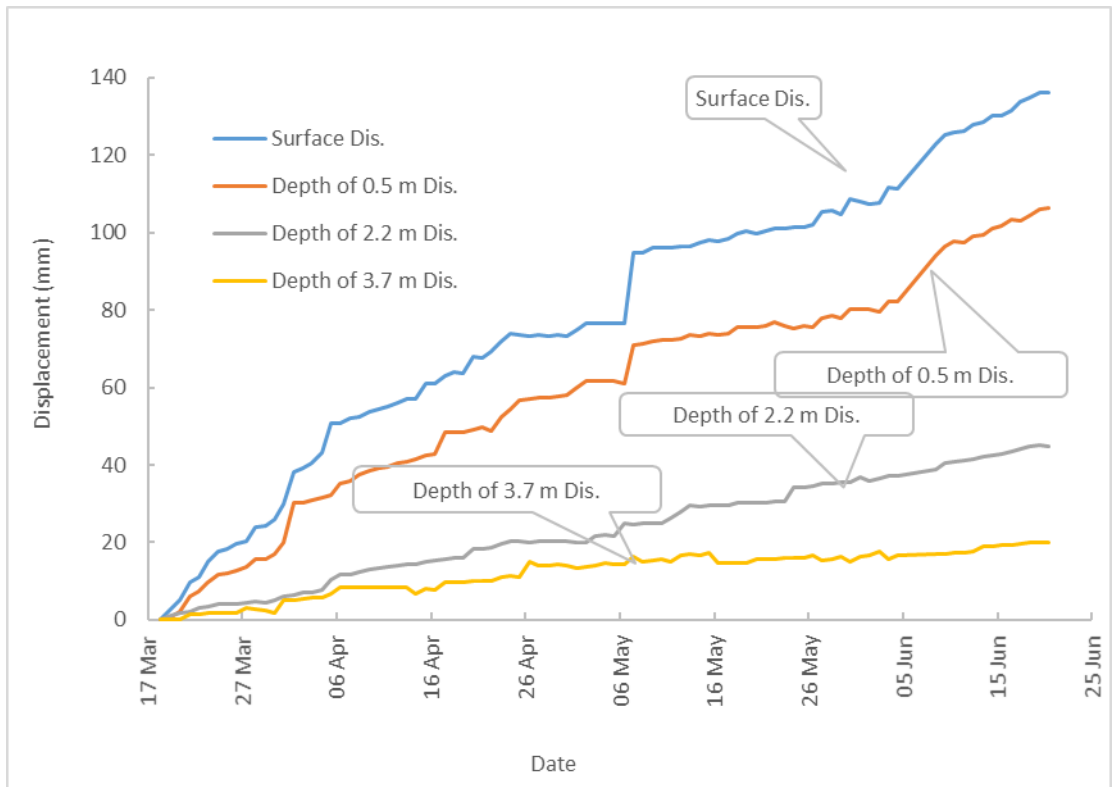


Figure 3.10. Displacements monitoring results at different distances from rockbolt head SB-09 Masoudi et al. (2019)

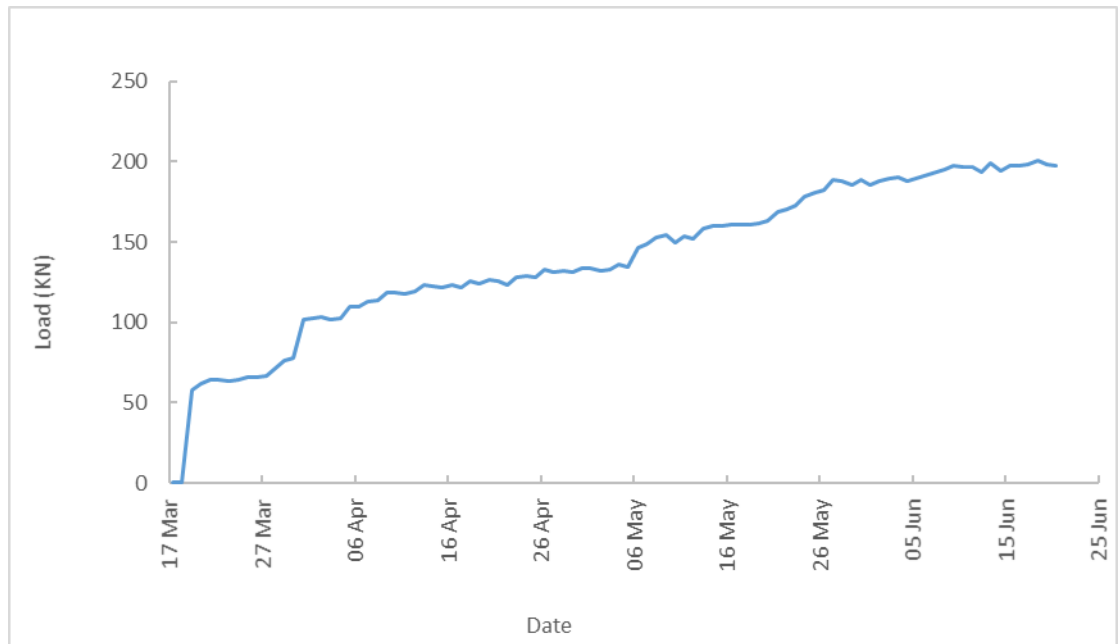


Figure 3.11. Load monitoring in the shank of rockbolt SB-09 Masoudi et al. (2019)

As shown in Figure 3.6 and Figure 3.7 the rockbolt No. 7 which is installed at the wall of array 3 was able to tolerate about 112 mm of deformation to reach to the final loading capacity, the rockbolt No. 8 (Figure 3.8. and Figure 3.9) installed at the corner was able to tolerate about 128 mm, and the rockbolt No. 9 (Figure 3.10. and Figure 3.11) installed at the roof was able to tolerate about 137 mm.

In order to investigate the load and deformation capacity, and estimate the energy dissipation capacity of the rockbolt, deformations and loads measured at the same times in each pair of graphs were extracted and depicted in Figure 3.12. The distribution of the displacement along each rockbolts and the energy absorption of each one are varying, although in comparison with full encapsulated rebar rockbolt it is evident that total energy absorption capacity of all of the bolts increased considerably (Masoudi & Sharifzadeh, 2018).

As can be seen in Figure 3.6 to Figure 3.12 during the period of study, the rockbolt no. 7 at the wall has experienced about 112 mm of deformation from which about 97.5 mm is related to the free length and the collar encapsulated length (from the surface to the depth of 2.2 m). The rockbolt no. 8 has tolerated about 128 mm of deformation. Where 99 mm of the deformation occurred from the surface to the beginning of the main encapsulation length (0.0 m to 2.2 m). The rockbolt No. 9 at

the roof has experienced about 137 mm from which about 67% (91.5mm) of it tolerated along free length and collar encapsulated length. Generally, most portion of the deformation was tolerated by the free length in all cases. Since this type of rockbolt does not have much elongation capacity, the results show significant improvement in rebar rockbolt deformability.

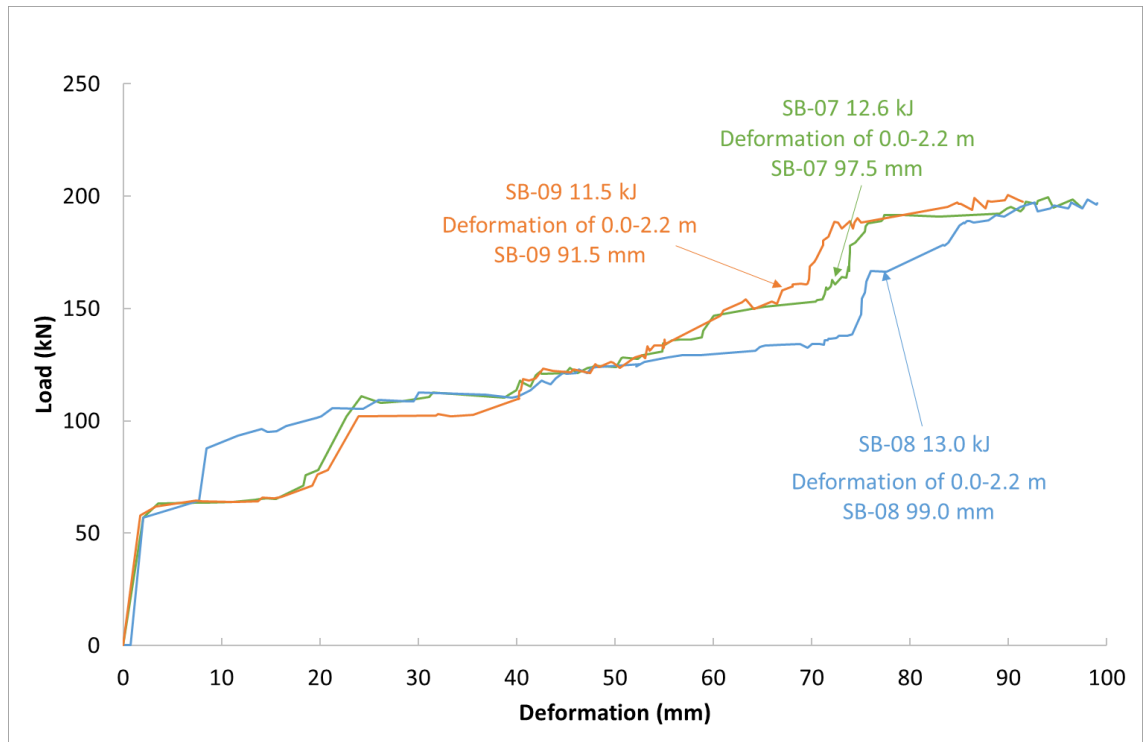


Figure 3.12. Changes of load versus deformation of the modified rebar rockbolt  
Masoudi et al. (2019)

Comparison of the results of the available load in the shank of the rockbolt with the applied deformation shows consistency in the whole range of monitoring except between 130 kN and 190 kN, which is around the yielding load of the rockbolt to the ultimate failure point. In this range, the load pattern differs from the deformation pattern because it is in the plastic zone of the rockbolt material. This behaviour shows that some part of the yielding of the rockbolt occurs under the dynamic impact, then recovers to the elastic range at the following stable condition. This impact load increase (impact ultimate strength) could reach 20% to 30% higher than its ultimate static strength. Determining this portion of the jumping in the load of the shank of the rockbolt needs continuous dynamic monitoring of the rockbolt during the impact

that has not been carried out before in the field. The field experiments show that continuous dynamic monitoring can be achieved using the proposed deformometre (Figure 3.5).

The practical experiments also show that the deformation capacity and energy dissipation capacity of steel rebars improve with partial encapsulation of rebar rockbolts.

### **3.3. DISCUSSION ON MODIFIED REBAR PERFORMANCE IN SEISMIC PRONE ZONES**

Modified rebar rockbolts in comparison with frictional rockbolts show much higher strength, (as well as deformation capability) specifically in seismic conditions. They are able to tolerate higher load compared to their ultimate strength in the static condition and compared to frictional contact because of their involvement with the ground through their anchoring system. Improving the rebars rockbolts, promote the entire rock support system and results in an effective safe workplace.

A suitable ground support system in the seismic prone zones should have enough resistance as an integrated system. The capacity of the support system is governed by the weakest link in the reinforcement of surface support. Having the collar encapsulation prevents the rockbolt to be the weakest link by removing those weaknesses in heading anchorage of the rockbolt. The low resistance of the bearing plate, nut, thread, and loose surface rock cover with the resistance of the coupled collar length to the ground so that the ultimate strength of the head anchorage goes higher than the strength of the shank of the rockbolt. Therefore rockbolts can perform their function entirely.

The free length or decoupled part of the rebar increases the deformability of the rockbolt and prevents the local failure due to concentrated deformation which leads to rockbolt failure unless the local deformation was more than the capacity of the whole free length. The decoupled part of the rockbolt is an important part of it so that many discontinuity opening or ejection of a volume of rock located in this depth. Without the free length in this part, early rupture of the rebars likely occurs or there is a high risk of the support failure.

The main difference between Cement and Resin partially encapsulated rockbolts is the constant quality of the resin compared with cement grout, while the latter needs a quality control program to assure the optimized performance.

One advantage of the proposed method is the economical effectiveness of it in different condition. The experiments in this research show an increase of the deformation capacity, and energy dissipation capacity of the rock bolt two-three times in comparison with ordinary type. The proposed modification has not been investigated accurately from an economical point of view while it is obviously worthy compared to the bolt price. Based on previous experience (of the candidate oversea), and depends on the manning costs and material price, the economical evaluation varies in a range of 10% to 30%. But since this part of the research was not at the centre of interest, the respected data have not been acquired.

Considering that proposed rockbolt modification is an easy, functional, and low-cost practice with high performance in seismic prone zones and significant improvement in the capacity of the deformation, avoids early failure, improves head anchorage, not leaving a weak link in reinforcement, connecting elements, and terminating arrangement, while rockbolts have enough strength in the anchorage.

### **3.4. SUMMARY AND RESULTS**

Rockbolts tolerate the load contained by the surface support and have to have enough length to be able to transfer it to the stable ground in depth while being not too long because of economic reasons and implementation limitations. The encapsulation length in the stable zone has the role of load transfer to the ground. Therefore uncertainty of the encapsulation length dimension should be minimised. Experiments show that there is a Minimum Required Encapsulation (Embedment) Length (MREL) for rockbolts in different situations that the designer has to take this into considerations.

Modifications applied on ordinary rebar rockbolts improves their performance in a rock support system specifically in seismic conditions. Considering a free length in the middle of the bolt by a piece of HDPE or PVC smooth pipe over the rockbolt to



decouple it from surrounded cement material, allows the rockbolt to be able to absorb more ground deformation than conventional fully encapsulated.

Collar embedment underneath the bearing pad and plate improves the head anchorage of the rockbolt and avoid any early failure in this part due to pre-existing rock breakage under the bearing pads, low resistance of bearing plates, the possibly lower ultimate strength of the threaded part, etc. The proposed length for collar embedment is the same as Minimum Required Encapsulation Length (MREL).

The Main Encapsulation Length (MEL) that transfers the applied load to the surrounding ground should be conservatively considered. Therefore, laboratory or preferably on-site testing is required to evaluate the as Minimum Required Encapsulation Length (MREL) which is the minimum length of the encapsulation that the interface resistance is more than the ultimate strength capacity of the shank of the rebar. Applying an engineering factor of safety to the MREL leads the designers to consider an appropriate MEL.

Prior to a rockbolt project, an on-site test plan to determine the optimised practical MREL for minimising the risk of support failure is recommended. Monitoring and observations will assist the engineers in modifying the whole system along with the progress. Since this type of rebars are always available and frequently employed in ground support systems along with other types of rockbolts and support elements, these modifications will improve the performance of the whole ground support system.

This page intentionally left blank

## **4. FIELD TESTING ON PROGRESSIVE DECOUPLING OF PARTIALLY ENCAPSULATED ROCKBOLTS AND MULTI-STRAND TENDON**

### **4.1. INTRODUCTION**

After installation of a reinforcement element in the underground, it is expected the load in the element to be increased in conjunction with the progress of the structure. In this condition, the anchorage system of the rockbolt gets activated and the shank of the bolt goes under the increasing load. In fully or partially encapsulated rockbolts, load needs to be transferred to the ground through the encapsulation length. As previously discussed, the encapsulation needs a minimum required length to be able to tolerate the load and transfer it to the surrounding ground. Lack of enough encapsulation length concludes to the anchorage failure of the rockbolt. Load concentrated on the first segment of the encapsulated length exceeds the strength of the segment and transfers to the next segment while the first segment only shows its descending residual strength. The phenomenon can progressively keep ahead toward the distal end of the encapsulation length. In other words, the increase of the free length along with the decrease of the encapsulation length would happen. Therefore, if the encapsulation length was not enough, progressive decoupling of it concludes to lose the rockbolt functionality.

In this chapter a brief background to progressive decoupling, then, the field experiment procedure was given, and finally, four representative practical experiments on rock bolt and multi-strand cable bolt were presented.

### **4.2. DECOUPLING PROCESS BACKGROUND**

The behaviour of the encapsulated length of reinforcement element under increasing load condition depends on multiple variables. Therefore prediction of encapsulated length behaviour needs sophisticated approaches. The most prospective reasons for load growth and hence decoupling process are listed as follows.

- Geometrical change due to advances in the face or bench of the opening (excavation sequences)
- Change in stopping geometry
- Time (due to time-dependent behaviour of the ground)
- Applying external loads
- Seismic events
- Failure of other elements
- Changing in available water condition
- The setting time of the grout material if exist

The realistic load distribution along a partially encapsulated rockbolt has been explained and discussed in section 2.2.3.3 and depicted in Figure 2.12. the detailed process of progressive decoupling is illustrated in Figure 4.1.

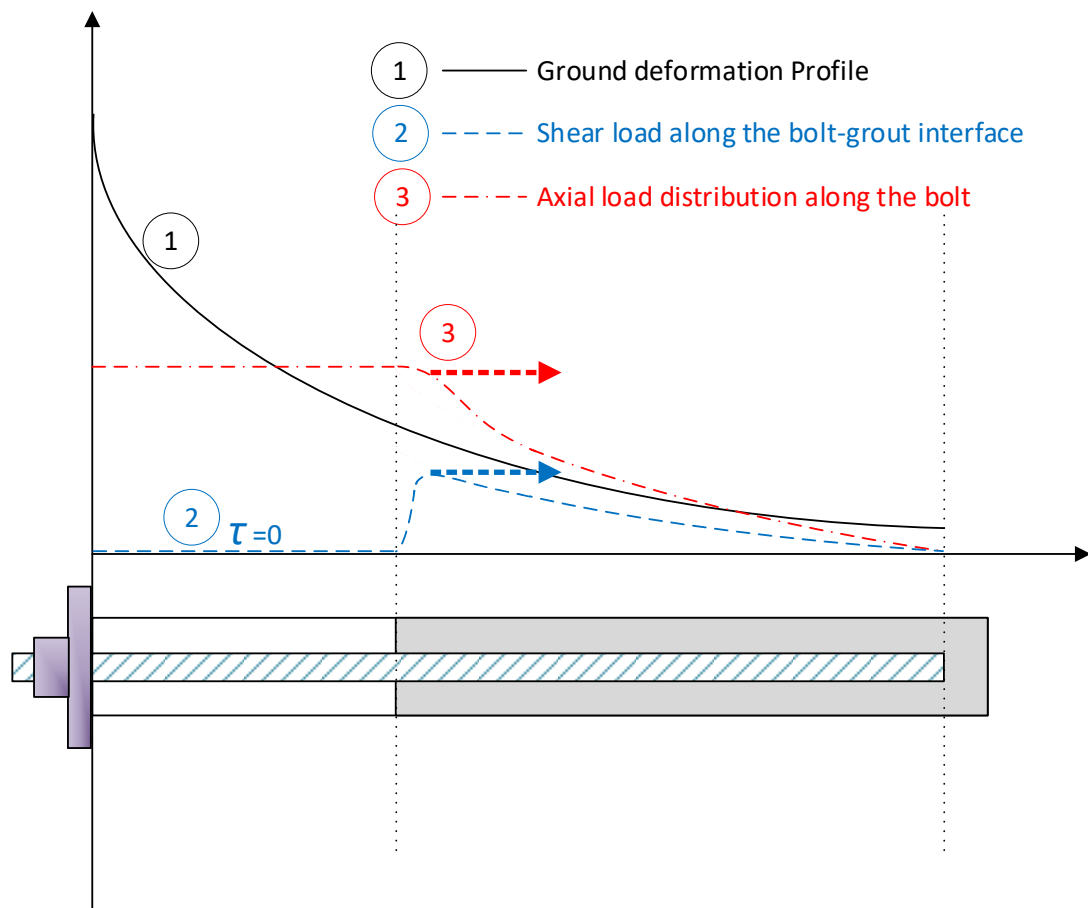


Figure 4.1. Change of the load distribution in partially encapsulated reinforcement element in uniform media

As it can be seen in Figure 4.1 with increasing the load and deformation, probable developments of the shear load pick point move toward the distal end of the rockbolt. In other words, the first segments are failed and the load transferred to the next segment, therefore, in this phenomenon gradually the free length increases and encapsulation length reduces. Development of the movement in the ground causes more anchorage length to be activated in encapsulated part, and the applied load cannot overcome to its strength unless the encapsulation length is not enough and the whole activated anchorage force in the encapsulated part is less than the applied load.

Charlie C Li et al. (2016) experiments on 20 mm diameter rebars show that in laboratory condition the Minimum Required cement Encapsulated Length (MREL) is between 25 cm to 36 cm for the water to cement ratio of 0.40 to 0.50 (UCS of 37 to 28 MPa). In addition to this, the experiments show that the encapsulation length could decrease up to 15 cm, in other words, the free length can increase up to 15 cm in a viable strength range of cement grout for 20 mm diameter rebars in laboratory condition. It can vary for other diameters specifically in field condition and actual quality of the cement grout and other limitations. In the following section some other experiments in actual condition have been carried out and the results discussed.

### **4.3. FIELD TESTING TO ASSESS THE DECOUPLING PROCESS**

Several experiments have been performed on multi-strand cable tendons and monobar tendons installed on roof and wall of an underground powerhouse cavern as a part of the long-term support system. A stressing test program including comprehensive and simple acceptance test designed and performed to insure about the future correct functioning of all tendons. In terms of the progressive decoupling, the results show that it could be greater than a few centimetres and seemingly variety of parameters are involved in determining the effective required encapsulated and free length. The installation and test procedure in different locations were based on standards such as DIN 4125, DIN EN 1537, PTI, BS 8081, and FHWA-IF-99-015 “ground anchorages and anchored structures” of Federal Highway Administration (FHWA). At

the following, the stressing procedure of the test have been explained then the results have been discussed.

#### **4.3.1. STRESSING PROCEDURE**

The stressing test is a non-destructive comprehensive loading with a hydraulic jack to a certain proof load predetermined by the designer. Depend on the application and the designated working load ( $F_w$ ) of the tendon, proof load varies up to 1.5 times of  $F_w$  or final lock-off load. In all non-destructive tests of tendons, the proof-load should be considered greater than 1.25  $F_w$  as the minimum value and less than 75% of the tendons nominal ultimate capacity. It also should be less than 90% of the tendon yield strength.

In the initial step, the load increases from zero to  $F_a = 0.2 F_w$  as the initial load step to avoid any deformation corresponding to the loosening of the head arrangement including nut, bearing plate, concrete pad, changing the alignment, and probable loos surface rock underneath the pad. A dial gauge on a tripod set to measure the deformation of the head of the tendon. It is obvious that the tripod locates in a place far enough from the tendon's location to avoid any induced deformation due to the loading. Then the load increases to the first load step of  $F_1 = 0.5 F_w$ . At the load step, the creep of the tendons needs to be measured therefore the load value has to be maintained constant during the observation time. The deformation is recorded via the dial gauge at 1, 2, 3, 5, 10, and 15 minutes to calculate the creep that can be determined with Equation 4.1.

$$Creep = \Delta L_{cr1} / \text{Log} (t_2/t_1) \quad (4.1)$$

Where  $\Delta L_{cr1}$  is differential deformation ( $\Delta L = L_2 - L_1$ ) at first load step occurred during the time steps corresponded to  $t_1$  and  $t_2$  under constant load.

After the observation period, the load decreases to the initial value of  $F_i$  to measure the reversible elastic deformation. At this stage, the (apparent) free length can be calculated by having Equation 4.2.

$$\text{Free Length} = (E)(A)(\Delta L_E)/(\Delta F) \quad (4.2)$$

Where: E is the young modulus of the tendons, A is cross-section of the tendons,  $\Delta L_E$  is elastic deformation of the tendon during the unloading, and  $\Delta F$  is differential load in the load step ( $\Delta F = F_1 - F_a$ ).

Another parameter that needs to be recorded is residual deformation. The residual deformation refers to the amount of plastic deformation that happens in the process of loading and unloading. It means that after unloading to  $F_a$  the dial gauge does not return to zero and some part of the total deformation remains unrecovered in the tendons permanently. This fact could be a reason of plastic deformation of the encapsulated part of the tendon, movement of the rockmass around the anchorage zone, the movement of the tendon in the surrounded encapsulation material, or a combination of these reasons.

Comparing three measured or calculated parameters from the test, the calculated creep, the calculated (apparent) free length, and the measured residual deformation, to predetermined values, allows the test to be continued to the next step. There are three criteria for acceptance of a tendon based on every standard. The creep and the residual deformation have to be less than a certain value as two of the acceptance criteria, and the free length has to stay in a standard range around its original designed value as the third criterion in which the last one is at the centre of the interest in this chapter.

In the next step of the stressing test, load increases to a higher level of  $F_2 = 0.75 F_w$  then the same procedure similar to the first step is followed for measurement and calculation of the creep at the constant load of  $F_2$ , the free length based on recovered deformation during unloading, and the residual deformation when load completely returns to the initial load ( $F_a$ ). Figure 4.2 schematically and conceptually depict the measured values during the second cycle of loading. This Figure also shows the third stage of the loading while in the experiments explained in this chapter the tendons have been undergone to five cycles of loading and unloading.

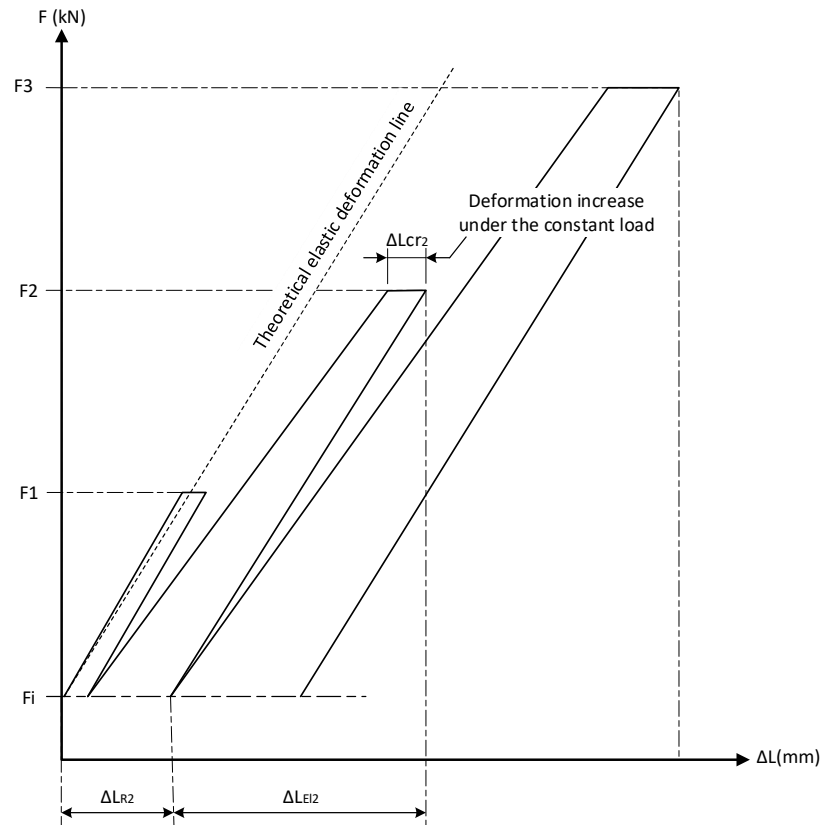


Figure 4.2. Schematic stressing steps and measured values during the second cycle of loading.

It is predicted that the free length develops in each load step to a greater length. In other words, under the increasing loading condition, the encapsulation length is reduced and therefore the free length is increased gradually corresponding to the level of the loading.

As it has been mentioned, the tendons have been tested for five loadings steps of F1, to F5 and the shortening of the encapsulation length is calculated respectively. The observation time increases for the higher load steps up to 120 minutes in case of successful experiments and can be extended based on different circumstances. The results show a greater amount of decoupling of the encapsulated length of tendons than what it is expected. Since the considered encapsulation length was excessively large, none of the tendons rejected or failed. The experiments also show that the encapsulation length should not be less than three meters in the stable depth of the hole.



### 4.3.2. EXPERIMENT RESULTS

The results of a field experiment on three types of the reinforcement elements consisting; multi strands tendons, monobar tendons, and partially encapsulated rock bolts were presented herewith.

#### 4.3.2.1. The first experiment on multi-strand cable bolt

In the first experiment, a multi-strand with 10 m length contains six strands of 0.5 inches with an initial cement encapsulated length of 5.0 m have been tested. Total free length of the tendons was 5.8 meter comprising 5-meter nominal free length and 80 cm of the predicted length for stressing equipment. The multi strands experienced 5 cycles of loading and unloading between an initial load step of  $F_a=120\text{kN}$  to each load step of  $F_1=254\text{kN}$ ,  $F_2=388\text{kN}$ ,  $F_3=522\text{kN}$ ,  $F_4=656\text{ kN}$ , and  $F_5=F_p=790\text{kN}$ . Apparent free length calculated by measuring elastic deformation in each unloading step via Equation 4.2.

Therefore by having cross-section area ( $6 * 100\text{ mm}^2 = 600\text{ mm}^2$ ), and Young modulus of the tendon material ( $E=200\text{ GPa}$ ), the apparent free length of the tendon have been calculated for every cycle of loading-unloading by measuring the elastic deformation in unloading part of each cycle. The summary of properties of the multi-strand and the loading step of the experiment abstracted in table 4.1 and 4.2 respectively.

Table 4.1. Properties of the monobars for the first experiment

Type	multi-strand	Total Length (m)	10
Yield Stress	1,580 MPa	Free Length (m)	5
Yield Load	984 kN	Encapsulated Length (m)	5
Ultimate Stress	1,860 MPa	Extra Free Length (m)	0.80
Ultimate Load ( $F_{ult}$ )	1,092 kN	Diameter of each (mm)	13 (0.5 inch)
Young Modulus	200 kN/mm <sup>2</sup>	Cross section area (mm <sup>2</sup> )	6*100 = 600

Table 4.2. Loading steps of the monobars in the first experiment

Load step	Load (kN)	Comment / Criteria
Initial Loading (Fa)	120	10% $F_{ult}$
First loading step (F1)	254	25% $F_{ult}$
Second loading step (F2)	388	37.5% $F_{ult}$
Third loading step (F3)	522	50% $F_{ult}$
Forth loading step (F4)	656	62.5% $F_{ult}$
Fifth loading step (F5)	790	75% $F_{ult}$
Working Load (Fw)	400	

The load-deformation of the multi-strand tendon in the first experiment depicted in Figure 4.3

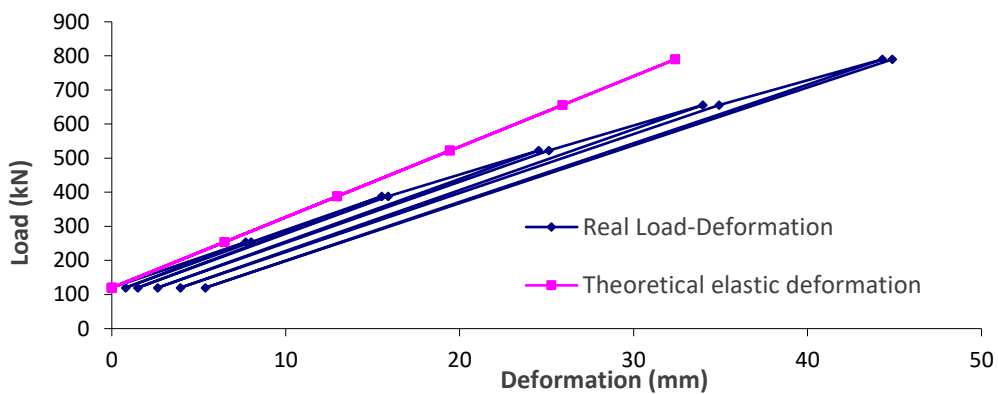


Figure 4.3. Load-deformation of a multi-strand during the stressing process in the first experiment

Figure 4.4 depicts a decrease in encapsulated length (and increase in free length) up to 1.25 m in a 5 metre of encapsulated length of the multi-strand under a comprehensive stressing test. It can be seen at the figure that by increasing the load in each load step the encapsulated length reduces from 5 metres at the load of zero to 3.75 metre at the load of 790 kN and respectively on the other graph the free length increased from 5.8 at the load of zero to 7.05 metre at the maximum load of 790 kN.

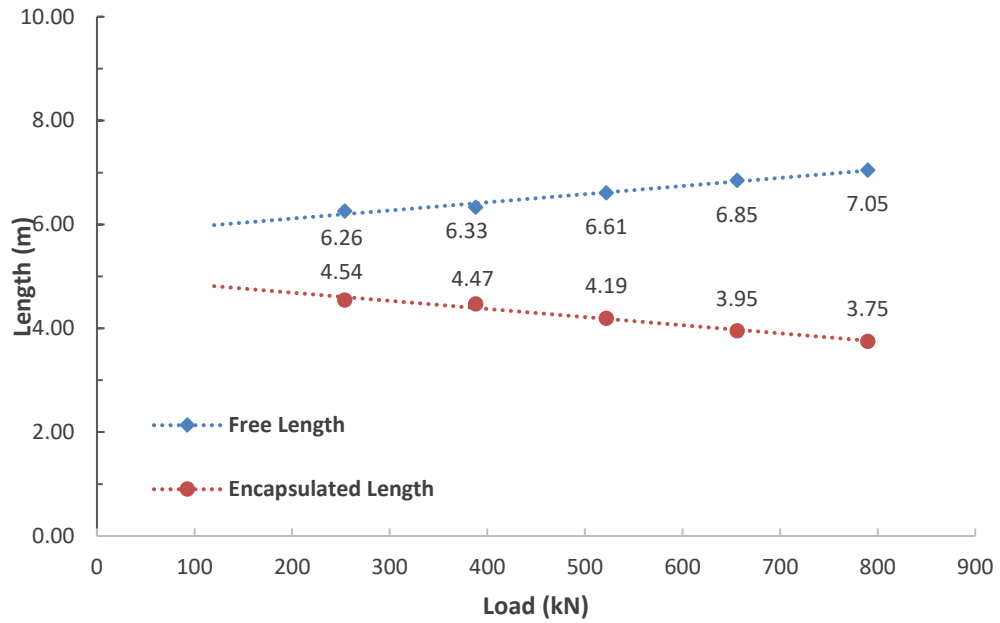


Figure 4.4. Encapsulation length/Free length calculation of a multi-strand tendon under increasing load

#### 4.3.2.2. Second experiment on rockbolts of a cavern crane runway beam

The second set of experiments have been carried out on 20 rockbolts (monobar tendons) out of 200, installed on the overhead crane runway concrete beam of an underground powerhouse cavern during the construction. As it has mentioned, the total number of the monobars of the beam was 180 while only 18 of them had been selected for the comprehensive stressing non-destructive test (CST). The rest of the monobars had been tested in a simple stressing non-destructive test (SST). The test procedure already has been discussed in 4.3.1 base on DIN-EN 1537 and DIN 4125. The properties of the monobars presented in table 4.3.

Table 4.3. Properties of the monobars for the second experiment

Type	Monobar	Total Length (m)	15
Yield Stress	950 MPa	Free Length (m)	10
Yield Load	1,650 kN	Encapsulated Length (m)	5
Ultimate Stress	1,050 MPa	Extra Free Length (m)	0.40
Ultimate Load ( $F_{ult}$ )	1,820 kN	Diameter (mm)	47
Young Modulus	205.94 kN/mm <sup>2</sup>	Cross section area (mm <sup>2</sup> )	1,735

The load steps of the tests presented in Table 4.4.

Table 4.4. Loading steps of the monobars in the second experiment

Load step	Load (kN)	Comment / Criteria
Initial Loading (Fa)	200	10% $F_{ult}$
First loading step (F1)	450	25% $F_{ult}$
Second loading step (F2)	685	37.5% $F_{ult}$
Third loading step (F3)	900	50% $F_{ult}$
Forth loading step (F4)	1,150	62.5% $F_{ult}$
Fifth loading step (F5)	1,200	67% $F_{ult}$
Working Load (Fw)	600	

The design working load for each of these tendons was  $F_w = 600$  kN that the tendons were locked-off on it after successful tests. Figure 4.5 shows the 5 cycles of loading of the monobar in comparison with the theoretical elastic deformation line.

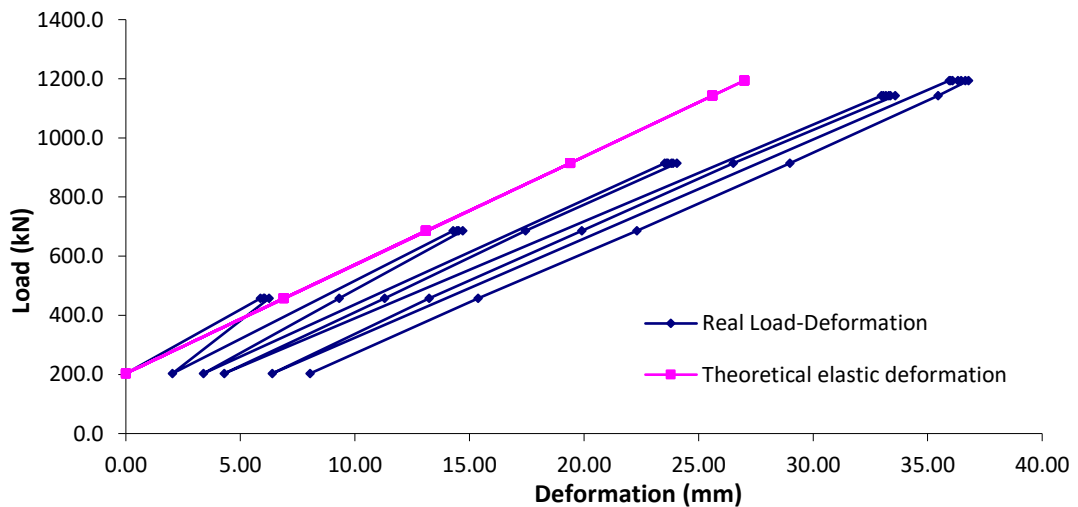


Figure 4.5. Load-deformation profile during the stressing process of the second experiment

Three criteria have been checked in each test including the creep, the residual (plastic) deformation after stressing, and the variation of the free length.

The creep measured at each load step in 15 minutes at F1 and F2, 60 Minutes at F3 and F4, and 120 minutes at F5 under the constant load. The deformation recorded

at time steps of 1, 2, 5, 15, 30, 60, and 120 minutes in order to calculate the creep by the equation 4.2

The creep calculation in each step has been drawn in Figure 4.6 shows that the creep of the encapsulated length is lower than 1.0 mm in each load step and lower than 2.0 over the whole range of loading observation.

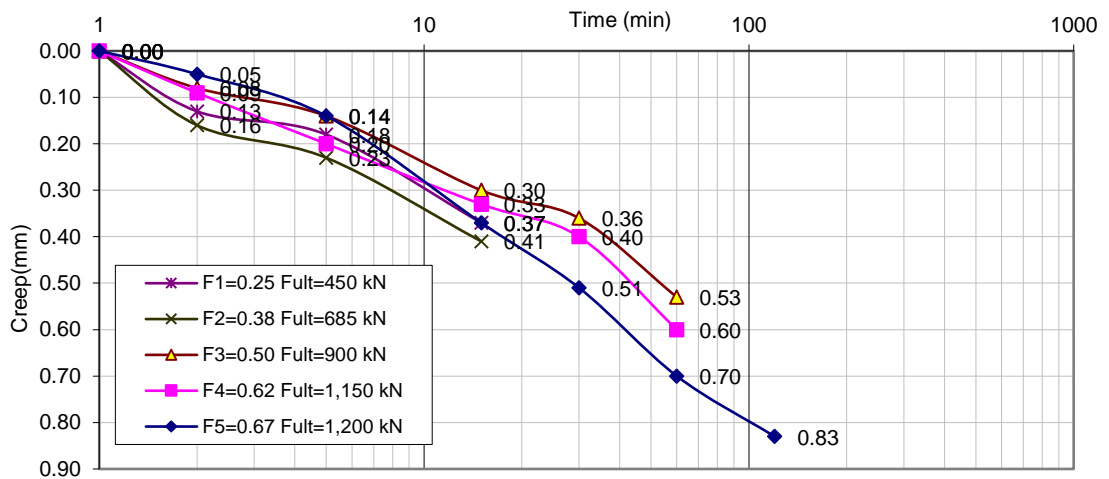


Figure 4.6. Creep results for the monobar tendon for the second experiment

Another criterion that has checked in this test was the residual deformation that is mostly related to the encapsulation length of the bolt. In this experiment it was 8.04 mm ( $\Delta L_{EI}=8.04$  mm) that was less than 10 mm as the predetermined acceptable amount for residual deformation.

As it can be seen, Figure 4.7. shows the development of the free length illustrating the decoupling of some part of the encapsulated length.

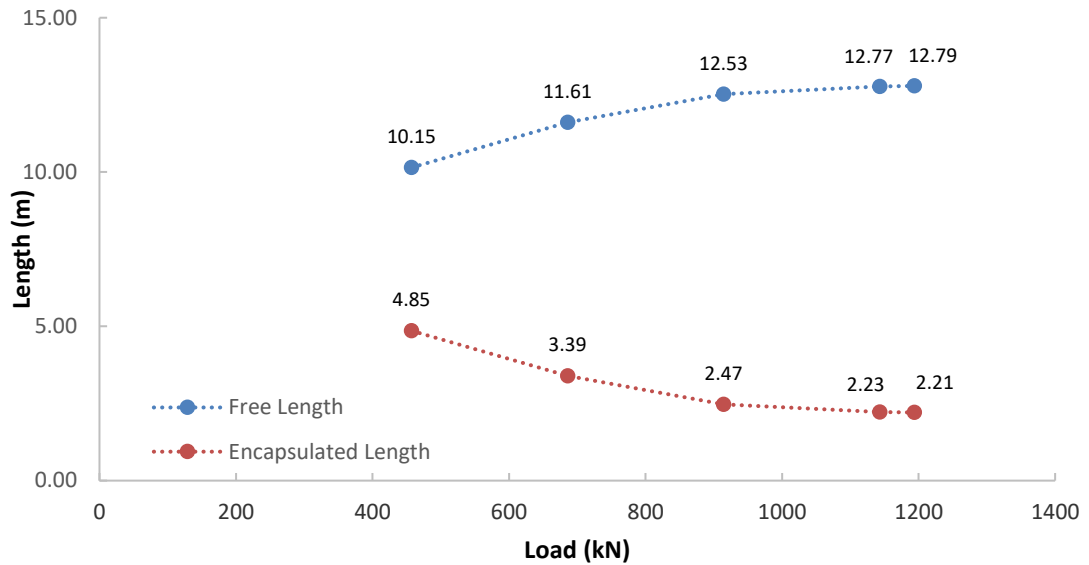


Figure 4.7. The free length - the encapsulation length variation under increasing loading in the second experiment

The free length that was considered in design, manufacturing and assembling of the tendon was 10 m but as it can be seen in Figure 4.5, the free length would be increased from 10 m at the beginning of the test at a load of Zero to 12.79 m at the proof load of 1,200 kN. The encapsulation length respectively would be decreased from 5 m in the starting point to 2.21 m at the ending point. In other words, it seems that the length of the encapsulated part would be decoupled 2.79 m under the loading process. Probably all of this amount is not because of decoupling but it has been discussed later in this chapter.

#### 4.3.2.3. Third experiment on rockbolts of a cavern walls

The third set of experiments have been carried out on a type of rockbolts (monobars) very similar to the monobar tendons in the second experiments. These monobars installed on the wall of the same underground powerhouse cavern during the construction. The number of the monobars was more than 1000 but 50 of them had been selected for the comprehensive stressing non-destructive test. The test procedure already has been discussed in 4.3.1 base on DIN-EN 1537 and DIN 4125. The properties of the monobars presented in table 4.5.

Table 4.5. Properties of the monobars for the third experiment

Type	Monobar	Total Length (m)	15
Yield Stress	950 MPa	Free Length (m)	10
Yield Load	1,650 kN	Encapsulated Length (m)	5
Ultimate Stress	1,050 MPa	Extra Free Length (m)	0.40
Ultimate Load ( $F_{ult}$ )	1,820 kN	Diameter (mm)	47
Young Modulus	205.94 kN/mm <sup>2</sup>	Cross section area (mm <sup>2</sup> )	1,735

The load steps of the tests presented in table 4.6.

Table 4.6. Loading steps of the monobars in the third experiment

Load step	Load (kN)	Comment / Criteria
Initial Loading ( $F_a$ )	180	0.20 $F_w$
First loading step ( $F_1$ )	430	50 $F_w$
Second loading step ( $F_2$ )	660	0.75 $F_w$
Third loading step ( $F_3$ )	890	1.0 $F_w$
Forth loading step ( $F_4$ )	1,120	1.25 $F_w$
Fifth loading step ( $F_5$ )	1,350	1.50 $F_w$
Working Load ( $F_w$ )	890	

The design working load for each of these tendons was  $F_w = 890$  kN that the tendons were locked-off on it after successful tests.

The profile of loading-unloading load-deformation of the monobar during 5 cycles of loading has been depicted in Figure 4.8.

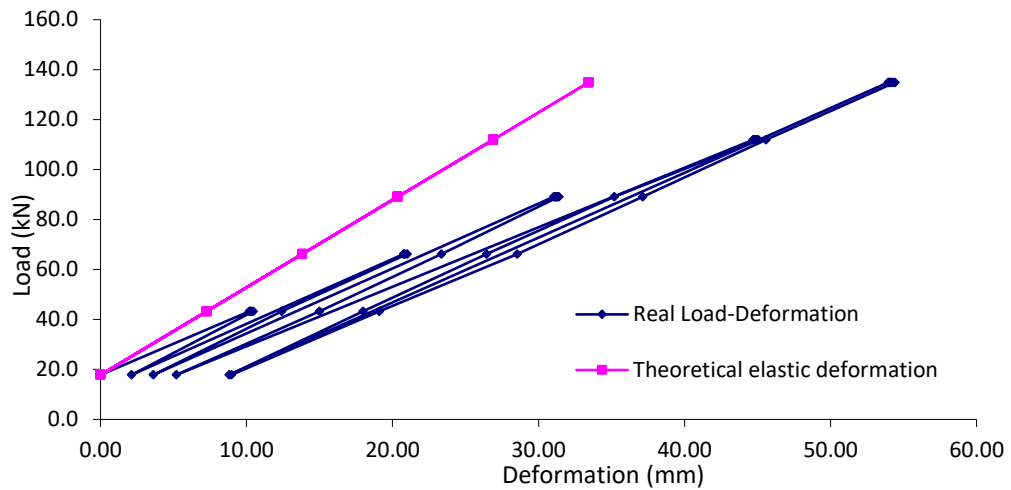


Figure 4.8. The profile of load-deformation of the monobar in the third experiment

Similar to the second experiments, three criteria have been checked in each test including the creep, the residual (plastic) deformation after stressing, and the variation of the free length.

The creep measured at each load step in a period of 15 minutes at F1 and F2, 60 Minutes at F3 and F4, and 120 minutes at F5 under the constant load. The deformation recorded at time steps of 1, 2, 5, 15, 30, 60, and 120 minutes in order to calculate the creep by the equation 4.2

The creep calculation in each step has been drawn in Figure 4.9 shows that the creep of the encapsulated length is lower than 1.0 mm in each load step and lower than 2.0 mm over the whole range of loading observation.



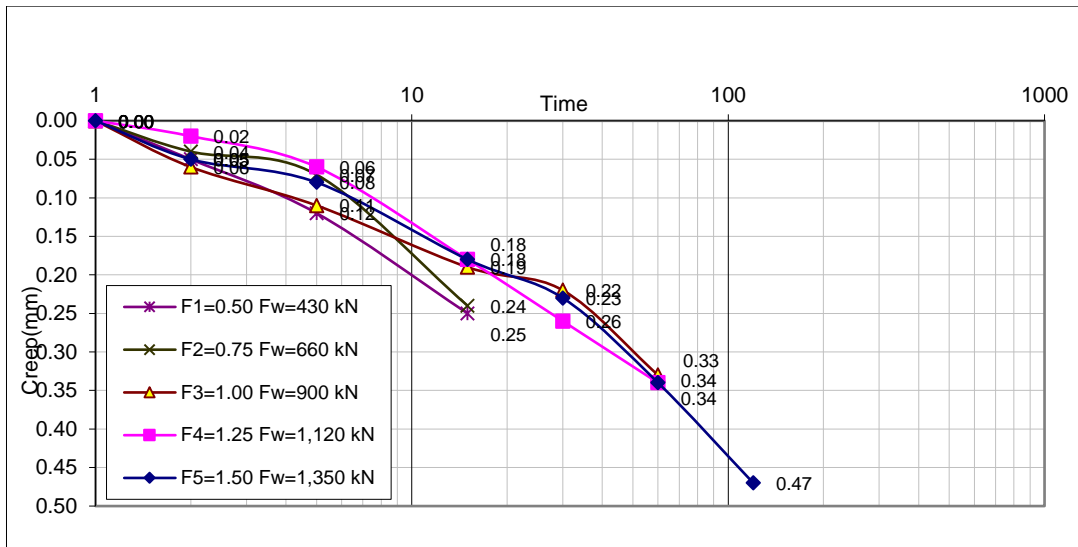


Figure 4.9. Creep result for the monobar tendon in the third experiment

Another criterion that has checked in this test was the residual deformation that is mostly related to the encapsulation length of the bolt. In this experiment  $\Delta L_{EI}$  was 8.97 mm that was less than 10 mm as the predetermined acceptable amount for residual deformation.

Figure 4.10 shows the development of the free length illustrating the decoupling of some part of the encapsulated length.

Very similar to the previous experiment, the free length of the tendons in this experiment was 10 meter but the graph in the Figure 4.10 show that the free length would be increased from 10 m at the beginning of the test at a load of Zero to 12.41 m at the proof load of 1,350 kN. The encapsulation length respectively would be decreased from 5 m in the starting point to 2.59 m at the end of the loading test. In other words, it means that the encapsulated length would be decoupled 2.41 m under the loading process.

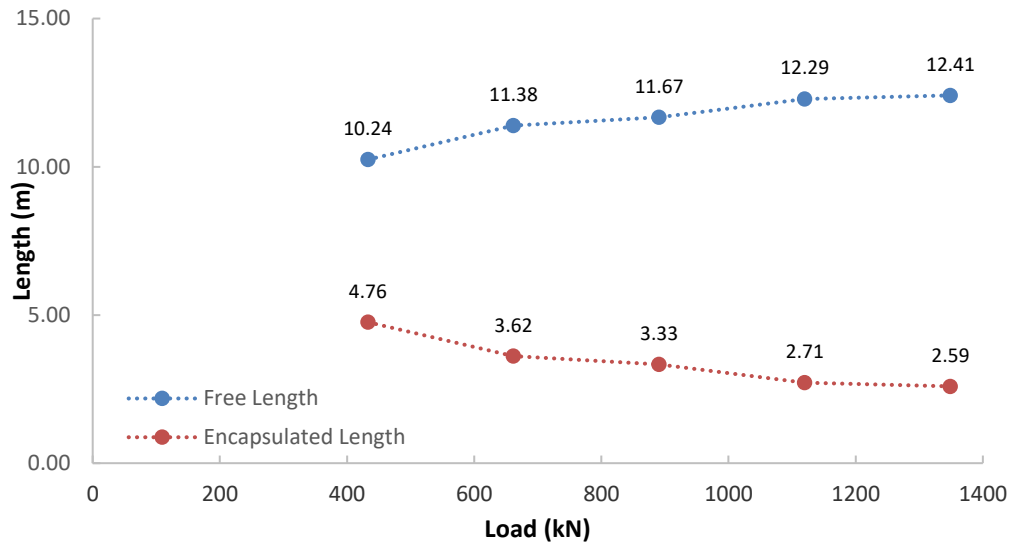


Figure 4.10. The free length and the encapsulation length under increasing loading on monobar tendon third experiment

#### 4.3.2.4. Fourth experiment on partially encapsulated rockbolts on a cavern crane runway beam

The fourth set of experiments have been carried out on a smaller size of rockbolts (monobars). These rockbolts installed on the overhead crane runway concrete beam of the underground Transformer cavern of the same project during the construction. The number of the rockbolts was 200 while 20 of them had been selected for the comprehensive stressing non-destructive test (CST) and the rest tested in the simple stressing non-destructive test (SST). The test procedure already has been discussed in 4.3.1 base on DIN-EN 1537 and DIN 4125. The properties of the monobars presented in table 4.7.

Table 4.7. Properties of the monobars for the fourth experiment

Type	Monobar	Total Length (m)	15
Yield Stress	950 MPa	Free Length (m)	11
Yield Load	525 kN	Encapsulated Length (m)	4
Ultimate Stress	1,050 MPa	Extra Free Length (m)	0.40
Ultimate Load ( $F_{ult}$ )	630 kN	Diameter (mm)	26.5
Young Modulus	205.94 kN/mm <sup>2</sup>	Cross section area (mm <sup>2</sup> )	552

The load steps of the tests presented in Table 4.8.

Table 4.8. Loading steps of the monobars in the fourth experiment

Load step	Load (kN)	Comment / Criteria
Initial Loading (Fa)	60	0.20 Fw
First loading step (F1)	158	50 Fw
Second loading step (F2)	235	0.75 Fw
Third loading step (F3)	315	1.0 Fw
Forth loading step (F4)	395	1.25 Fw
Fifth loading step (F5)	475	1.50 Fw
Working Load (Fw)	315	

The design working load for each of these tendons was  $F_w = 315$  kN that the rockbolts were locked-off on it after successful tests.

The profile of load-deformation of the fourth experiment has been depicted in Figure 4.11.

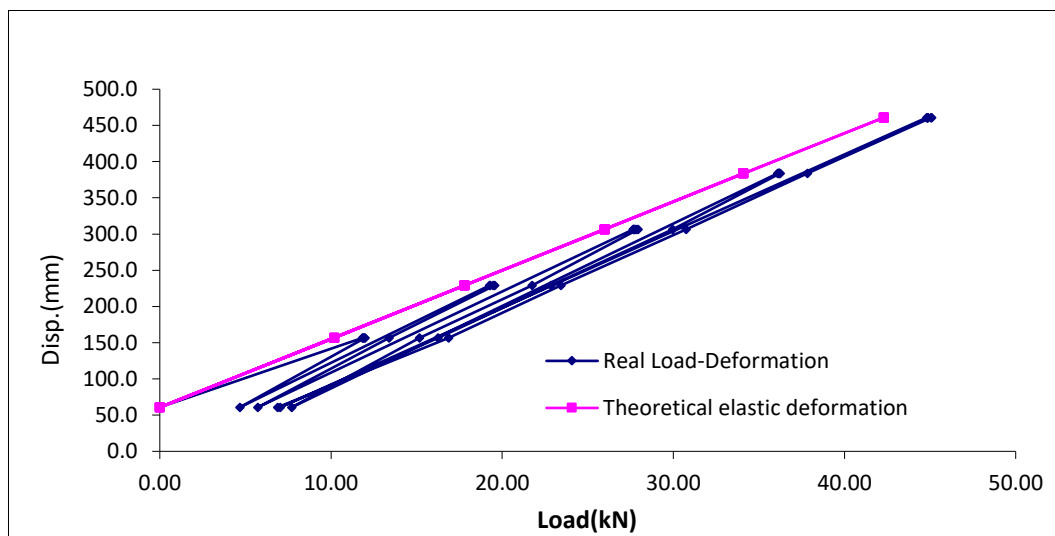


Figure 4.11. The profile of load-deformation of a rockbolt in the fourth experiment

Similar to the previous experiments, three criteria have been checked in each test including the creep, the residual (plastic) deformation after stressing, and the variation of the free length.

The creep measured at each load step in a period of 15 minutes at F1 and F2, 60 Minutes at F3 and F4, and 120 minutes at F5 under the constant load. The deformation recorded at time steps of 1, 2, 5, 15, 30, 60, and 120 minutes in order to calculate the creep by the equation 4.2. The calculated creep in each step concluded that the creep of the encapsulated length is lower than 1.0 mm in each load step and lower than 2.0 mm over the whole range of loading observation. Since the creep was not in the centre of interest of this research, the graphs have not depicted here.

Another criterion that has checked in this test was the residual deformation that is mostly related to the encapsulation length of the bolt. In this experiment,  $\Delta L_{EI}$  was 4.91 mm for one of the tests and 6.88 mm for another one. In all cases, they were less than 10 mm as the predetermined acceptable amount for residual deformation.

Very similar to the previous experiment, the free length of the tendons in this experiment was 10 meter but the graph in Figure 4.6 shows that the free length would be increased from 10 m at the beginning of the test at a load of Zero to 12.41 m at the proof load of 1,350 kN. The encapsulation length respectively would be decreased from 5 m in the starting point to 2.59 m at the end of the loading test. In other words, it means that the encapsulated length would be decoupled 2.41 m under the loading process.

Figure 4.12 shows the development of the free length illustrating the decoupling of some part of the encapsulated length.

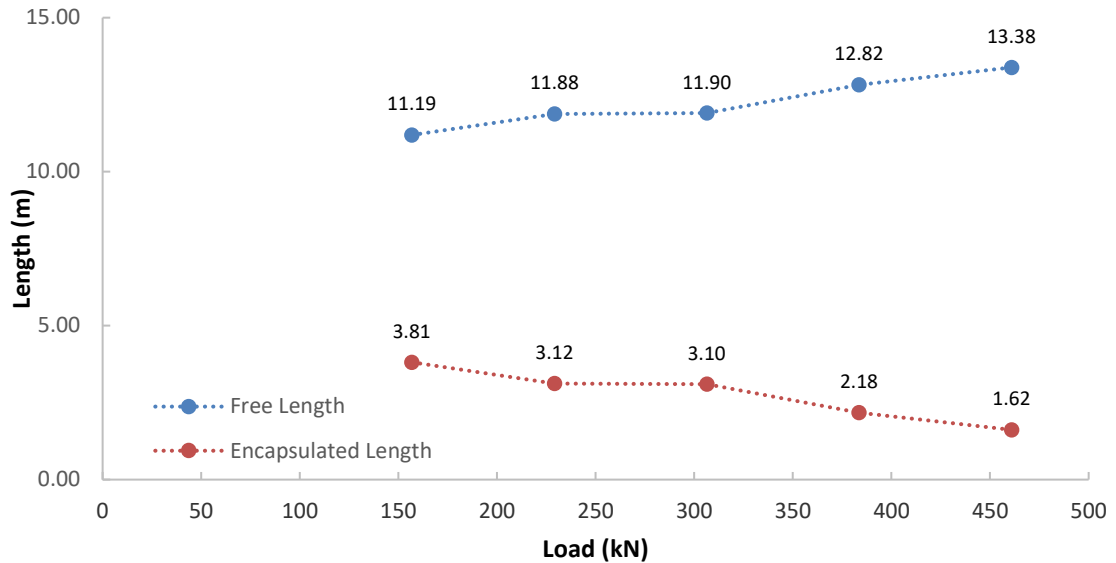


Figure 4.12. The free length and the encapsulation length under increasing loading condition on rock bolt fourth experiment

#### 4.4. SUMMARY AND RESULTS

As it is explained in this chapter and depicted in the figures the progress of the decoupling in the encapsulated length of a rockbolt is an inevitable consequence of loading phenomenon. Ground movement applies the load to the surface support on the tunnel wall, then it transfers to the shank of the rockbolt through the head arrangement including nut, bearing plate and pad. Transferring the load to the ground occurs through the initial segments of the encapsulation material (cement or resin) that is coupled the bolt to the ground. Induced movement in the coupled part transfers the load to the next segments concluding to activate anchorage in a certain portion of the encapsulated length of the rockbolt until diminishing the total applied load.

The concentration of the load over the beginning of the encapsulation length sometimes overcome the bond strength then the decoupling occurs in the bolt-cement or the cement-ground interface. Overcoming the bond strength is not a brittle failure because neither cement nor ground behaves in an elastic way. Moreover the available confinement and lateral stress over rockbolt that increases along with dilation of the encapsulation material increase the friction, therefore even

if the detachment occurs in the interface, the bond strength is still available because of the friction.

The explained experiments showing an obvious increase in the apparent free length that drives from the calculation of the elastic deformation recovered from the bolt during the unloading process. The phrase of “Apparent” refers to the fact that the calculated value for free length is not the exact free length of the rockbolt. In one hand, some part of the recovered deformation is related to elastic displacement of the ground that happens along with the encapsulated segments of the rockbolt due to the load transferred to the surrounding rock, while on the other hand there is some part of movement not recovered due to the friction in the interface of the detached bond.

The calculated apparent free values order show that the decoupling is not limited to only a few centimetres but it can be much greater than that. The coupled section is concerned with the decoupling failure, which is common at the rockbolt-grout interface. This fact shows the importance of the encapsulation length design that has to be considered in the first stage of design not only based on laboratory experiments but also practical field test plan.

## 5. ROCKBOLT BEHAVIOUR UNDER DYNAMIC (SEISMIC) CONDITION

### 5.1. INTRODUCTION

The energy dissipation capacity of a rockbolt depends on its deformation capabilities along with its load-bearing capacity. Rockbolts such as conventional steel rebar are strong with high load capacity, but normally they do not have much deformation capacity. These kinds of bolts are so-called strength bolts. Rockbolts such as split sets have a large capacity of deformation but they are not strong because they start to slip at a small applied load. The second type of rockbolts is so-called ductile rockbolts (Charlie Chunlin Li, 2010). Additionally, hot-rolled steel rebar rockbolts show an extension in length of yield under constant load followed by strain hardening (C. C. a. Li, 2017). This property of hot-rolled steel rebars is also useful for increasing the energy dissipation capacity of the rebar rockbolts.

Rockbolts have various kinds of anchoring mechanisms some of which will be discussed in the following sections. Ordinary rockbolts are those rebars which lie in a hole entirely coupled with the rock using cement or resin encapsulation. This type of bolt shows an appropriate stiffness under the loading stage of the bolt, but this kind of rockbolts have low deformation capacity. Specifically, a small amount of a local deformation due to a discontinuity opening overloads the related section and cause a local failure in the shank of the bolt. End anchoring or two-point anchoring of the rockbolts (using expansion shell) can increase the deformation capacity of the rockbolts by the distribution of the deformation of local expansions or discontinuity opening in the rock, over the whole free length of bolts. In this case, anchor movement (slip) due to load concentration on, or creep of, the anchor point could cause loading on the bolt shank being released. Partial anchoring (having a bond length at the end of the bolt) is a way to avoid the creep but the nut and bearing plate at the head of the rockbolt do not have enough load capacity under dynamic loading conditions (or even sometimes in static conditions) (MING Cai & Champaigne, 2009; C. C. Li et al., 2014; J. Player, Thompson, et al., 2009). Bearing face plate sometimes shows lower resistance in comparison to the rockbolt strength under the loading

conditions (Jan & Palape, 2007; C. C. Li et al., 2014; J. Player, Thompson, et al., 2009; T. Stacey, 2012). Ductile rockbolts such as split sets accommodate large ground deformation by slippage of their cylindrical surface over the borehole's wall and have a load capacity due to the available friction in-between which usually is not high enough. Other yielding bolts such as Swellex, Cone bolt, D-bolt, Garford, etc. are more expensive and need special equipment to install as well as trained operators.

Ideal yielding rockbolts are those that have both high strength and large capacity of deformation. The area under the curve of load-deformation of a reinforcement element during the process of loading replicates the amount of energy that the element can dissipate. As a rule, the more area under the curve that a support element has, the more energy dissipation capacity it has. Therefore increasing the deformation capacity of a rockbolt without reducing its ultimate strength will increase its energy dissipation capacity as well as increasing the ultimate strength of a bolt-type without reducing its deformation capability.

For a mine support design, it is a necessary step to find the capacity of a rockbolt and in dynamic condition, the energy absorption capacity of a bolt is focused. There are different testing facilities to test and measure the bolt capacity but because of different reasons, none of them is similar to others. Therefore, their results are not completely comparable with each other but still, they can provide information for the designer to have an index or guide for design considering all inconsistencies in results. In this chapter different behaviour of rockbolt under dynamic loading is discussed. A significant part of the data has been achieved by Direct Impact tests of DIT.

## **5.2. EXPERIMENTS WITH NEW CONCEPT MINING DYNAMIC IMPACT TESTER**

The experiments in this research have been done in drop testing facility of the New Concept Mining of South Africa. The drop testing facility called New Concept Mining Dynamic Impact Tester (NCM DIT) is one of the most qualified testing machine constructed in the laboratory of New Concept Mining Company in South Africa. New Concept Mining (NCM) has built up the Dynamic Impact Tester (DIT) equipped for testing rockbolts, without any interferences to mining tasks. The restrictions of the



dynamic axial load testing strategy are known, however, the DIT gives a proficient facility, on which an enormous number of reinforcement elements can be evaluated under controlled conditions.

During the quick improvement of new rockbolt items, it is significant to evaluate the impacts of high strain rates applied by rockburst on ground support systems. Further explanation of the testing machine its development history, mechanical structure, dynamic component, instrumentation, etc. presented by Knox and Berghorst (2018)

### **5.3. THE BEHAVIOUR OF THE ROCKBOLTS UNDER DIFFERENT APPLIED PARAMETERS**

In this section different behaviour of the several types of rockbolts have been discussed. The effect of the magnitude of the applied energy of multiple drops, number of drops, the length of the bolts, and the velocity of the impacts are the parameters that have been discussed.

#### ***5.3.1. INTRODUCING THE ROCKBOLT TYPES***

Different types of rockbolt and mechanisms have been tested in this research. First, a short explanation of the rockbolts types and the mechanisms explained then the detail of experiments is discussed. A significant portion of experiments has been carried out over rockbolts produced by New Concept Mining rockbolts including Par1 Bolt, Par1 Resin Bolt, MP1 bolt, and Vulcan Bolt. Following subchapters contain the description of each of these Bolts.

##### ***5.3.1.1. Par1***

The Par1 Bolting system is an end-anchored yielding bolt that is grouted post-installation and can be supplied with attachment points for meshing and lacing. The end anchor provides immediate support upon installation and two pairs of double paddles act as additional anchors once the bolt is grouted.

The Par1 Bolt with 16mm, 18mm or 20mm bar has been tested in this research. The unit has an elongation of 23% in static conditions and 15% under dynamic loading. The unit is provided with a collapsible load indicator to confirm correct

tensioning of the unit when installed. The end of the bolt protruding from the hole has a threaded section over which a washer is placed and held in place by a nut, which is also used for pre-tensioning of the unit. A specially designed seal ensures easy grouting of the installed Par1 with minimal spillage of grout during pumping. An optional non-return valve can be incorporated in the grout seal to prevent any leakage of grout once the pumping system is disconnected.

The Par1 Bolt can be used when the following parameters are requested by the ground condition.

- High yield ability
- High energy absorption
- Fully mechanised or manual installation and grouting
- Immediate support
- Pre-tensionable with load indicator
- Easy grouting with no spillage
- Includes attachment points for meshing and lacing directly onto the bolt

Table 5.1. Par1 Bolt Performance specifications

	Ø16	Ø18	Ø20
Dimensional Specifications			
Bar diameter	Ø16.3mm, DIN 405 RD 18	Ø18.3mm, DIN 405 RD 20	Ø20.3mm, DIN 405 RD 22
Length of bolt	1.0m to 3.0m	1.0m to 3.0m	1.0m to 3.0m
Typical length of thread (adjustable)	300mm	300mm	300mm
Steel Specifications			
Yield strength typical	500MPa	500MPa	500MPa
Yield load typical	100.5kN	127kN	157kN
Ultimate tensile load typical	128kN	162kN	229kN
Elongation*			
Average	26.13%	26.13%	26.13%
Standard deviation	2.17%	2.17%	2.17%
Guaranteed static	15% to 30%	15% to 30%	15% to 30%

\*Tested as per SANS 6892-1:2010 (Ed. 1.00)

The typical quasi-static load-deformation behaviour of the Par1 bolt has been depicted in Figure 5.1.

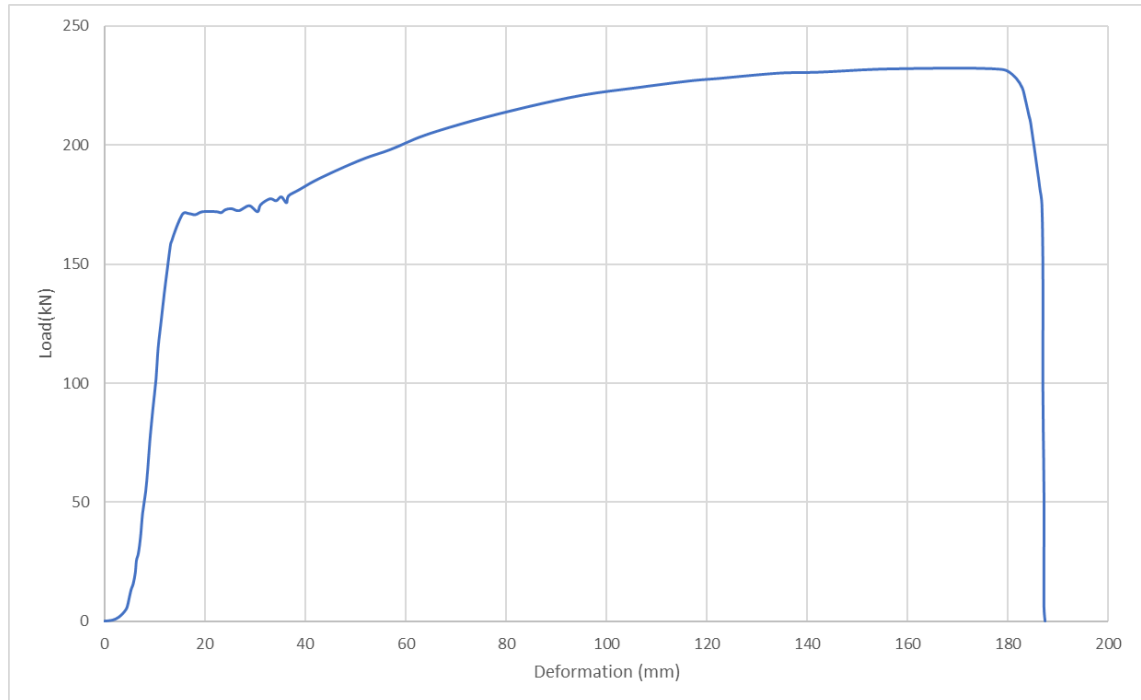


Figure 5.1. Typical Quasi-Static Performance of a Par1 Bolt  
2.2m long (1.3m between paddles)

#### 5.3.1.2. Par1 Resin Bolt

The Par1 Resin Bolt is a resin or grout anchored yielding bolt considering (in case) attachment points for meshing and lacing.

The resin provides the anchor with immediate support upon installation for tensioning. The anchor has a pair of five paddles which assist in the mixing of the resin and act as additional anchors when the resin is set.

The Par1 Resin Bolt with 16mm, 18mm or 20mm bar is tested in this research. The unit has an elongation of 23% in static conditions and 15% under dynamic loading. The unit is provided with a collapsible load indicator to confirm correct tensioning of the unit when installed, and to assist in post auditing of the installation.

The end of the bolt protruding from the hole has a threaded section over which a washer is placed and held in place by a nut. The nut is also used for pre-tensioning of

the unit. The Par1 Resin Bolt is supplied with a shear pin to facilitate spinning prior to pre-loading. The pin shears to facilitate the tensioning process.

The bolt can be used when the following parameters are requested by the ground condition:

- High yield ability
- High energy absorption
- Immediate support
- Pre-tensionable with load indicator
- Includes attachment points for meshing and lacing directly onto the bolt

Table 5.2. Par1 Resin Bolt Performance Specifications

	Ø16	Ø18	Ø20	Ø22	Ø25
Dimensional Specifications					
Bar diameter	Ø16.3mm, DIN 405 RD 18	Ø18.3mm, DIN 405 RD 20	Ø20.3mm, DIN 405 RD 22	Ø22.3mm, DIN 405 RD 24	Ø25.2mm, DIN 405 RD 27
Length of bolt	1.0m to 3.0m	1.0m to 3.0m	1.0m to 3.0m	1.0m to 3.0m	1.0m to 3.0m
Typical length of thread (adjustable)	170mm	170mm	170mm	170mm	170mm
Steel Specifications					
Yield strength typical	500MPa	500MPa	500MPa	500MPa	546MPa
Yield load typical	100.5kN	127kN	157kN	208kN	268kN
Ultimate tensile load typical	128kN	162kN	229kN	289kN	356kN
Elongation*					
Average	26.13%	26.13%	26.13%	25.4%	25.4%
Standard deviation	2.17%	2.17%	2.17%	2.17%	2.17%
Guaranteed static	15% to 30%	15% to 30%	15% to 30%	15% to 30%	15% to 30%

\*Tested as per SANS 6892-1:2010 (Ed. 1.00)

The typical quasi-static load-deformation behaviour of the Par1 Resin bolt has been depicted in Figure 5.2.

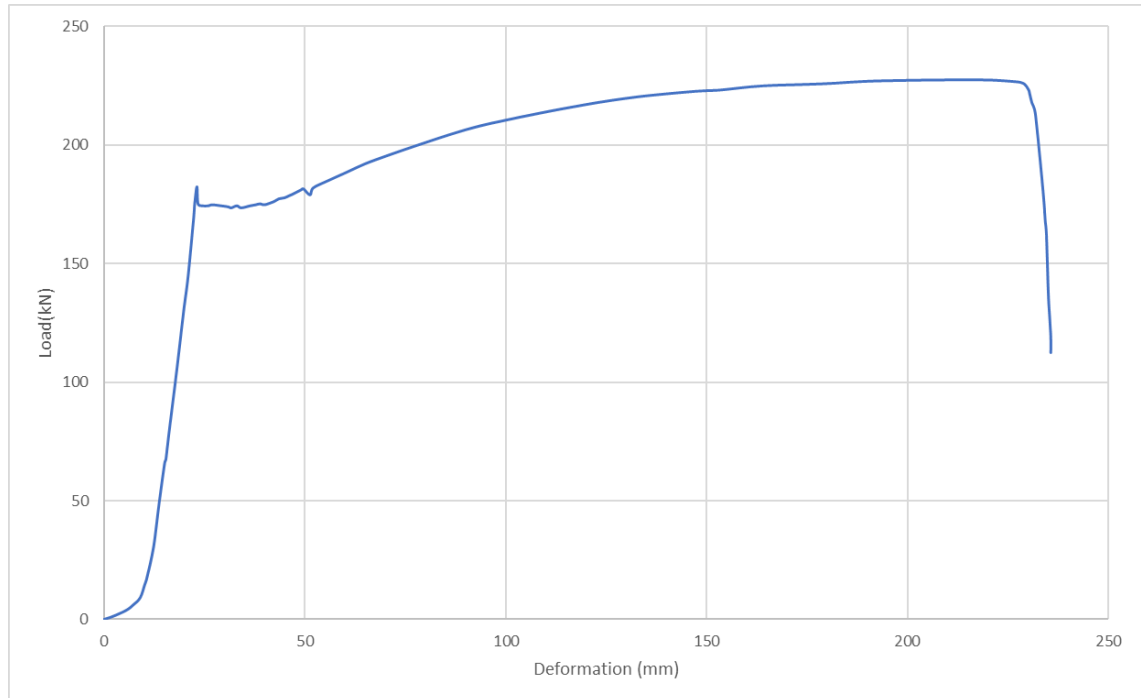


Figure 5.2. Typical Quasi-Static Performance of a 2.7m Par1 Resin Bolt

### 5.3.1.3. MP1 Bolt

The MP1 Bolting system is a mechanised end-anchored yielding bolt that is grouted post-installation. The end anchor provides immediate support upon installation and two pairs of double paddles act as additional anchors once the bolt is grouted. The end anchor is shielded by a grouting sleeve which is activated on the collapse of the grout sleeve spacer.

The MP1 has been tested with 16mm, 18mm or 20mm bar diameter in this research. The unit is provided with a collapsible load indicator to confirm correct tensioning of the unit when installed.

The end of the bolt protruding from the hole has a threaded section over which a washer is secured by a nut, which is also used for pre-tensioning of the unit. A specially designed sleeve ensures easily mechanised or manual grouting of the installed MP1 with minimal spillage of grout during pumping.

This bolt can be used when the following parameters are requested by the ground condition.

- Very High yield ability
- Very High energy absorption
- Immediate support
- Pre-tensionable with load indicator
- Easy grouting with no spillage
- Can include an alternate faceplate with attachment points for meshing and lacing directly onto the bolt

Table 5.3. MP1 Performance Specifications

	Ø16	Ø18	Ø20
Dimensional Specifications			
Bar diameter	Ø16.3mm, DIN 405 RD 18	Ø18.3mm, DIN 405 RD 20	Ø20.3mm, DIN 405 RD 22
Length of bolt	1.0m to 3.0m	1.0m to 3.0m	1.0m to 3.0m
Typical length of thread (adjustable)	300mm	300mm	300mm
Steel Specifications			
Yield strength typical	500MPa	500MPa	500MPa
Yield load typical	100.5kN	127kN	157kN
Ultimate tensile load typical	128kN	162kN	229kN
Elongation*			
Average	26.13%	26.13%	26.13%
Standard deviation	2.17%	2.17%	2.17%
Guaranteed static	15% to 30%	15% to 30%	15% to 30%

\*Tested as per SANS 6892-1:2010 (Ed. 1.00)

The typical quasi-static load-deformation behaviour of the MP1 bolt has been depicted in Figure 5.3.

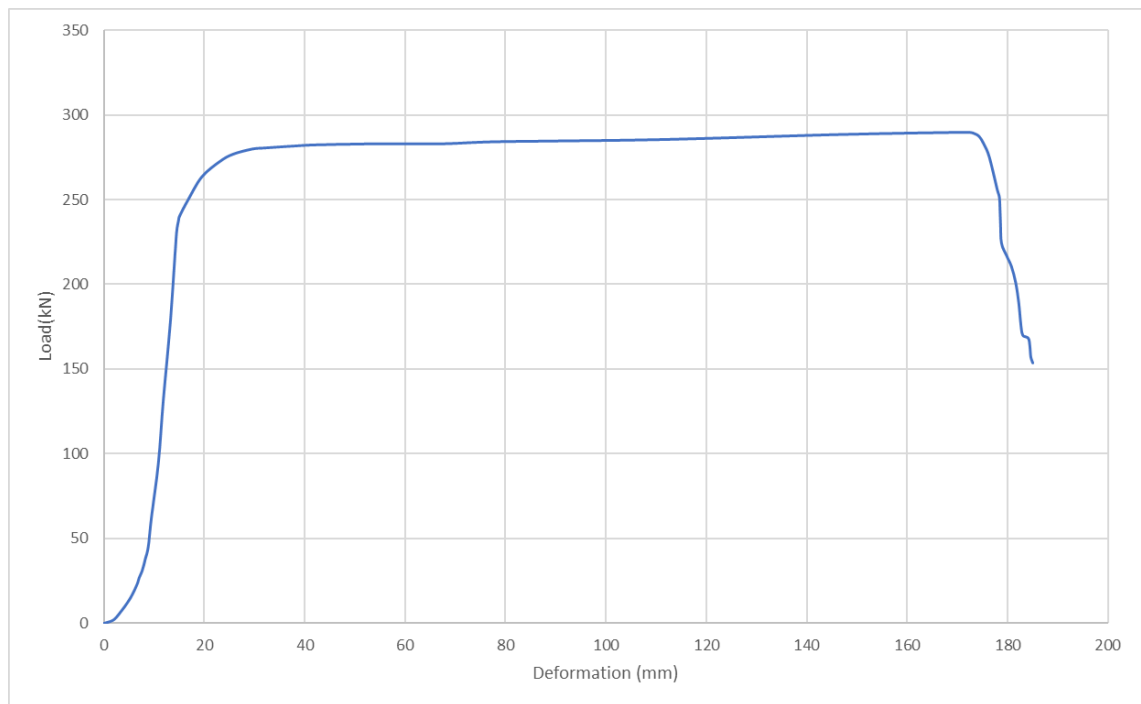


Figure 5.3. Typical Quasi-Static Performance of a Ø20 MP1 2.7m long (1.8m between paddles)

#### 5.3.1.4. *Vulcan bolt*

The Vulcan Bolt is an integrated primary and secondary support system, that offers instantaneous support, with full load capacity on installation. The unique design creates an active support system with a full column frictional bond without the use of resin or grout and also gives excellent resistance to shear. This system provides a consistent load performance over a range of hole sizes, with the ability to accommodate an irregular rock face.

The Vulcan Bolt delivers improved efficiency to the current support cycle. The system can be installed with mechanised equipment, and an auditable, positive clamping force is introduced into the rock mass. The Vulcan Bolt support system will accommodate a secondary mesh washer (either push on or screw on).

The Vulcan Bolt is pre-tensioned by tightening the nut. A collapsible load indicator is provided to confirm correct tensioning when installing.

Depend on the application the Vulcan Bolt can be employed in lengths from 0.9m up to 3.0m.

Table 5.4. Vulcan Bolt Performance Specifications

Bolt Diameter (mm)	Ø18	Ø20
Peak Load (kN)	175	210
Frictional Unit Diameter (mm)	Ø39 or Ø46	Ø39 or Ø46
Hole Size Range (mm)	36 – 38 for Ø39 43 – 45 for Ø46	36 – 38 for Ø39 43 – 45 for Ø46

The typical quasi-static load-deformation behaviour of the Vulcan bolt has been depicted in Figure 5.4.

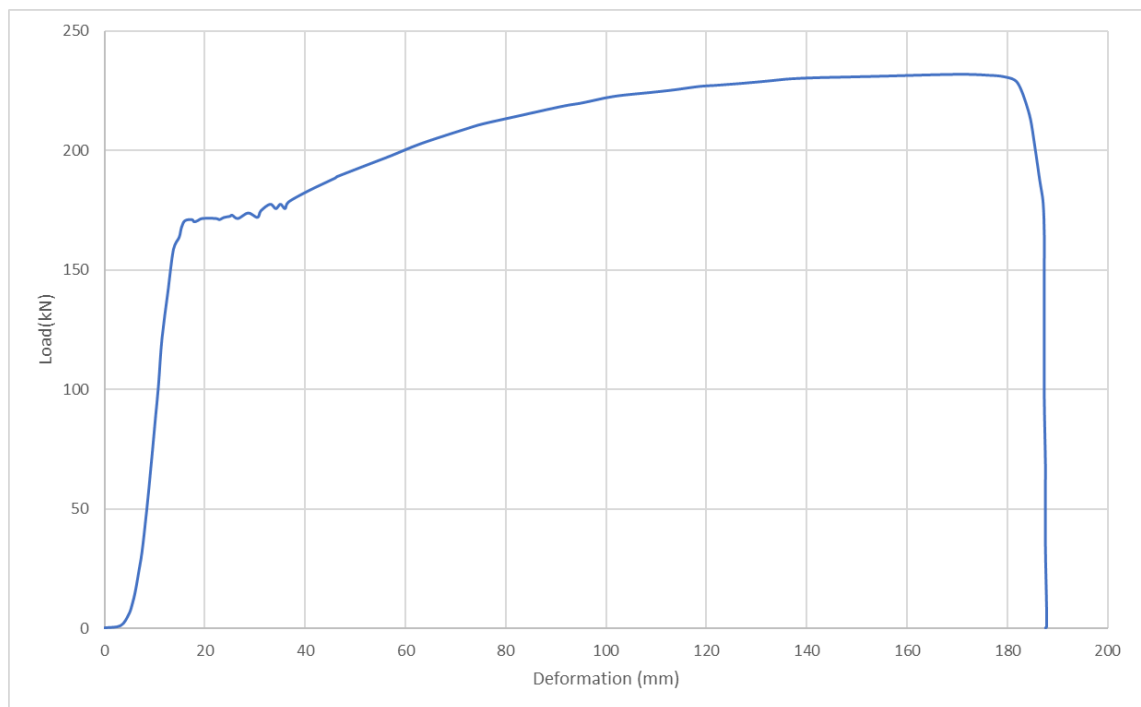


Figure 5.4. Typical Quasistatic Bar Performance (1.3m Vulcan Bolt)

### 5.3.2. THE BEHAVIOUR OF REBAR UNDER DYNAMIC IMPACT TEST

As a rule, when the velocity of loading goes up, higher maximum loading capacity is expected. Comparison between the behaviour of rebar under the static loading test and dynamic impact test clearly depict this phenomenon, as shown in Figure 5.5.



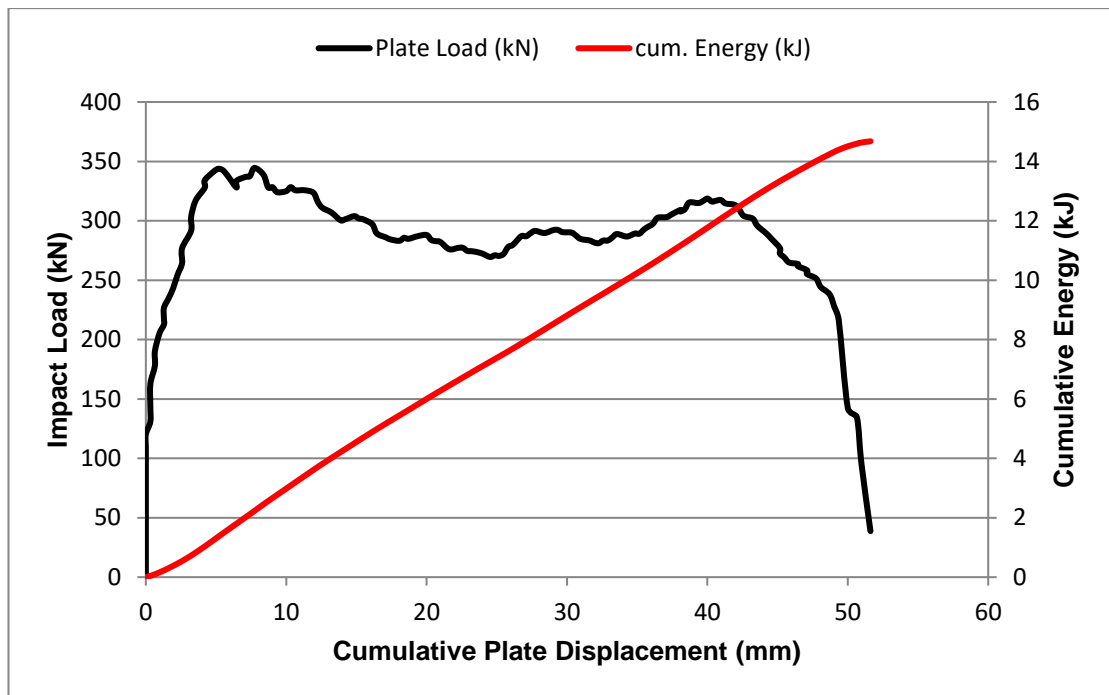


Figure 5.5. Cumulative Displacement and Energy of rebar subjected to drop test

As it can be seen in the graph, the maximum load impact load applied to the bolt reaches 345 kN while rebar under static loading condition can just tolerate 190 kN. Additionally, the total deformation of the bolt reached to about 52 mm while it is about 25 mm to 35 mm in a static loading test.

To calculate the absorbed energy, the plate displacement must be rectified with reducing the toe displacement. The graph depicted in Figure 5.6 shows the Impact load and displacement versus plate load and toe displacement.

The graph depicted in Figure 5.7 shows the dynamic capacity of three different rebars with a diameter of 18, 20, and 22mm subjected to dynamic drop load. The applied impact energy was about 30.1 kJ, while every bolt has failed with receiving about 11.3 to 15.1 kJ of energy before the failure.

The number of the test was not enough to conclude, as it can be seen, increasing the diameter of the rebar had not much effect on energy absorption capacity or even the total deformation capacity of the bolt. Of course, it needs more dynamic tests to have a statistically accepted number of the test to be able to have a reliable result and conclusion. The obvious fact is the significant increase in energy

absorption/dissipation capacity of the bolts under the dynamic loading condition in comparison to that of the static loading test.

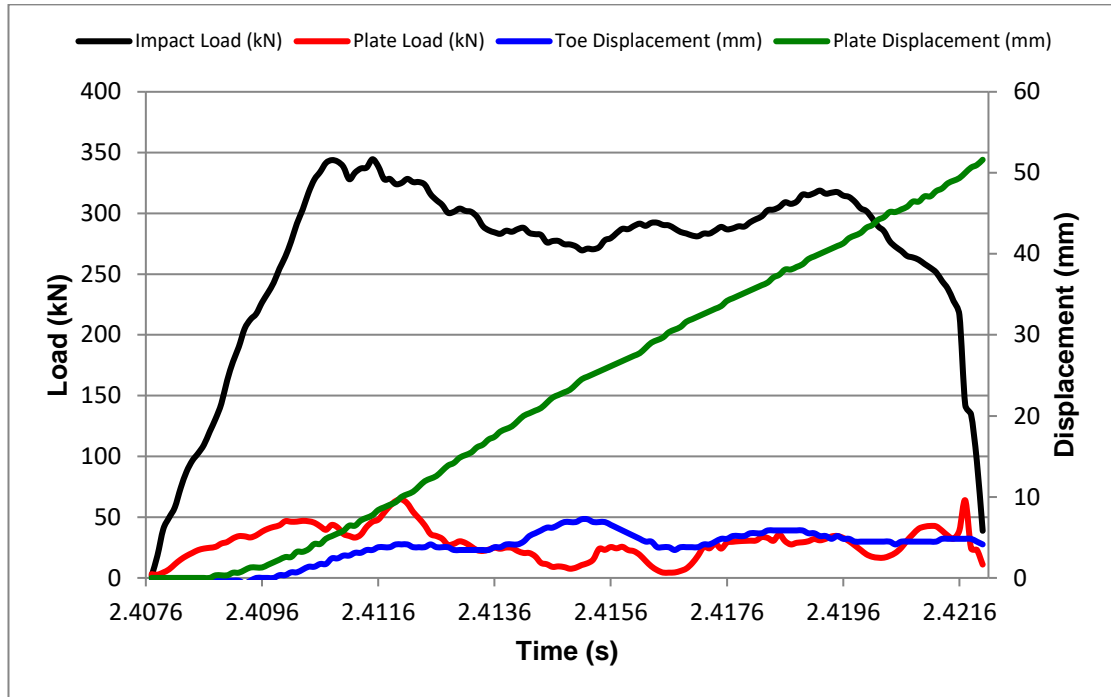


Figure 5.6. Impact load, Plate load, Toe displacement, and Plate displacement of rebar subjected to a drop test

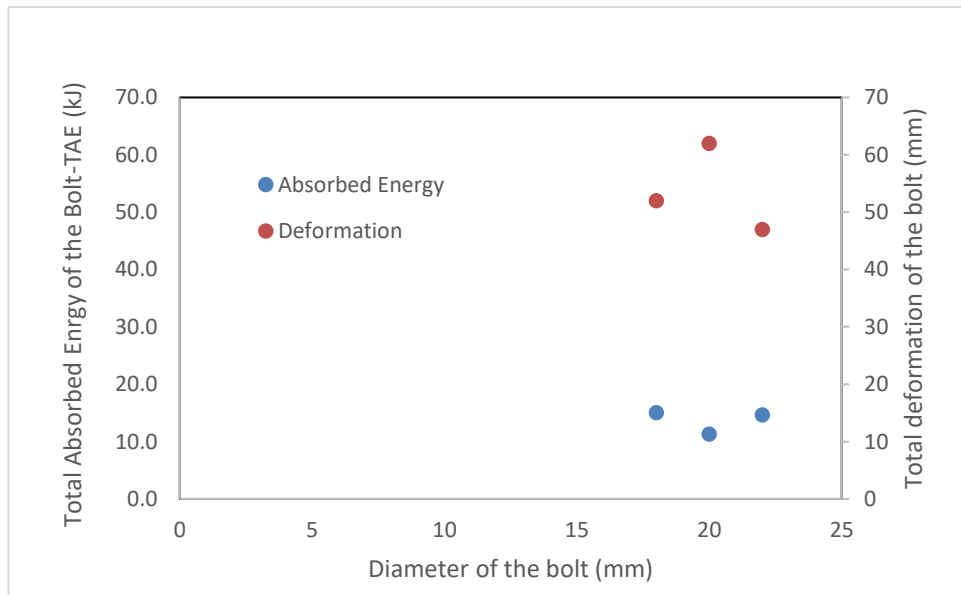


Figure 5.7. Dynamic Capacity of the Rebar subjected to dynamic Drop load

### **5.3.3. THE BEHAVIOUR OF THE DYNAMIC BOLTS CONCERNING THE APPLIED ENERGY OF THE MULTIPLE DROPS AND NUMBER OF DROPS**

To assess the effect of the multiple drops on energy absorption of the Vulcan Bolt 104 drops in 52 sets of multiple drops have been carried out. This experiment started by multiple dropping of the weight of 1,181 kg from the height of 1.5 m over the bearing plate of the rockbolt. The drop weight reaches a velocity of 5.43 m/s and produces impact energy of 17.4 kJ. The bolts were with 2 m length and 20 mm diameter cast in continuous steel tubes and by receiving a number of 3 or 4 impacts failed. Bolts in this experiment have a capacity of dissipating average impact energy of 49.7 kJ with 170.9 mm elongation in length. The experiment continued by increasing the weight or height or a combination of the both including the impact energy increments of 23.4 kJ, 30.3 kJ, 40.1 kJ, in which mostly failed by two drops while increasing the impact energy to 46.7 kJ concluded to failure of the most specimens at first drop. Total energy absorption/dissipation of the bolt in such condition have been accumulatively calculated as the energy absorption capacity and measured the accumulative deformation as maximum deformation capacity of each bolt.

The results show that increasing the amount of impact lead the bolt to earlier failure. As it can be seen in Figure 5.8 a lower total energy absorption capacity have been calculated in cases of stronger impacts. On the other hand, although the deformation capacity changes and increases the total amount of the occurred deformation, it stays in a range of 170 to 180 mm.

The calculation and graphs prepared for all drops as well as the average energy and deformation capacity measurement in each category of applied energy. The averaged measured capacities give a better understanding of the decrease in energy dissipation capacity and increase in deformation capacity of the bolt because the number of tests in each group was not the same, therefore, in order to avoid the error of the weighting, the average capacities have to be considered. Figure 5.9 to Figure 5.13 show the interpreted results.

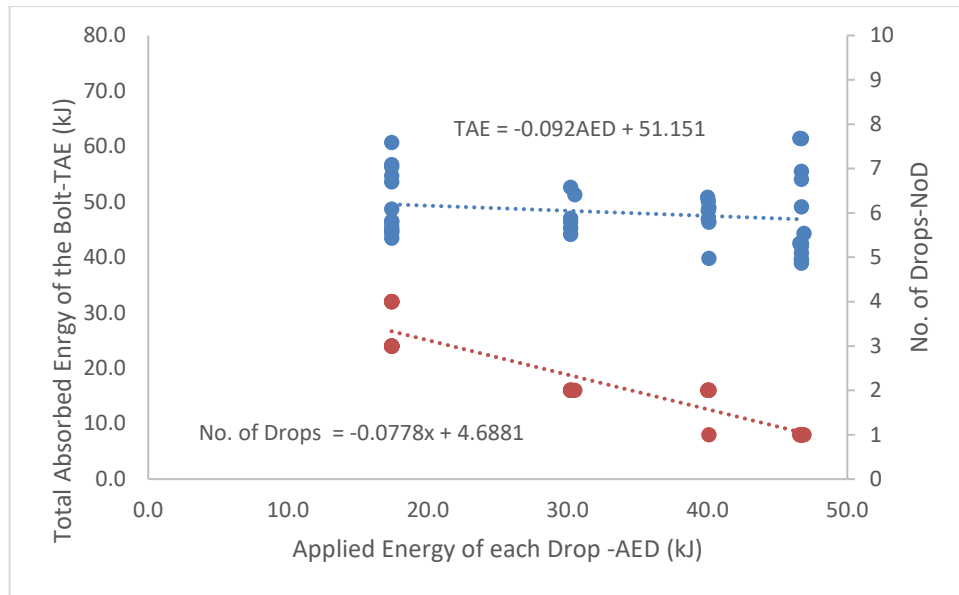


Figure 5.8. Dynamic Capacity of the VB-D20-L2.0 bolt subjected to multiple Drops

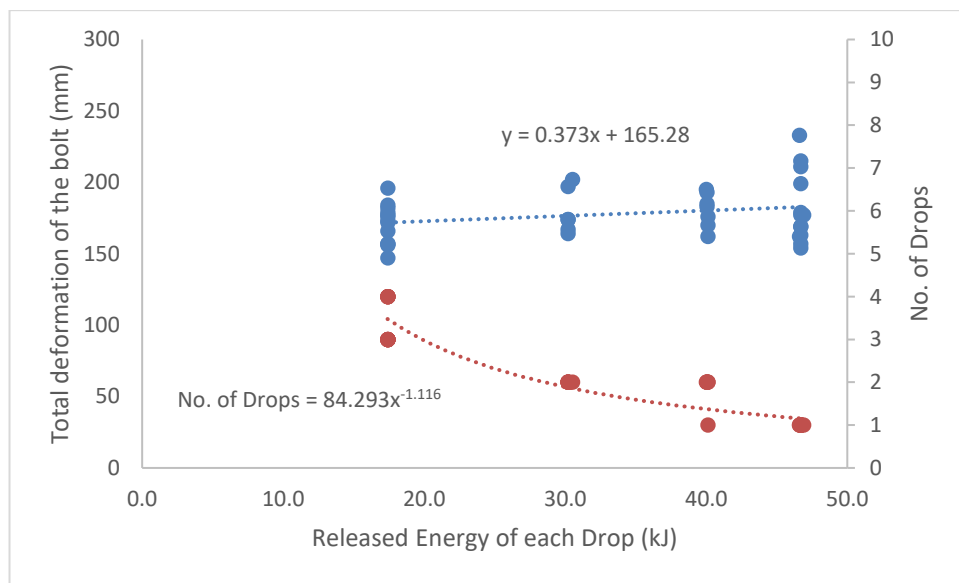


Figure 5.9. Total deformation of the VB-D20-L2.0 bolt in respect to the applied energy of multiple Drops and number of Drops

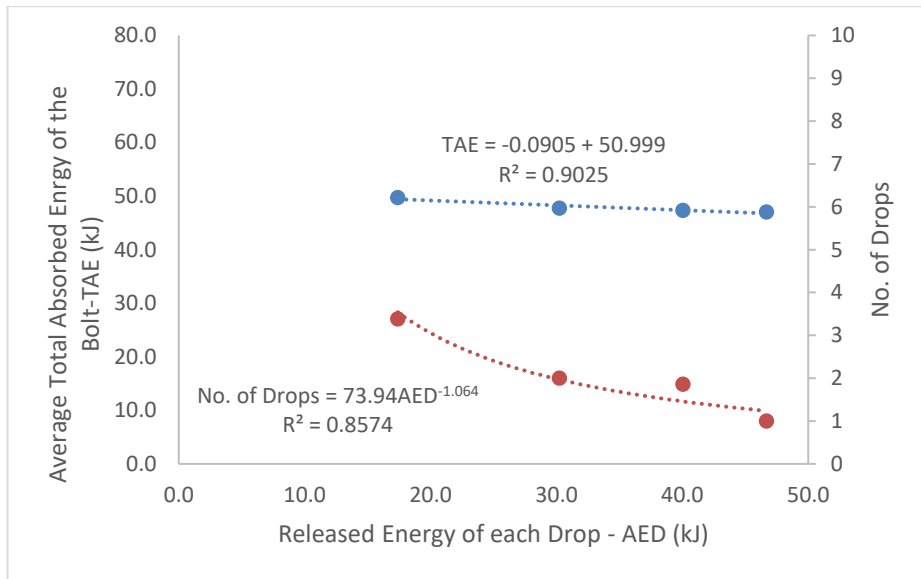


Figure 5.1. The total absorbed energy of the VB-D20-L2.0 bolt in respect to the applied energy of multiple Drops and number of Drops

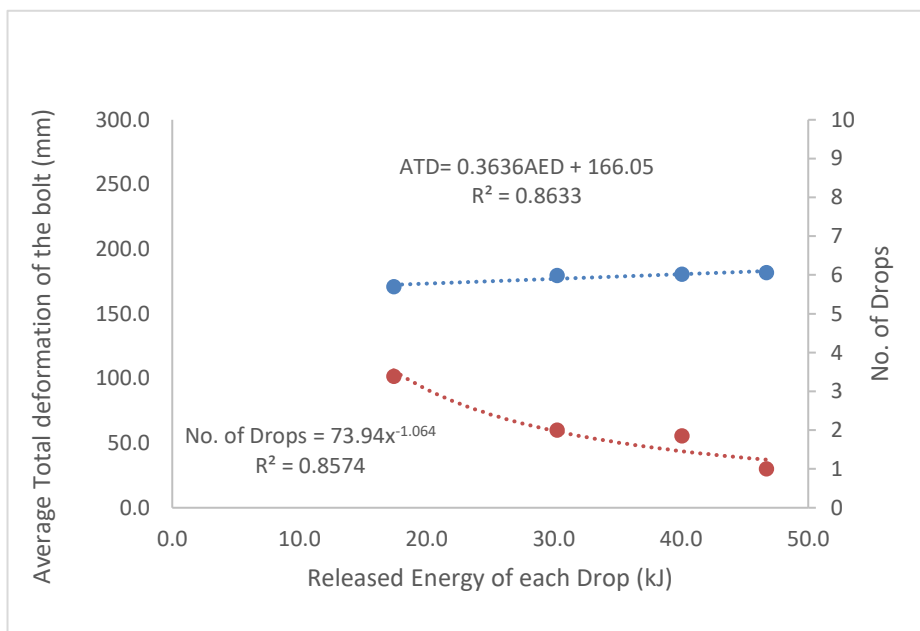


Figure 5.2. Total deformation of the VB-D20-L2.0 bolt in respect to the applied energy of multiple Drops and number of Drops

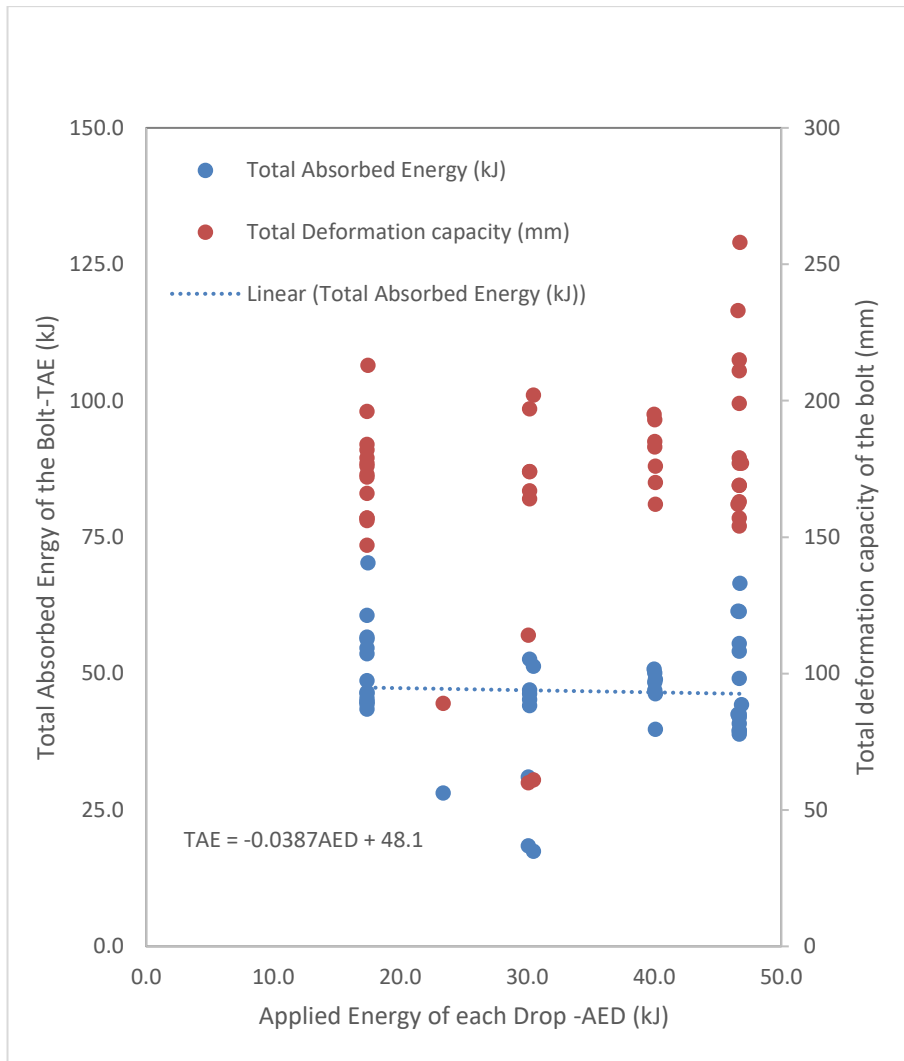


Figure 5.3. Dynamic Capacity of the VB-D20-L2.0 bolt subjected to multiple Drops

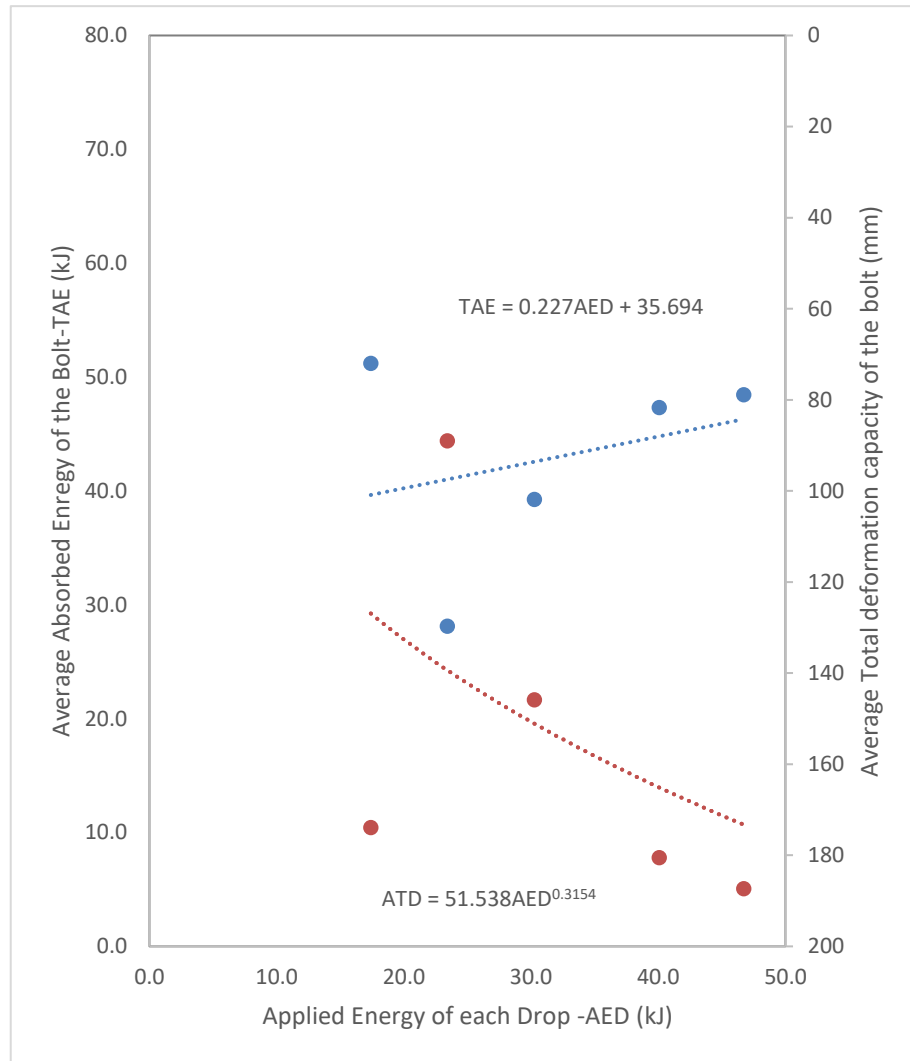


Figure 5.4. Dynamic Capacity of the VB-D20-L2.0 bolt subjected to multiple Drops

Some other experiments have been carried out on other types of the bolts so-called MP1 while the results show similar behaviour. The structure of an MP1-2024 bolt presented by Knox and Berghorst (2018).

The MP1-2024 is a 2.4 m  $\varnothing$ 20 mm yielding rockbolt. Upon insertion, the shell at the distal end of the bolt is ejected from the grout sleeve, providing a mechanical anchor against which pretension can be applied. A grouting nozzle placed over the grout sleeve allows the grout to be pumped up the internal bore of the sleeve, then back down through the bore of the hole, providing a full column. Once the grout is cured, the paddle pairs at the distal and proximal ends of the bar form anchor point between the grout and the rockbolt. During squeezing or a rockburst, the bar

between the paddles de-bonds from the grout, absorbing the energy via deformation.

The MP1-2024 was tested in a split tube configuration where the load was indirectly applied to the tendon. The load applied to the lower split tube is transferred through the grout to the proximal paddle set and measured by Plate Load Cell and Impact Load Cell (Figure 5.14).

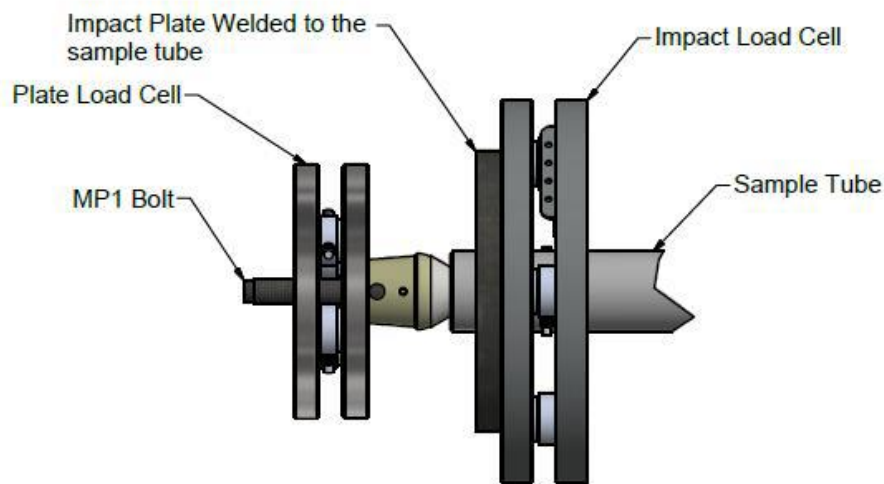


Figure 5.14. Illustration of the MP1 Split Tube Instrumentation (Loadcell)

A total number of 120 drops included in 38 multiple drops on the bolts that had a length of 1.8 to 3.0 meter, a diameter of 20 mm and resin encapsulated have been tested. The drops categorized with applied impact energies of 8.1, 17.4, 30.2, 37.4, and 46.7 kJ.

As shown in following Figures 5.15 to 5.20 the bolts energy dissipation capacity was dropped by increasing the impact energy from accumulative energy dissipation capacity of 64.4 kJ to 48.8 kJ while accumulative deformation capacity was in an average range of 177 to 202 mm. obviously, the number of drops in each multiple drops test set decreased with the increase of the applied impact energy. This behaviour can be seen in the following graphs.



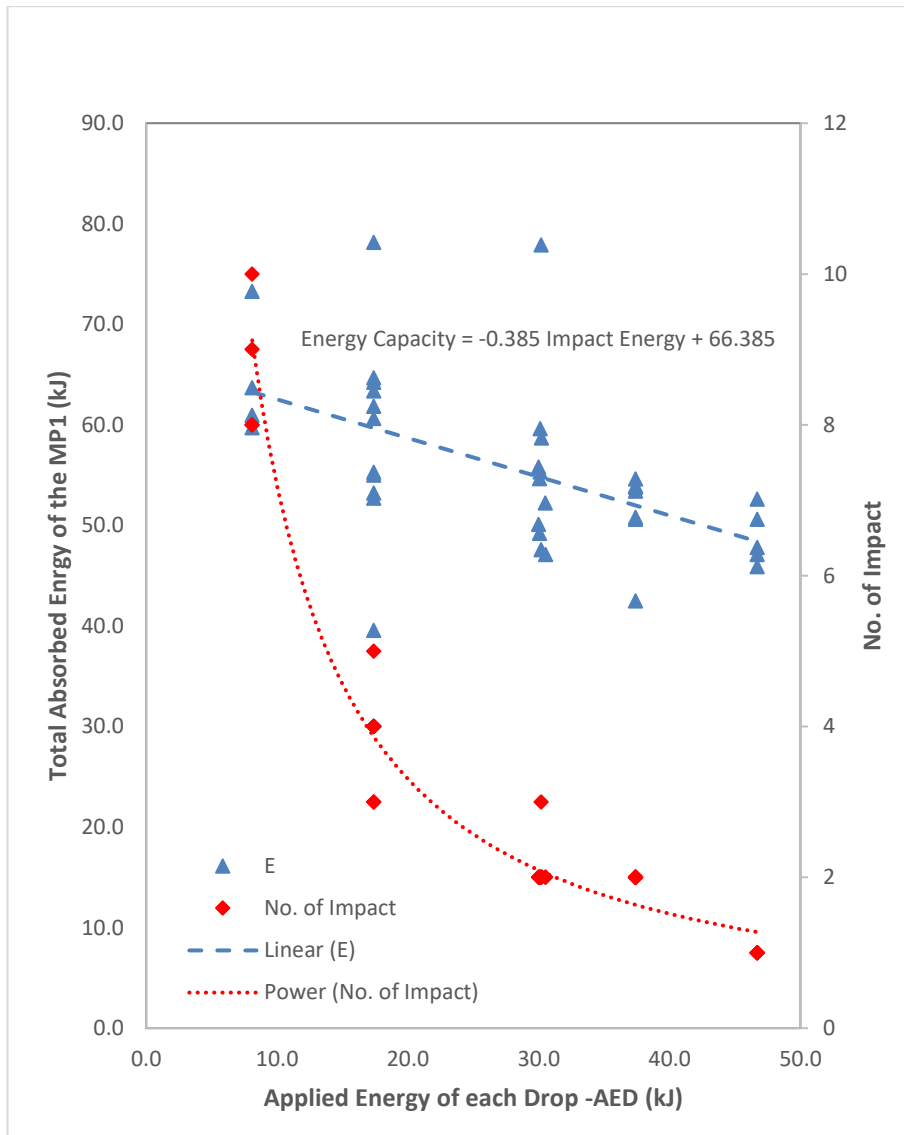


Figure 5.15. Dynamic capacity of the MP1 bolt subjected to multiple drops

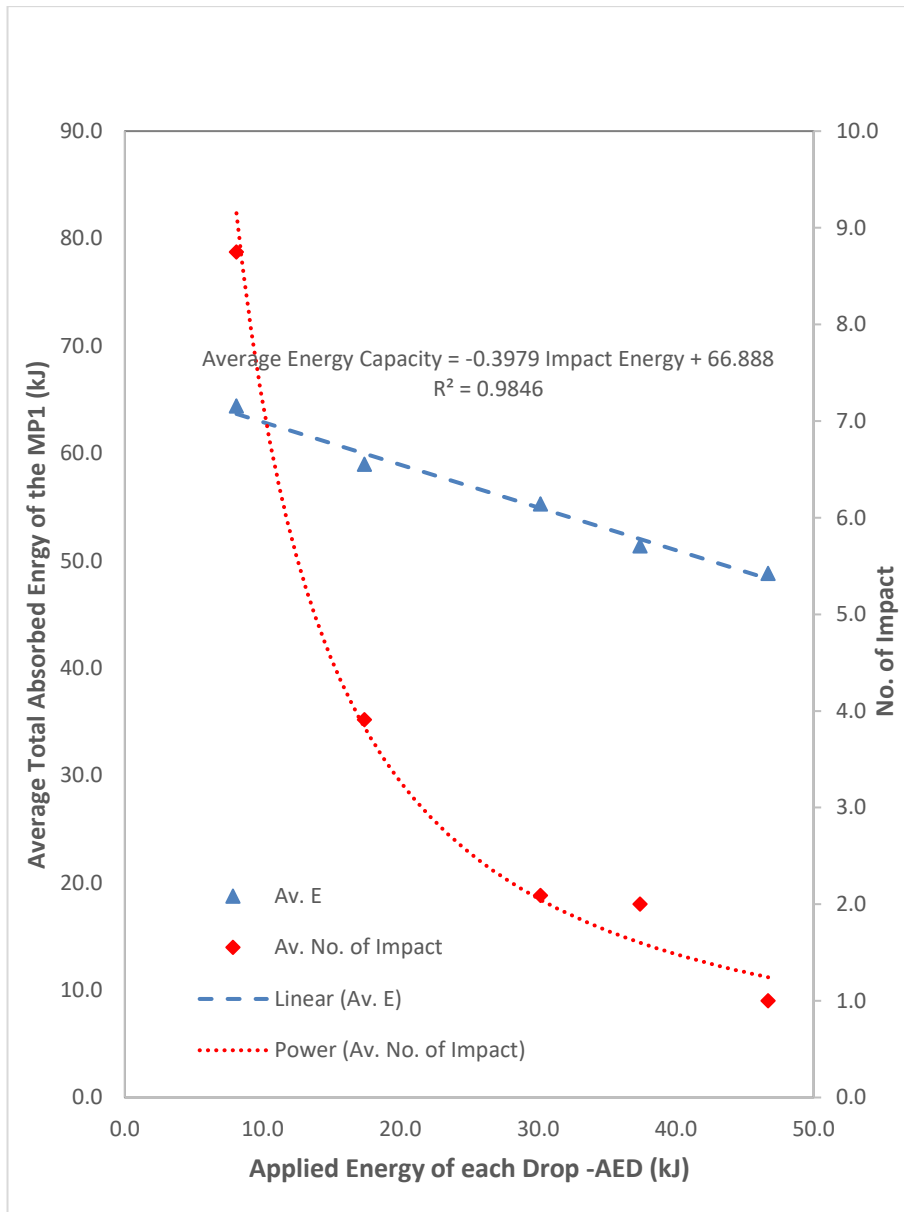


Figure 5.16. Dynamic capacity of the MP1 bolt subjected to multiple drops

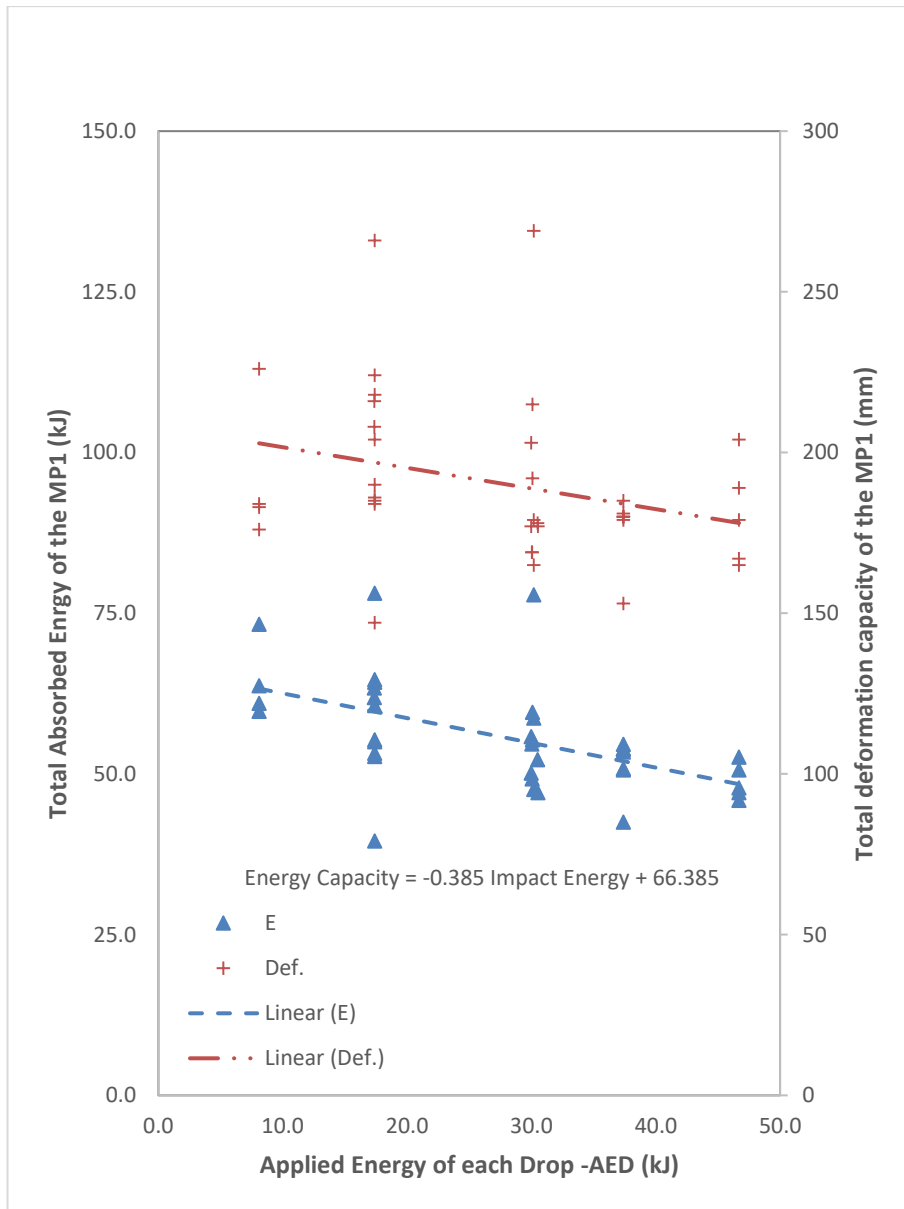


Figure 5.17. Dynamic capacity of the MP1 bolt subjected to multiple drops

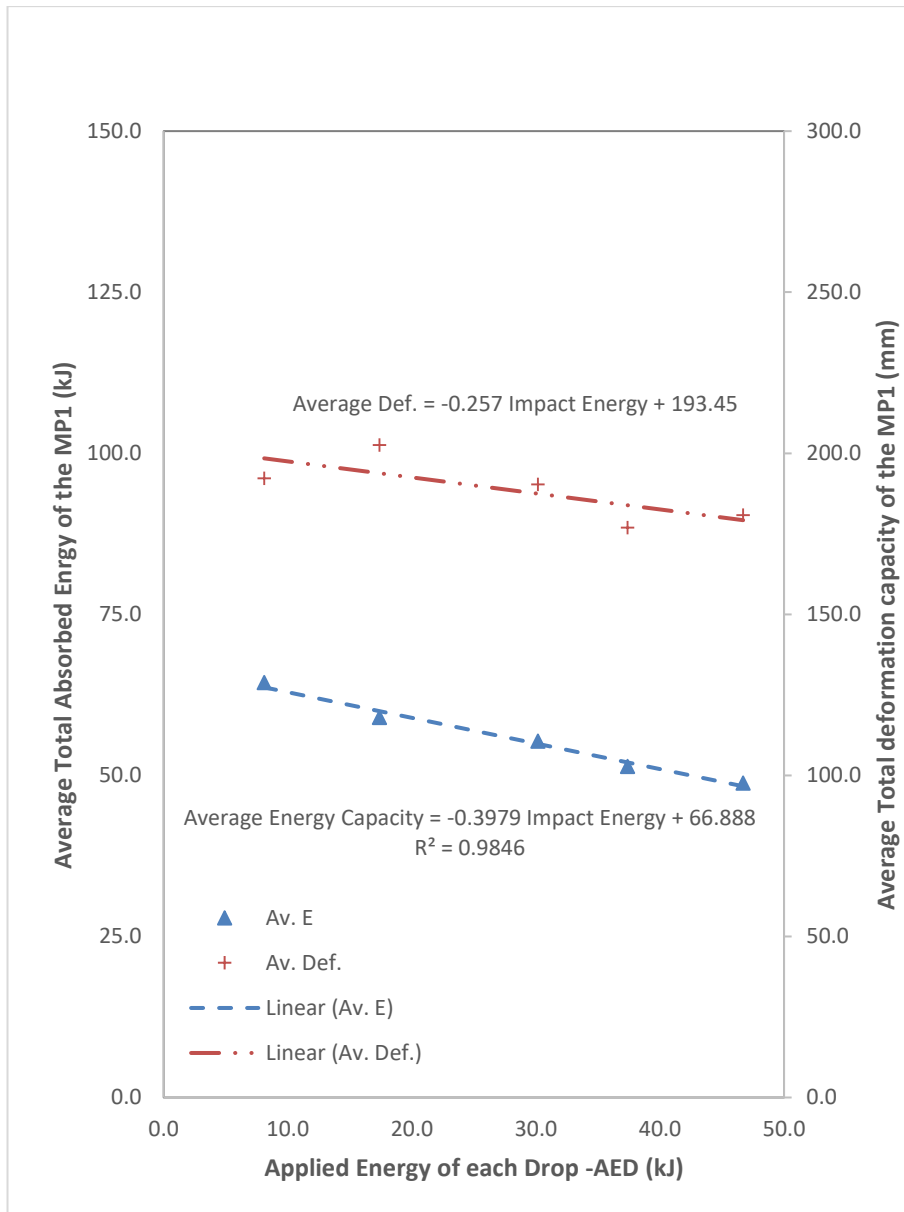


Figure 5.18. Dynamic capacity of the MP1 bolt subjected to multiple drops

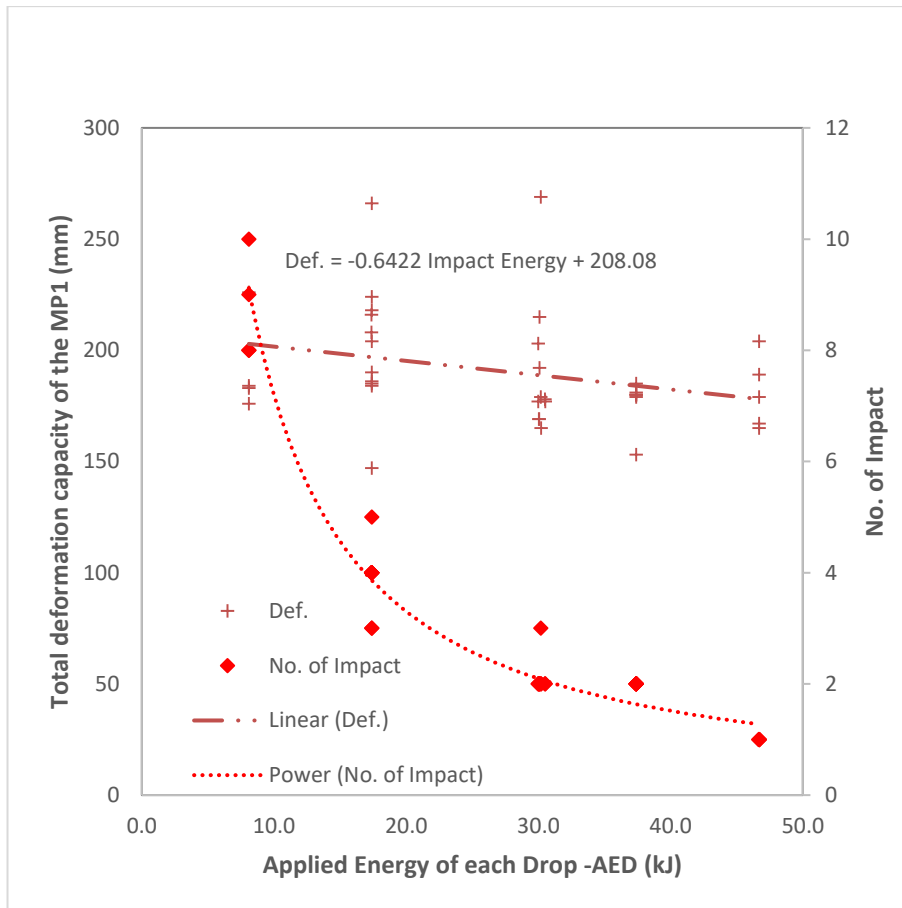


Figure 5.19. Deformation capacity of the MP1 bolt subjected to multiple drops

#### 5.3.4. DYNAMIC BEHAVIOUR OF THE BOLT WITH RESPECT TO THE LENGTH OF THE BOLT

Increasing the length of the bolt logically should have an increase in the deformation capacity and consequently in energy absorption capacity of the bolt. To assess such effect a set of 10 Vulcan Bolt has been added to the previous experiment. The new bolts have a length of 2.4 m with the similar other specifications as of the bolts in the previous experiments. The tests have been carried out with the applied energy of 46.7 kJ in each drop. As it had been expected, the results show an increase in the accumulative energy absorption capacity from 48.4 kJ for 2.0 m length bolts to 58.6 kJ for 2.4 m of length, and an increase in the accumulative deformation capacity from 187.4 mm for 2 m length bolts to 219 mm for 2.4 m length.

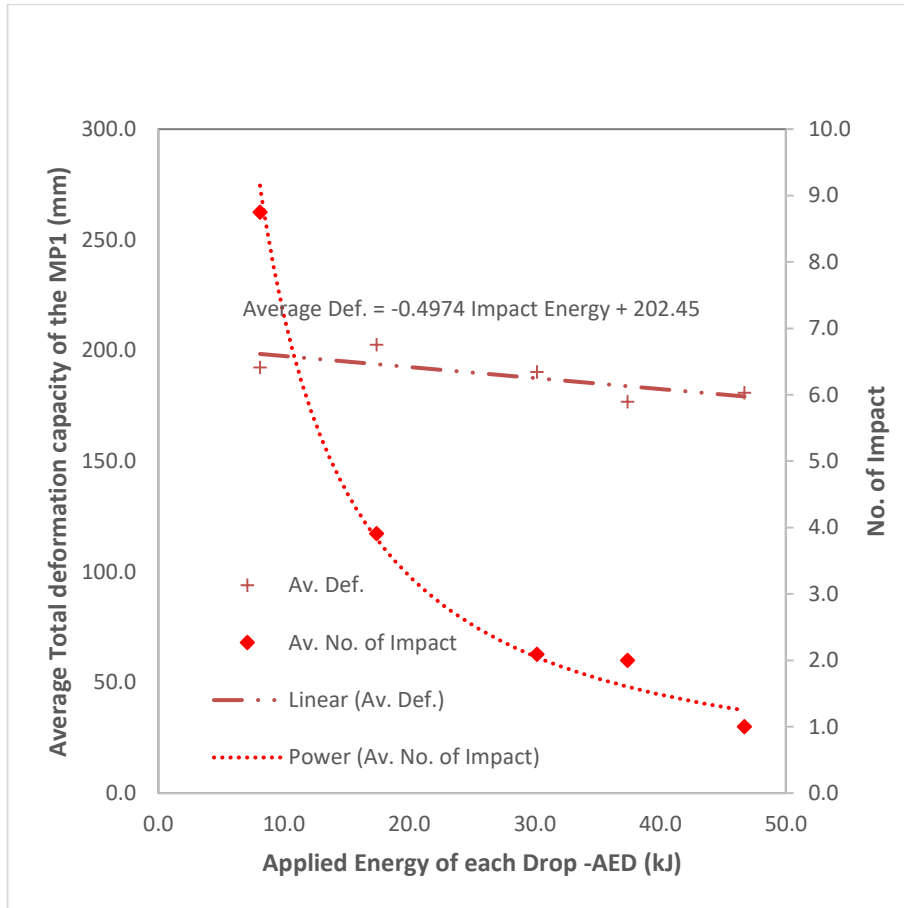


Figure 5.5. Deformation capacity of the MP1 bolt subjected to multiple drops

Some other tests have been done on Par1 bolts with a length of 2.1, 2.4, and 2.5 m with a diameter of 20 mm. The results were the same as depicted in Figure 5.21 and Figure 5.22.

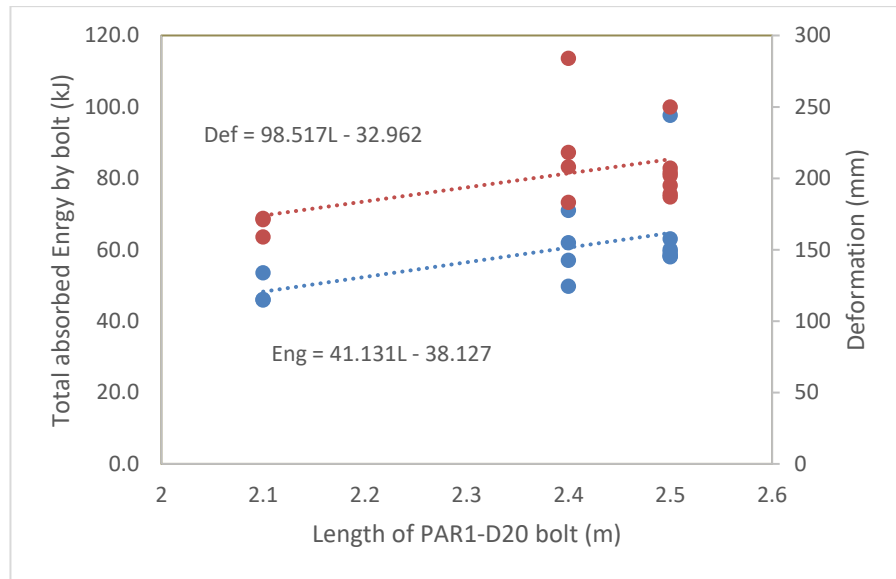


Figure 5.6. Dynamic energy absorption and deformation Capacity of the PAR1-D20-L2.1-2.5 bolt subjected to multiple Drops

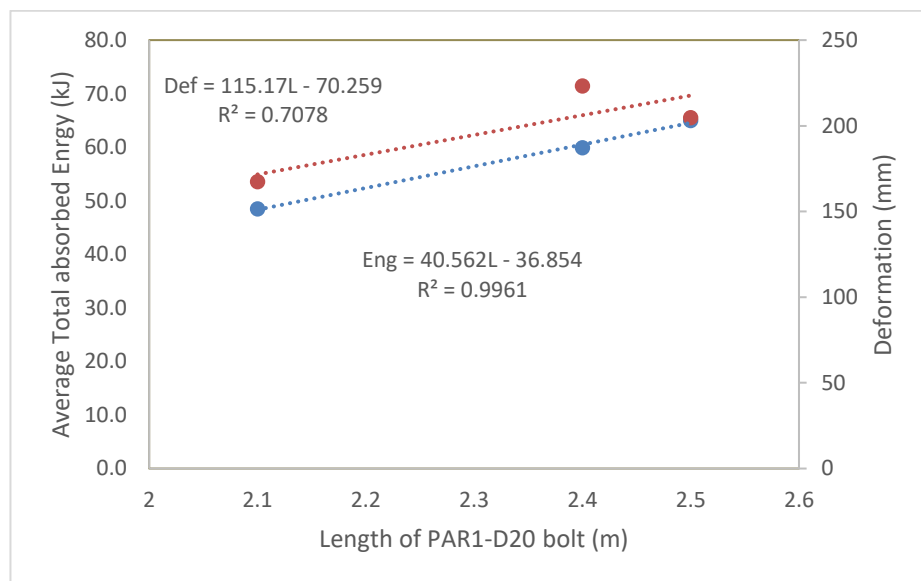


Figure 5.7. Dynamic energy absorption and deformation Capacity of the PAR1-D20-L2.1-2.5 bolt subjected to multiple Drops

### 5.3.5. THE EFFECT OF ENCAPSULATION MATERIAL ON ROCKBOLT CAPACITY

In an experiment, a set five test has been carried out using encapsulation material of cement grout and 5 test using a type of resin grout. Seemingly the resin

encapsulation material gives better flexibility to the bolts and consequently a more appropriate energy absorption capacity. In this set of experiments the average deformation capacity of the bolts increased from 212.8 mm for the cemented bolt to 231.5 mm for the resin grouted bolts, and consequently increase in energy dissipation capacity from 55.5 kJ to 64.7 kJ for the cement grouted and resin grouted bolts respectively.

### ***5.3.6. THE EFFECT OF THE VELOCITY OF THE IMPACTS ON ROCKBOLT CAPACITY***

To assess the effect of the velocity of the different impacts on energy dissipation and deformation capacity of the bolts, further work consist of a number of subsections were needed including further development of the machine, research and expanding the capabilities of the facility.

The focus on the work in respect of the machine was to improve the understanding of the input parameters: the kinetic energy and the velocity at impact. Therefore, the first improvement to the machine provided the capability to accurately measure the impact velocity of the Trolley prior to and during impact. This achieved by tracking the trajectory of the Trolley with an additional Line Scan camera, thus increasing the field-of-view of the lower line-scan imaging system to 2.8 m. The trajectory of the Trolley to be tracked prior to the impact, allowing for the losses in the system to be accounted for and the drop height adjusted. In addition, this allows for the rebound velocity to be calculated enabling the coefficient of restitution and the system dampening to be calculated, further improving the understanding of the impact.

The standard was to calculate the impact mass based on the sum of the average value of the plates used and the mass of the Trolley. In order to improve the accuracy of the stated impact mass, a pair of load cells added. Currently, the impact mass can be determined as the difference in the mass measured before and after releasing the mass.



Following the above development in the testing facility, some experiments have been carried out on Par1 bolts with the length of 2.4 m and diameter of 20 mm, resin grouted with an average impact energy of 11.6 kJ. To do this the weight and height of the drops changed each set and accumulative energy absorption and deformation capacity of the bolts calculated. During this experiments, a total number of 111 drops in 20 multiple drops with 5 different average velocity of impact have been carried out containing 21 drops of 4 multiple drops with the impact velocity of 2.7 m/s, 21 drops of 4 multiple drops with the impact velocity of 3.4 m/s, 22 drops of 4 multiple drops with the impact velocity of 4.4 m/s, 22 drops of 4 multiple drops with the impact velocity of 5.4 m/s, and 25 drops of 4 multiple drops with the impact velocity of 6.4 m/s. The results show a slight increase in energy dissipation capacity of the bolts from the velocity of 2.7, 3.4, 4.4, 5.4, and 6.4 m/s from 61.1, 64, 62.2, 63.9, and 64.3 kJ, and dissipation energy with a pick in between the range, and 194.3, 198.3, 208.8, 196.8, and 196.5 mm of accumulative deformation capacity.

The results depicted in Figures 5.23 to Figures 5.28.

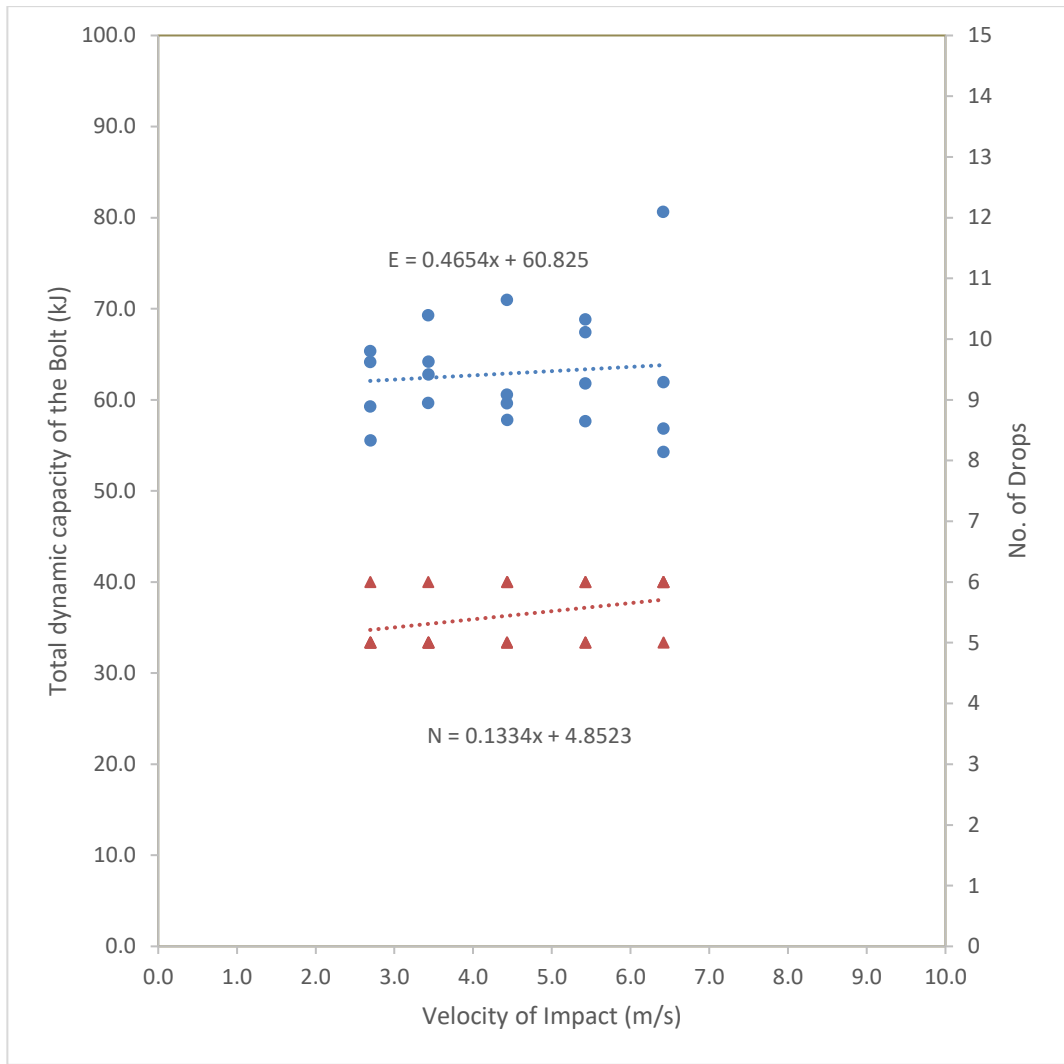


Figure 5.23. Effect of the impact velocity on the dynamic capacity of the bolts

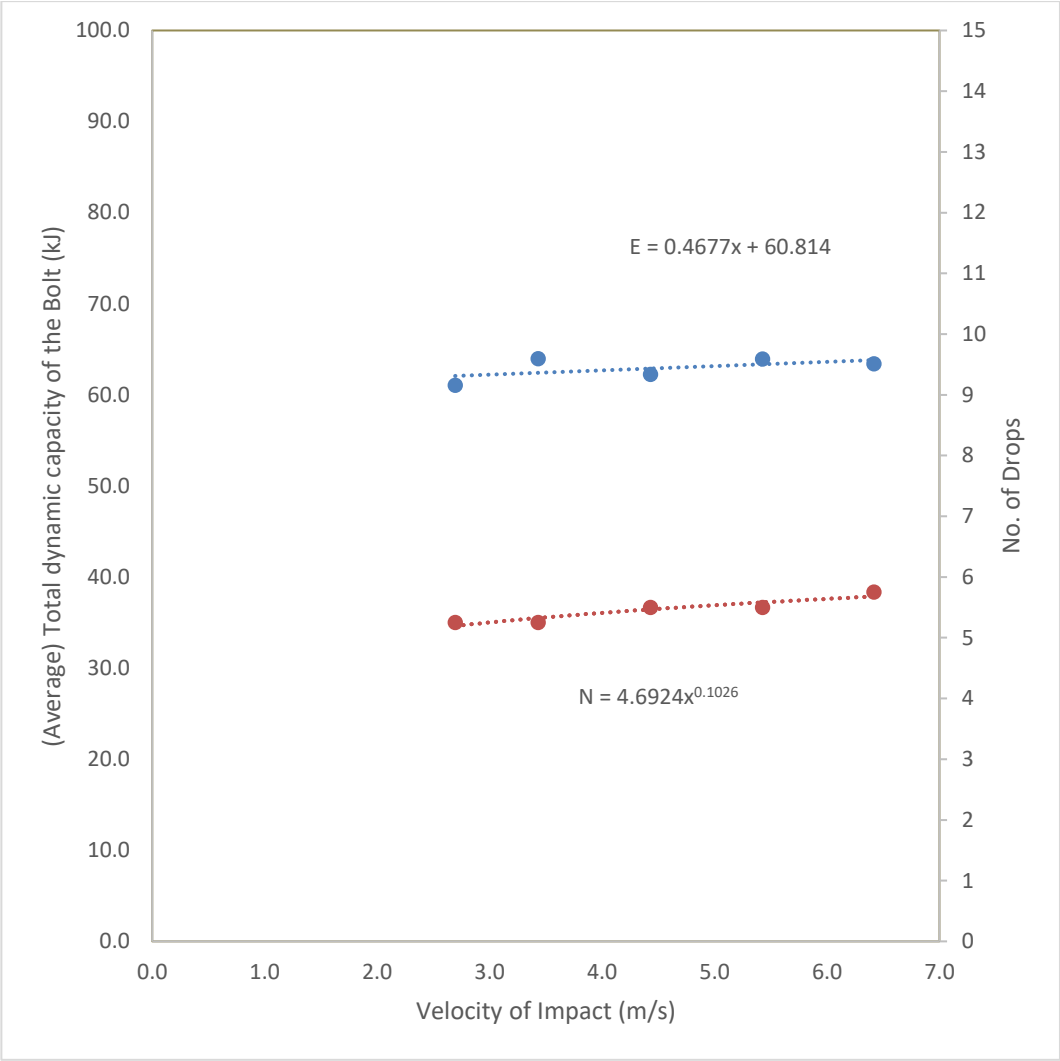


Figure 5.24. Effect of the impact velocity on the average dynamic capacity of the bolts

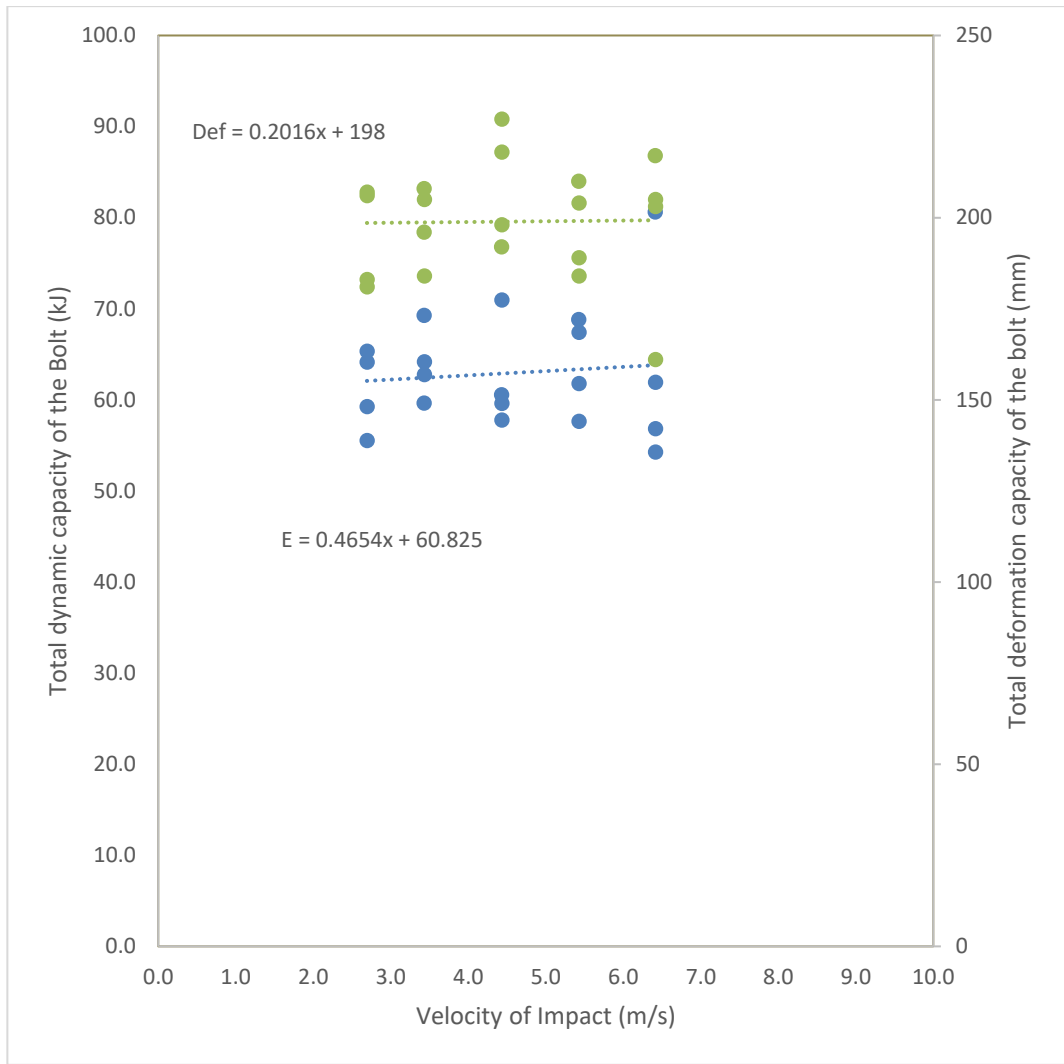


Figure 5.25. Effect of the impact velocity on the dynamic capacity of the bolts and their total deformation capacity

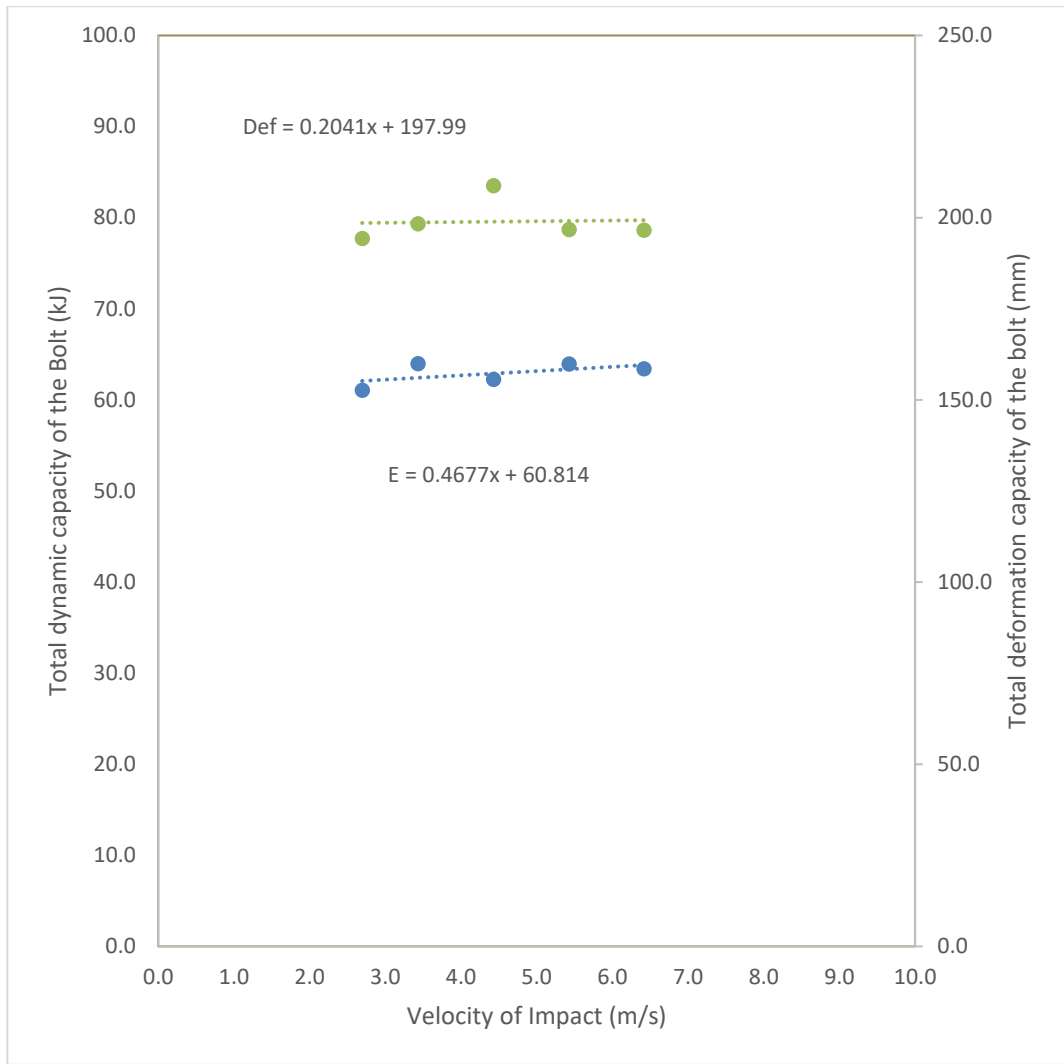


Figure 5.26. Effect of the impact velocity on the average dynamic capacity of the bolts and their average total deformation capacity

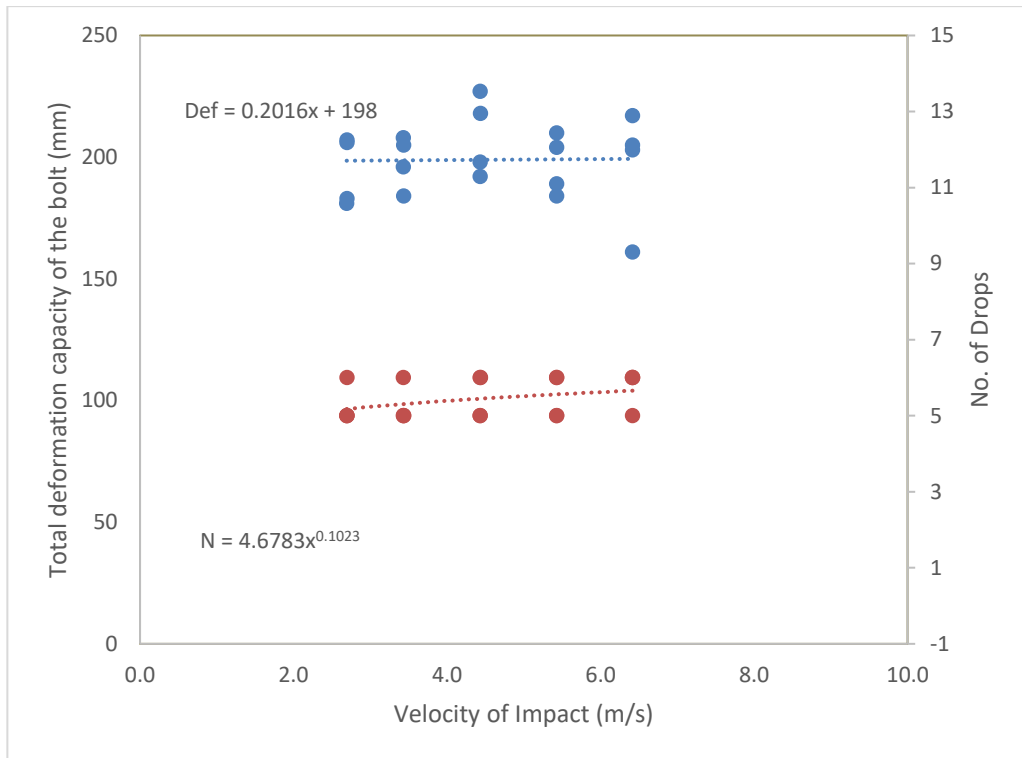


Figure 5.27. Effect of the impact velocity on deformation capacity of the bolts

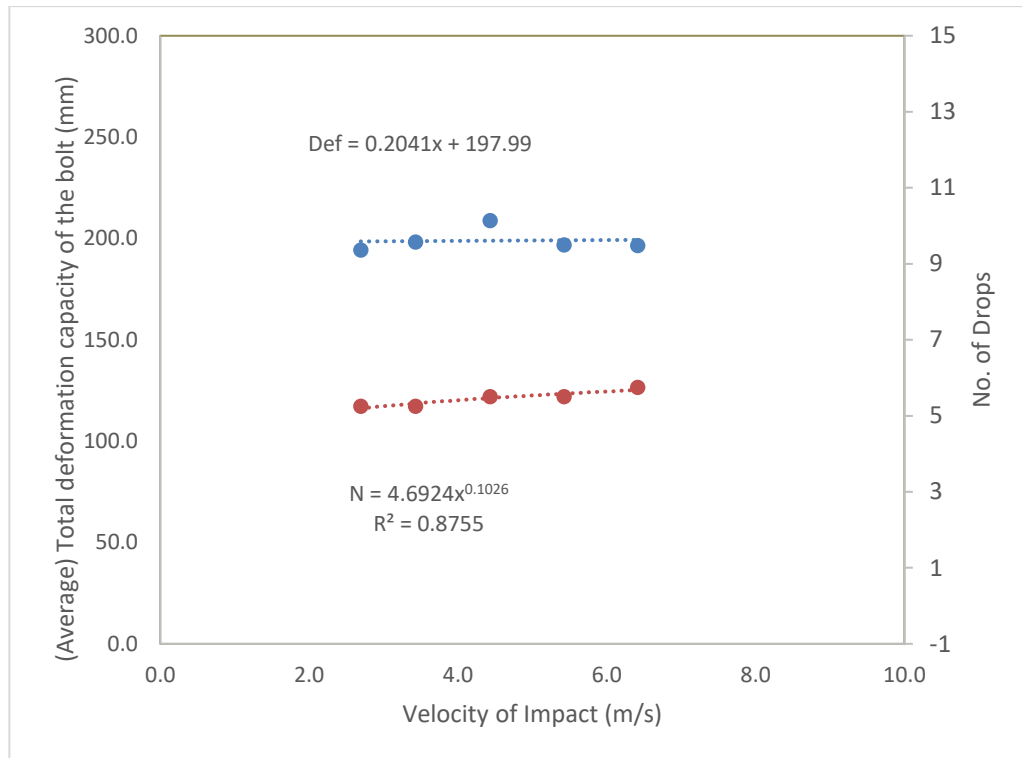


Figure 5.28. Effect of the impact velocity on average deformation capacity of the bolts

#### 5.4. SUMMARY

As it explained in this chapter, a large number of laboratory experiments have been carried out using the New Concept Mining Dynamic Impact Tester (NCM-DIT) that has been constructed in the laboratory of the company in South Africa. The experiments include 338 drop tests on 113 prepared samples consist of 104 drop tests on 52 samples of Vulcan bolt, 120 drop tests on 38 prepared samples of MP1 bolt, and 111 drop tests on 20 prepared samples of Par1 bolt as well as 3 experiments on 3 prepared samples of rebars. The results of the tests on different effective factors described and illustrated in the chapter some of which are summarised as follows:

Rebars show higher loading capacity under a dynamic impact as well as performing a higher deformation capacity. As it explained in one of the experiments, a 22 mm diameter rebar showed about 345 kN of peak load capacity during a dynamic impact instead of 190 kN in a static loading test, and 52 mm of deformation during the seismic impact while it was about 25 mm to 35 mm in a static test. It replicates about

50% to 80% of the increase in the loading and deformation capacity under a dynamic impact condition in comparison with a traditional static loading test.

Experiments on 20 mm diameter and 2.0 m length Vulcan bolts showed a decrease in the total amount of absorbed energy along with applying higher impact energy of each drop. On the contrary, the total deformation capacity slightly increased while the total deformation stayed in a range of 170 mm to 180 mm. These experiments simply showed that same kind of bolt can show higher capacity when they are under a lower level of seismic events in comparison with them while they are experiencing a higher level of dynamic impacts.

Experiments on MP1 bolts showed a similar behaviour Vulcan bolt when they are confronting different levels of dynamic impacts. On the other hand, another set of experiments on Par1 showed an increase in loading and deformation capacity both along with increasing the length of the bolt.

Experiments on Par1 bolts indicate a slight increase in energy absorption capacity as well as its deformation capacity of Par1 bolts when it goes under the higher velocity of the dynamic impacts. It is worth mentioning that the total amount of deformation stays in a range of 190 mm to 210 mm.



## **6. DISCUSSION ON RESULTS**

### **6.1. INTRODUCTION**

Ground support system design in a seismically active ground or rockburst prone area needs specific consideration regarding evaluation or estimation of the released or transferred energy to the surface of the opening on one hand and knowing the energy absorption or dissipation capacity of the support system on the other hand. Design of a support system at a certain location underground requires an evaluation of both ground demand and support capacity, in order to design a reliable support system. The presented methods in the evaluation of ground demand have a large degree of uncertainty while the testing methods of the support system are also capable of simulating the conditions occurring in the ground with a similar uncertainty in comparison to the real condition.

Having an estimation of both factors, the ground demand and the support capacity is essential, therefore, even with a large amount of uncertainty, designers can compare these two factors to define a factor of safety. In addition, the methods could be modified and calibrated in a certain area by the probable occurrence of seismic activities similar to observational methods. Comparison of the support systems tested by multiple facilities assists with promoting the design for the next step.

### **6.2. DISCUSSION ON STATIC EXPERIMENT RESULTS**

As explained in chapter 4 static experiments showed that there is an expectation of progressive decoupling on the encapsulated part of the rockbolt along with increasing loading process. The first segment of the encapsulated part goes under the load with deformation that transfers from the shank of the bolt to the beginning segments and the first segment's strength fails when it reaches to its ultimate shear strength then it can tolerate only some decreasing amount of the load as its residual shear strength. This phenomenon continually happens for the consequently

segments with increasing deformation in the surrounding ground and consequently rockbolt.

It seems that the decoupling does not start considerably in the start of the loading but it would start after a certain amount of deformation and load transfers depend on a variety of parameters such as the difference in stiffness between rock bolt, annulus cement and surrounding ground.

Another fact is that the decoupling is a nonlinear process, despite some test results shows linear behaviour in the range of tested conditions. In Figure 6.1, two trendlines overlaid on the variation of the free length and the encapsulation length along with the increasing load in five steps for the monobar (explained in Figure 4.5) from the second set of the experiments. As it can be obviously seen in the graph, the gradient of the trendline of the free length development does not intercept the Y-axis at its exact initial free length. Theoretically, the intercept point of the trendline, on the free length development points with Y-axis represents the free length at the beginning of the loading process. Therefore, the graph shows that the trend of free length increasing is not linear. At low loading levels, the slope of the trendline almost horizontal compared to the trend line when the load increases. In other words, it has a positive or upward curvature representing that the rate of the free length increasing over the low level of the load is not as much as that when load increase significantly. Therefore, although the free length increasing does not start from the beginning, it starts after transferring a certain amount of deformation to the encapsulation part.

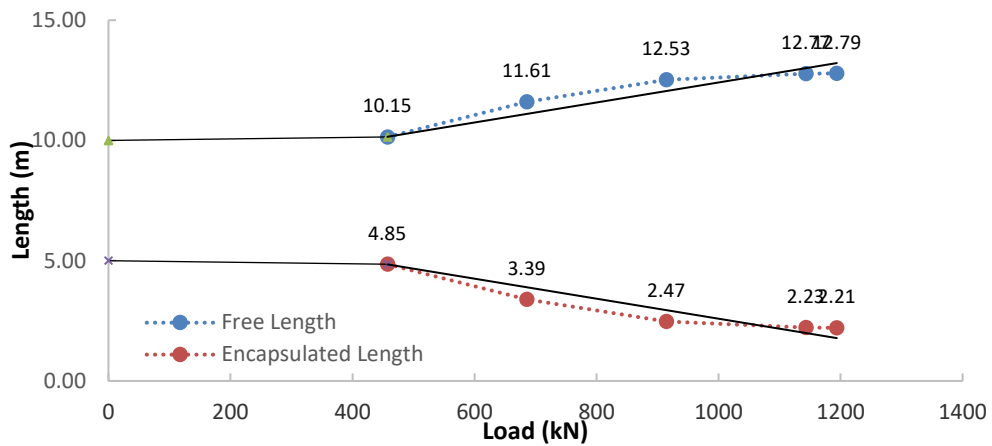


Figure 6.1. Trend of the free length - encapsulation length variation under increasing load in the second experiment

Figure 6.2 is related to the monobar explained in chapter 4 from the third set of the experiments. This graph also shows a very similar stream when overlaid with two trendlines. Additional to what has discussed in Figure 6.1, in both graphs a declining in the rate of development can be found at the end of the graph.

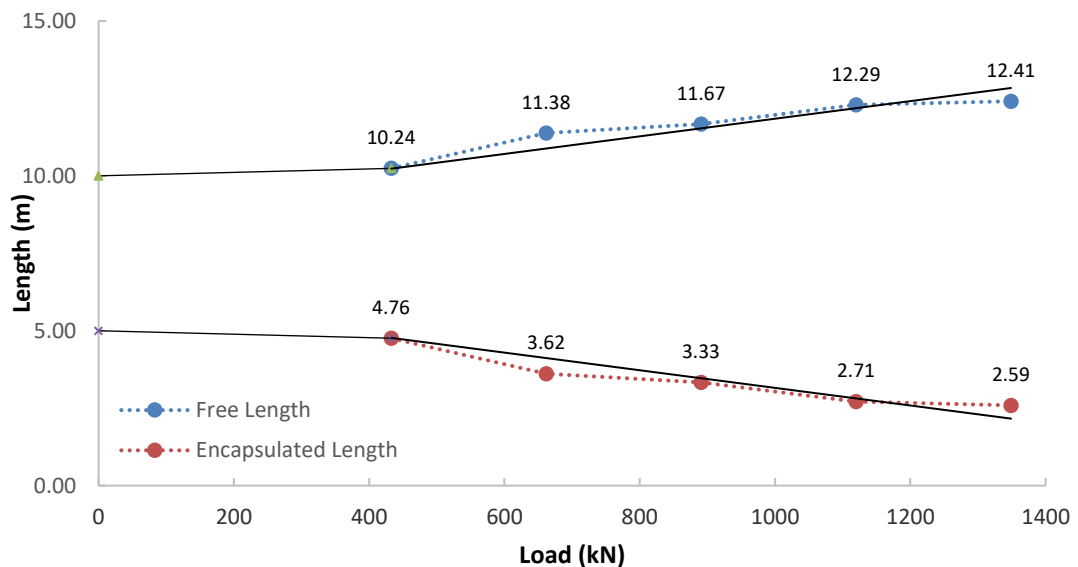


Figure 6.2. Trend of the free length - encapsulation length variation under increasing load in the third experiment

The negative curvature of the free length development in the above graph shows that enough anchorage length is activated in that level of the load and encapsulation length strength would be higher than the monobar ultimate load (at least the proof load) capacity. If the graph curvature at the end part of the loading range was not

negative, it would have not been concluded that there is enough encapsulation length. Therefore, the monobar interface could have failed in the latter case in the increasing loading condition instead of the failure in the shank of the bolt itself.

Figure 6.3 depicted the previous graph with an overlaid nonlinear trendline. As it can be seen in the graph of Figure 6.3 an order 3 polynomial double curvature trendline with a positive curvature in the beginning step of the loading process and negative curvature in the higher level of loading steps gives a better description for the behaviour of the free length development of the monobar under an increasing loading condition.

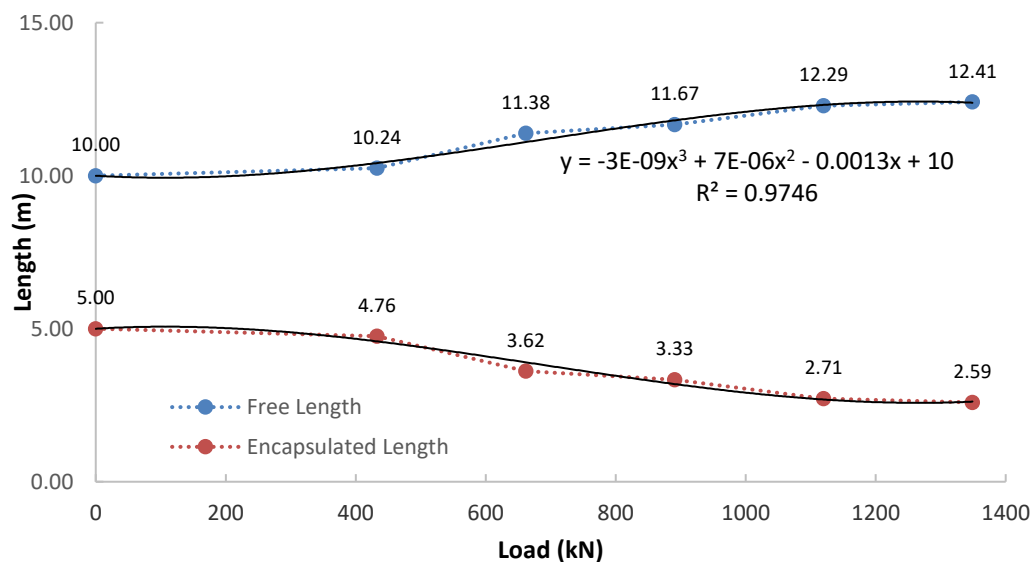


Figure 6.3. Non-Linear trend of the free length - encapsulation length variation under increasing load in the third experiment.

As it can be seen bi-linear relation cannot represent the important trend while a polynomial relation fitted on data so that it can lead not only to a better coefficient of determination but also depict the behaviour of the monobar at the high level of the loading process that has a negative or positive curvature. Having the negative curvature at the higher step of loading or converging the graph to horizontal shows the long-term stability of the rockbolt. This is proposed as a new criterion to ensure the long-term functionality of the rock bolt. A linear or bi-linear relation never can

depict such a key behaviour. Therefore, the best representative graph would be a double curvature polynomial.

Figure 6.4 depicted the non-linear trend of the free length and encapsulation length variation in the fourth experiment. In the same way with the previous experiment, an order three polynomial double curvature trendline fitted over the gathered data during the loading test. As it can be noticed the curvature of the graph is still positive at the end of the loading steps. One reason could be not enough anchorage length activation of the encapsulated part of the rockbolt and it cannot guarantee the adequacy of the encapsulation length in the installed rockbolt.

By equating the second derivative of the equation with zero the inflexion point of the graph can be found. For the presented graph in Figure 6.4, the inflexion point is hypothetically at the load of 950 kN. It means that over the viable loading range of this rockbolt with the ultimate strength of 580 kN the curvature of the graph stays positive. Although there is no confidence for having a stable rockbolt in long term or under an increasing loading condition, it does not refer to a certain failure of the rockbolt in the working range. In this case, it can be concluded to increase the encapsulation length of the rockbolt to be sure about the long term usage.

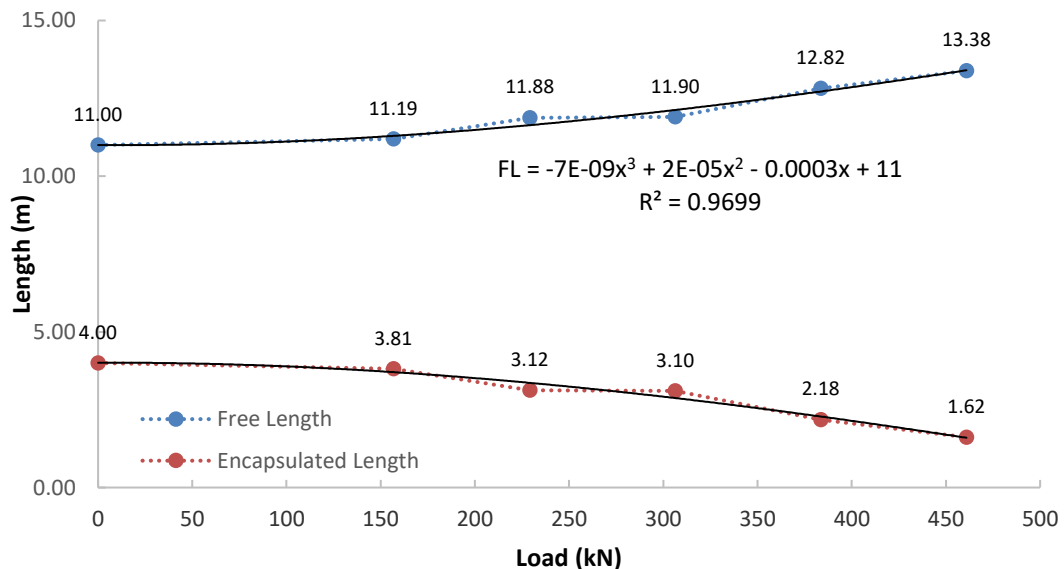


Figure 6.4. Non-Linear trend of the free length - encapsulation length variation under increasing load in the fourth experiment

On the contrary, in the previous experiment, the inflexion point is at the load of 780 kN while the monobar ultimate capacity is 1,820 kN. Therefore the concluded result along with the creep test and other controlling criteria, explained in chapter 4 assure the designer about having a sufficient encapsulation length and avoiding from an unexpected failure of the rockbolt.

### **6.3. DISCUSSION ON DYNAMIC TEST RESULTS**

The strain hardening behaviour of the rockbolts subjected to the static pulling test can be found by comparing and interpreting the load-deformation plot of the same bolts under multiple dynamic impacts. It seems that the dynamic behaviour of the rockbolts follows the static load-deformation plot of it under static testing condition. In other words, achieving a pick load along with the first drop, dropping down the strength afterwards followed by strain-hardening behaviour of the steel bolts under static loading.

Of course, this phenomenon is still under investigation and needs more research to be more transparent and to be sure that it is not because of the higher stiffness of the material in the earlier stage of the test.

Further explanation of this phenomenon presented in Knox and Berghorst (2018)

### **6.4. GROUND SUPPORT SELECTION STRATEGY**

In this part, the most common types of rockbolts are discussed and divided into different capacity categories. It is assumed that the surface support and connecting element of the support system (including shotcrete, mesh and nut) are acting appropriately and transfer the load to the rockbolt. Then the rockbolt would be the central element absorbing and dissipating energy.

Typical load-deformation behaviours of different rockbolts under the loading test are collected and illustrated in Figure 6.5. According to the load-deformation capacity, the rockbolts are classified into five groups namely, Stiff, Medium yielding, High yielding, Very high yielding, and Extremely high yielding rockbolts. As shown in the figure, a category of rockbolts, such as expansion shell and resin/grout

encapsulated rebars, are concentrated on the left side of the plot and represent stiff rockbolts with less than 50 mm deformation capacity and less than 5 kJ energy absorption capacity. The second category such as Split set, Swellex, Roofex and Yield-Lok are the rockbolts which can tolerate deformations between 50 mm and 100 mm with an energy absorption capacity between 5 kJ and 15 kJ. The D-Bolt, Conebolt, Swellex, Roofex, PAR1, Vulcan (20 mm, 2 m), and Yield-Lok which are high yielding rockbolts could lie in the next category. For deformation capacity, greater than 200 mm, Conebolt, Garford and Roofex (possibly with small spacing), Vulcan (20 mm, 2.4 m), and MP1 fall into the very high yielding category, and just Conebolt and Garford are suitable for the extremely high yielding category.

An important fact related to high yielding rockbolts is that they show different behaviour depending on loading conditions and other environmental circumstances. Loading velocity is one factor which can change the load and deformation capacity of yielding bolts, and the quality of installation is another important factor. As it can be seen in the graph, one of the Conebolts tolerates more than 300 mm deformation and absorbs or dissipates 60 kJ of the ground released energy. In comparison, two other Conebolts tolerate less than 150 mm and less than 300 mm and can dissipate 20 kJ and 35 kJ, respectively. Grout quality is a major factor for Conebolts. Strong cement grout could lead to higher initial loading and early rupture while soft cement grout leads the rockbolt to early sliding and not reaching its maximum load capacity. In both cases, the energy absorption capacity of a rockbolt dramatically drops. So before starting to implement a ground support scheme, it would be necessary to plan a test program to determine the conditions for optimum performance of the rockbolts. Examples of influencing parameters include grout mix design, curing time and preloading. The result of the test program should be used to develop a quality control plan.

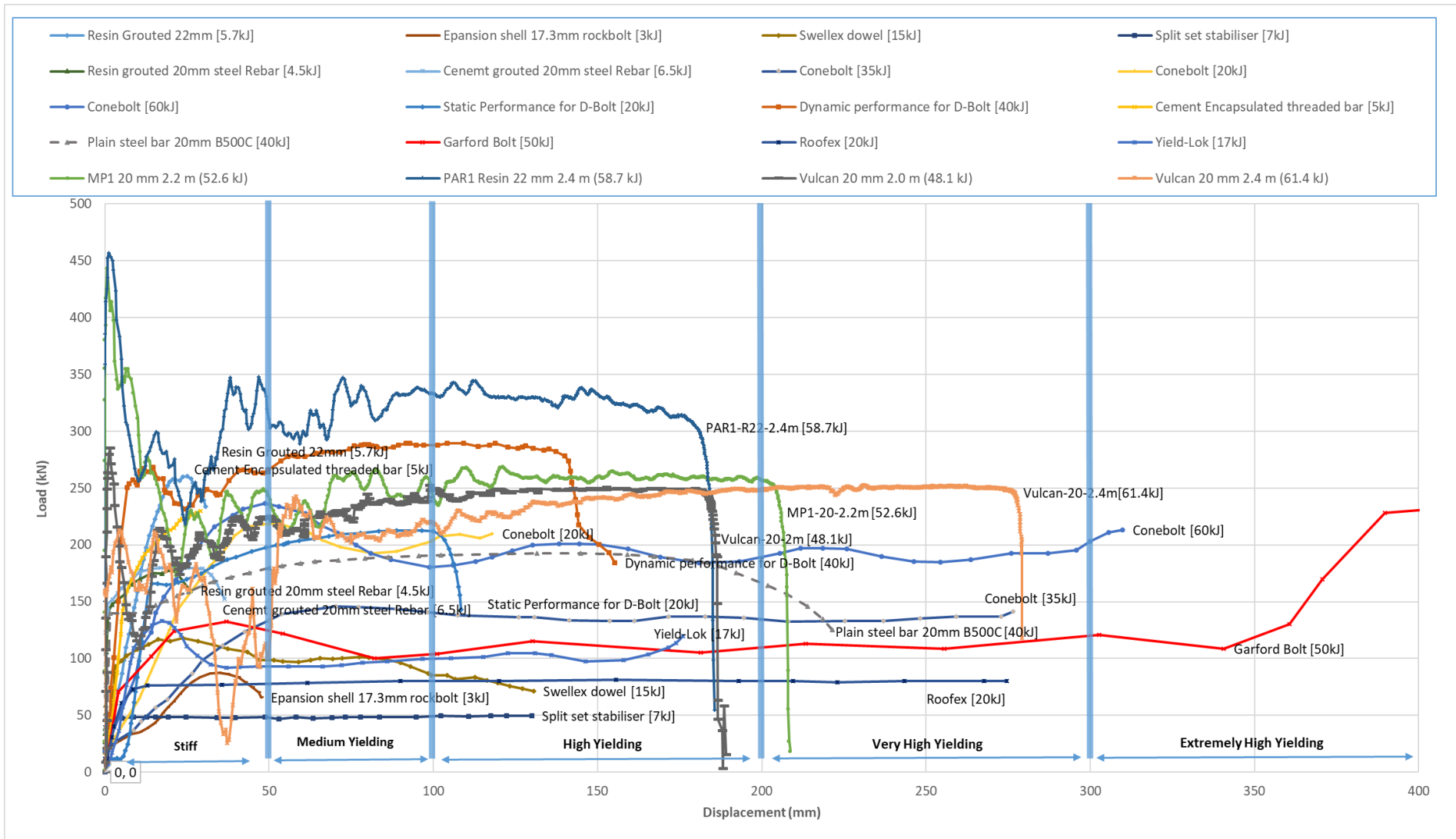


Figure 6.5. Load - Deformation behaviour of different Rockbolts (modified after Masoudi and Sharifzadeh, 2018)



Considering rockbolts' energy absorption as shown in Figure 6.5 and discussed above, suitable rockbolt type selection for various ground demand categories are proposed in Table 6.1. This table could be an initial guideline to narrow the choices, and it is evident that complementary studies such as dynamic tests are required for detail design. Although there are some newer types of rockbolt like Dynamic Omega-Bolt which can absorb 22 kJ to 35 kJ in static and dynamic conditions (Scolari, Brandon, & Krekula, 2017), they need more laboratory and industrial experimentation.

Table 6.1. Demand – Capacity based support selection modified after Masoudi and Sharifzadeh (2018).

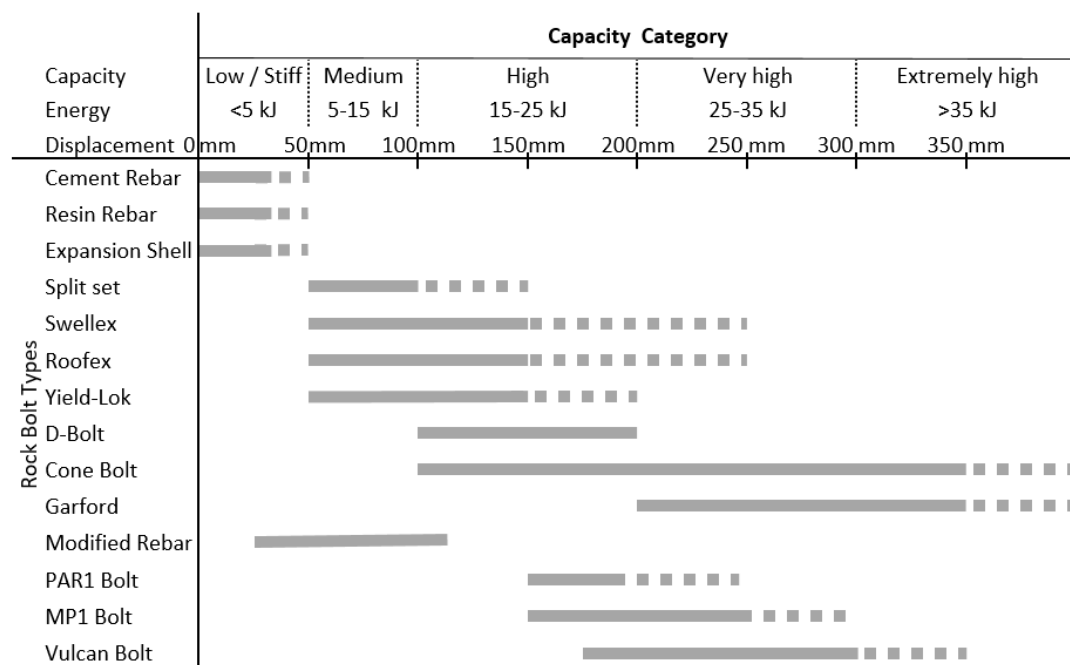
Ground Demand		Reinforcement Selection	
Surface Displacement (mm)	Energy (kJ/m <sup>2</sup> )	Recommended Reinforcement	Capacity Category
<50	<5	Expansion shell Rockbolt, Resin/Cement steel Rebar,	Low / Stiff
50–100	5–15	Split set, Swellex, Roofex, Yield-Lok, Modified Rebar	Medium
100–200	15–25	Swellex, D-Bolt, Conebolt, Roofex, Yield-Lok, PAR1, Vulcan (20 mm, 2 m)	High
200–300	25–35	Roofex, Conebolt, Garford, Vulcan (20 mm, 2.4 m), MP1	Very high
>300	>35	Conebolt ,Garford	Extremely high

As explained in sections 2.6, 2.6.1, 2.7, 6.4, the support system considered in three different elements including surface support, connecting elements, and reinforcement or rockbolts. In a seismic condition, all of the three elements have to

act their function successfully as well as the whole as an integrated system. In this research, the focus was on the reinforcement element of the support system and as an assumption, other support elements are acting their function appropriately.

Table 6.2 shows the energy dissipation capacity of different types of reinforcement. Choosing a specific type of rock reinforcement, the table shows the range of energy dissipation and deformation capacity under each named capacity category.

Table 6.2. Energy dissipation capacity category of different types of reinforcement modified after Masoudi and Sharifzadeh (2018).



Based on the expectation of the deformation and energy demand of a location, the ground demand relates to the relevant categories in this table. The range of suitable reinforcement for the category is proposed in the “Rockbolt Types” column. The expected deformation and ground demand are complicated though and come from the methods explained in section 2.5 as well as previous experiences and engineering judgments.

## **6.5. CONSIDERATIONS OF LINKING AND TERMINATING ARRANGEMENTS OF REINFORCEMENTS**

The reinforcement connects to the surface support by linking and terminating arrangements (connecting elements) like nuts and bearing plates, split set rings, or the sealing weld and soft ferrule on Swellex. The ejected mass applies the dynamic load to the surface support or containment support. The load needs to be passed via the linking and terminating arrangements and transferred to the ground through the reinforcement. Every one of these elements has to be able to tolerate the applied dynamic load independently and if any of them fail, the load would no longer be transmitted to the ground and ejection would occur from in-between the rockbolts (Daniel P. Heal, 2010; Kaiser et al., 1996).

Some experiments show that the capacity of the bearing plate under a dynamic loading condition is much less than their nominal load capacity (Jan & Palape, 2007; Simser & Potvin, 2007). Therefore, in designating each ground support system, it is critical to be sure that the linking and terminating elements have adequate impact loading capacity to transfer the load to the reinforcement and avoid of local failure of the surface support.

## **6.6. MODIFIED REBAR ROCKBOLT PERFORMANCE IN SEISMIC CONDITIONS**

The rebar rockbolts are frequently used in underground mining to control the bulking of the stress fractured ground even in seismic conditions. The seismic prone ground needs considerations to avoid the violent collapse of the wall or roof. Improving the rebars rockbolts, promote the entire rock support system and results in an effective safe workplace.

Modified rebar rockbolts in comparison with frictional rockbolts show much higher strength, specifically in seismic conditions. They are able to tolerate more load even compared with this ultimate strength in static condition due to their involvement with the ground via an anchoring system compared to frictional contact.

A suitable ground support system in the seismic prone area should have enough resistance as an integrated system. The capacity of the support system is governed by the weakest link in the reinforcement of surface support. Having the collar bonding prevents the rockbolt to be the weakest link by removing all weaknesses in heading anchorage of the rockbolt. The low resistance of the bearing plate, nut, thread, and loose surface rock cover with the resistance of the coupled collar length so that the ultimate strength of the head anchorage goes much higher than the strength of the shank of the rockbolt.

The free length or decoupled part of the rebar increases the deformability of the rockbolt and prevents any local failure due to concentrated deformation. The debonded part of the rockbolt is an important part of it so that many discontinuity opening or ejection of a volume of rock located in this depth. Without the free length in this part, early rupture of the rebars likely occurs or there is a high risk of the support failure.

Generally, it is an easy practice and cost less modification for seismic conditions that improve the capacity of the deformation, avoids early failure, improves head anchorage, not leaving a weak link in reinforcement, connecting elements, and terminating arrangement, while rockbolts have enough strength in the anchorage.

## **6.7. SUMMARY AND RESULTS**

The static experiments on multi-strand tendons, monobars, and rockbolts installed in underground caverns showed that their behaviour under increasing loading condition changes so that the free length of the rockbolt increased during the process of loading test. Similar to what happens in a loading test occurs during loading due to ground movement. In other words, the designed free length of the rockbolt increases because of the growing the load in the shank of the rockbolt. Increasing the free length of the rockbolt have an effective change in its stiffness and impresses the assembly effect of a group of bolts that have installed. Additionally, along with increasing the free length the encapsulated length decreases with the same order at least.

A third-order polynomial double curvature trendline with a positive curvature in the beginning steps of the loading process and negative curvature in the higher level of loading steps represents the development of free length subjected to increased loading. Having the negative curvature at the higher step of loading or converging the graph to horizontal shows the long-term stability of the rockbolt seemingly.

Dynamic tests show that the general load-deformation behaviour of the rockbolts subjected to dynamic impacts has a similar trend with what is happening in a static test so that it shows a peak on the first impact following by the strain hardening behaviour with the next impacts to the total failure.

Using the presented table and graph the reinforcement can be selected for an underground tunnel or stop depend on the expected or estimated energy demand in the preliminary stage. Final selection of the appropriate rockbolt can be achieved by further observation.

All elements of the reinforcement system including nut, plate, linking elements, head arrangement, encapsulation part and the shank of the rockbolt should have a similar impact capacity. As it has been discussed the modified rebar or similar modification on rockbolts can be a solution to avoid to have a weak link in the support system chain.

This page intentionally left blank

## **7. CONCLUSIONS, RECOMMENDATIONS AND CONTRIBUTIONS TO STATE OF KNOWLEDGE**

### **7.1. CONCLUSIONS AND RECOMMENDATIONS**

As explained in the beginning paragraph of the abstract and introduction, the research narrowed to a more specific area of the thesis title referring to the static and dynamic behaviour of rockbolts in the deep underground excavation. This minor alteration decided by the supervision team because of more suitability and usefulness of the narrowed research with the mining requirement in Western Australia in addition to lack of enough resources such as laboratory facilities and field experiments difficulties.

Under seismic conditions in deep underground mine excavations, energy dissipation capability and large deformation capacity of the support system are the primary objectives of the design. In this research, the ground demand and likelihood of a dynamic event have been estimated using different methods. Despite the accuracy concerns of these estimation methods due to many assumptions, they are still only available approaches for the selection of appropriate support system at preliminary design stages. The design could be scrutinised and verified or modified with performance observations during construction progress.

Rockbolts tolerate the containing load by the surface support and have to have enough length to be able to transfer it to the stable ground at depth while being not too long because of economic reasons and implementation limitations. The bond length in the stable zone has the role of load transfer to the ground. Therefore, the uncertainty of the bond length dimension should be minimised. Previous experiments show that there is a critical embedment length for rockbolts in different situations that the designer has to take this into considerations.

Stiff behaviour at the beginning of the loading, along with high strength and yielding capability by increasing deformation, are essential qualities of the support components under dynamic loading conditions in order to dissipate a sudden release of energy. To estimate the capacity of rock support systems exposed to seismic

events, a number of estimation methods including laboratory drop tests, simulated rockburst, back-calculation, momentum transfer concept, large-scale dynamic test as well as the New Concept Mining Dynamic Impact Tester (NCM-DIT) were discussed. Although various assumptions and interpretations are needed to employ the results of dynamic tests, more dynamic capacity measurement of support elements is required to cover the wide range of possible energy released and resulting deformation. On the other hand, ground support reacts in various ways under different circumstances. The velocity of ejection (dynamic loading velocity), quality of grouting of rockbolts and appropriate linking between all elements are some of the known factors that affect the performance of the ground support system. The arrangement of a test program before finalising the design is vital to ensure a successful design.

Ground demand is estimated using the methods discussed along with an associated degree of uncertainty. However, to begin with, the potential for rockburst could be assessed through laboratory tests on intact rocks. Estimation of failure thickness or potential block size and velocity of ejection could support the assumptions and results of the laboratory tests. Using rockburst damage potential, the previous result could be cross-checked, and this could also be summarised into a qualitative description. Using ground demand – support energy dissipation capacity table and graph, the rockbolt type selection was introduced. The selected rockbolt can be tested, verified, and modified by proper dynamic testing or observation of progress during construction. The reliability of the support elements would be monitored and back-calculated after initial installation and following excavation progress. This will allow the support selection and details to be modified based on monitoring and back-calculation, progressively and continuously.

Modifications on ordinary rebar rockbolts improved their performance in a rock support system specifically in seismic conditions. Leaving a free length in the middle of the bolt by a piece of smooth pipe over the rockbolt to decouple it from surrounded encapsulation material, allows the rockbolt to be able to absorb more ground deformation and consequently dissipate more energy than conventional full encapsulation.



Collar bonding underneath of the bearing pad and plate, improve the head anchorage of the bolt and avoid any early failure in this part due to pre-existing rock breakage under the bearing pads, low resistance of bearing plates, the possibly lower ultimate strength of the threaded part, etc. The proposed length for collar bonding is the same length as the minimum required encapsulation length achieved by laboratory tests followed by field complementary examination.

The main encapsulation length which plays the function of transferring the applied load to the surrounding ground should be conservatively considered. Therefore laboratory or preferably on-site testing is required to evaluate the Minimum Required Encapsulation Length (MREL) which is the minimum length of the encapsulated part that the bonding resistance is more than the ultimate strength capacity of the shank of the rebar. Applying an engineering factor of safety to the MREL leads the designers to consider an appropriate main encapsulation length.

Prior to a rockbolt project, an on-site test plan to determine the optimised practical required encapsulation length for minimising the risk of support failure is recommended. Monitoring and observations will assist the engineers to modify the whole system along with the progress. Since the ordinary type of rebars are always available and frequently employed in ground support systems along with other types of rockbolts and support elements, proposed modifications will improve the performance of the whole ground support system.

## **7.2. CONTRIBUTIONS TO THE STATE OF KNOWLEDGE**

Some of the key achievements during the practical and laboratory experiments are summarised and listed as follows:

- ✓ Different methods for estimation or indexing the ground energy demand during a seismic event have been collected, analysed, categorized and presented in section 2.5 including intact rock property approach, the method by having an estimation of the failure volume and the ejection velocity and the rockburst damage potential method.

- ✓ Various methods for measurement of the dynamic capacity of the reinforcement have been insightfully explained including the drop testing method, blast simulation, momentum transfer method, back-calculation, large scale dynamic test rig and NCM Dynamic Impact Tester (NCM DIT).
- ✓ Modifications on ordinary rebar rockbolt have been discussed and supported by presented field experiments. A method to determine the different part of modified rebar developed based on experiments results. The most important part of rebar including Collar encapsulated part, Free length, and Main encapsulated length has been determined by introducing of Minimum Required Encapsulation Length (MREL). The practical experiments for testing the modified rebars proved an extensive improvement in the performance of the ordinary rebars subjected to dynamic impacts. Using the static load-displacement history interpretation, it is found that, the bolts behave with higher load and deformation capacity.
- ✓ A new methodology and instrument for rockbolt in-borehole load monitoring developed and employed to investigate the variation of the load in the shank of the bolt installed in a borehole and subjected to a seismic event. The results showed the successful performance of the instrument in real situations.
- ✓ Progressive decoupling of the rockbolt encapsulated part anchored with the surrounded material have been investigated and four sets of supporting experiments explained in chapter 4. The experiments showed that the free length of rockbolts develops along with increasing the load in the shank of the installed rockbolts. It is proved that the amount of the decoupled length could be higher than what expected before with an order of one to two meters instead of previous experiences that was just a few centimetres.
- ✓ Decoupling of the encapsulated part of the rockbolt increases the free length that should have an order 3 polynomial double curvature trendline with a positive curvature in the beginning steps of the loading process and should have a negative curvature in the higher level of loading steps for being a stable rockbolt.

Having the negative curvature at the higher step of loading or converging the graph to horizontal shows the long-term stability of the rockbolt. This is proposed as a new criterion to ensure the long-term functionality of the rock bolt.

- ✓ The laboratory NCM DIT experiments on rebars showed the increasing of the ultimate load and deformation capacity of them under seismic event condition. There is no clear relation between the variation of the diameter on load and deformation capacity of rebars but this area definitely needs more investigation.
- ✓ The total energy absorption/dissipation capacity of the bolts decreases when they are subjected to the larger applied energy of each drop. It means that the rockbolts show lower total energy dissipation during stronger dynamic events. Therefore, when rockbolts used in mine excavations, the energy dissipation capacity of it should be re-evaluated when they are used in deeper situations. Capacity evaluation of rockbolts in shallower depth is not valid in deeper condition because of encountering the stronger seismic events. On the contrary, the deformation capacity of the rockbolts slightly increased when they are subjected to stronger impacts.
- ✓ The velocity of dynamic events is another important factor that has been investigated in this research. The results of experiments on many different types of samples show that there is increases in the total energy dissipation and also the deformation capacity of rockbolts when they are subjected to the higher velocity of impacts. In other words, when seismic events or ejection happens with larger velocity, rockbolts show a higher performance in terms of energy absorption/dissipation and deformation.
- ✓ Last but not least, the results of this research could significantly improve understanding of rock bolt behaviour and design in seismically active underground excavations.

### **7.3. RECOMMENDATION FOR FUTURE RESEARCH**

- ✓ Performance of rebar under seismic condition need more investigation specifically the relation of energy absorption and diameter
- ✓ Using the developed instrument (Deformometre) with continuous recording of the data in laboratory condition. Currently, it is ongoing in NCM laboratory facility as all equipment have been prepared and tested during this research
- ✓ Employing the developed instrument in a site using an automatic data acquisition system with a continuous data recording

## REFERENCES

- Cai, M. (2013). Principles of rock support in burst-prone ground. *Tunnelling and Underground Space Technology*, 36, 46-56.
- Cai, M., & Champaigne, D. (2009). The art of rock support in burst-prone ground. *Proceedings of RaSiM*, 7, 33-46.
- Cheng, L., & Feng, S. (1983). *Mechanism and strengthening effect of split set bolts*. Paper presented at the Proc. of Int. Symp. on Rock Bolting. Abisko.
- Farmer, I. (1975). *Stress distribution along a resin grouted rock anchor*. Paper presented at the International Journal of Rock Mechanics and Mining Sciences & Geomechanics Abstracts.
- Gaudreau, D., Aubertin, M., & Simon, R. (2004). *Performance assessment of tendon support systems submitted to dynamic loading*. École polytechnique,
- Haile, A., Grave, D., Sevume, C., & Le Bron, K. (1998). Strata control in tunnels and an evaluation of support units and systems currently used with a view to improving the effectiveness of support, stability and safety of tunnels.
- Heal, D. P. (2010). *Observations and analysis of incidences of rockburst damage in underground mines / Daniel P. Heal*. (Ph.D.), University of Western Australia, Perth, Western Australia. Retrieved from [http://repository.uwa.edu.au:80/R/-?func=dbin-jump-full&object\\_id=29995&silo\\_library=gen01](http://repository.uwa.edu.au:80/R/-?func=dbin-jump-full&object_id=29995&silo_library=gen01)
- Heal, D. P., & Potvin, Y. (2007). *In-situ dynamic testing of ground support using simulated rockbursts*. Paper presented at the Deep Mining 07, Perth, Australia.
- Hoek, E., Kaiser, P. K., & Bawden, W. F. (1995). Support of underground excavations in hard rock.
- Jan, V. S., & Palape, M. (2007). *Behaviour of steel plates during rockbursts*. Paper presented at the Deep Mining 07, Perth, Australia.
- Jin-feng, Z., & Ming-yao, X. (2016). Uplift Capacity of Shallow Anchors Based on the Generalized Nonlinear Failure Criterion. *Mathematical Problems in Engineering*, 2016.
- Kaiser, P. K., & Cai, M. (2012). Design of rock support system under rockburst condition. *Journal of Rock Mechanics and Geotechnical Engineering*, 4(3), 215-227.
- Kaiser, P. K., McCreath, D., & Tannant, D. (1996). Canadian rockburst support handbook. *Geomechanics Research Centre, Laurentian University, Sudbury*, 314.
- Knox, G., & Berghorst, A. (2018). *Increased agility for the research and development of dynamic roof support products*. Paper presented at the Proceedings of the Third International Conference on Rock Dynamics and Applications, CRC Press, Boca Raton.

- Kristjánsson, G. (2014). *Rock bolting and pull out test on rebar bolts*. Institutt for geologi og bergteknikk,
- Kwaśniewski, M., Szutkowski, I., & Wang, J. A. (1994). *Study of ability of coal from seam 510 for storing elastic energy in the aspect of assessment of hazard in Porabka-Klimontow Colliery*. Retrieved from Sci. Rept. Silesian Technical University:
- Kwaśniewski, M., & Wang, J. (1999). 3-D numerical modeling and study of mine tremors associated with coal mining in vicinity of major of faults. *Puols Inst Geophys*, 22(310), 351-364.
- Li, C. C. (2010). A new energy-absorbing bolt for rock support in high stress rock masses. *International Journal of Rock Mechanics and Mining Sciences*, 47(3), 396-404.
- Li, C. C., Kristjánsson, G., & Høyen, A. H. (2016). Critical embedment length and bond strength of fully encapsulated rebar rockbolts. *Tunnelling and Underground Space Technology*, 59, 16-23.
- Li, C. C., Stjern, G., & Myrvang, A. (2014). A review on the performance of conventional and energy-absorbing rockbolts. *Journal of Rock Mechanics and Geotechnical Engineering*, 6(4), 315-327.
- Li, C. C. a. (2017). *Rockbolting : principles and applications / Charlie Chunlin Li*: Oxford, Oxfordshire : Butterworth-Heinemann.
- Li, L., Hagan, P., & Saydam, S. (2014). *A Review of Ground Support Systems Performance Subjected to Dynamic Loading*.
- Linkov, A. M. (1996). Rockbursts and the instability of rock masses. *International Journal of Rock Mechanics and Mining Sciences & Geomechanics Abstracts*, 33(7), 727-732. doi:[http://dx.doi.org/10.1016/0148-9062\(96\)00021-6](http://dx.doi.org/10.1016/0148-9062(96)00021-6)
- Mark, C. (2016). Science of empirical design in mining ground control. *International Journal of Mining Science and Technology*, 26(3), 461-470.
- Masoudi, R., & Sharifzadeh, M. (2018). Reinforcement selection for deep and high-stress tunnels at preliminary design stages using ground demand and support capacity approach. *International Journal of Mining Science and Technology*. doi:<https://doi.org/10.1016/j.ijmst.2018.01.004>
- Morissette, P. N. R. (2015). *A ground support design strategy for deep underground mines subjected to dynamic-loading conditions*. UNIVERSITY OF TORONTO (CANADA),
- Myrvang, A., & Hanssen, T. (1983). *Experiences with friction rock bolts in Norway*. Paper presented at the Proc. of Int. Symp. on Rock Bolting. Abisko.
- Ortlepp, W., & Stacey, T. (1998). *Testing of tunnel support : dynamic load testing of rockbolt elements to provide data for safer support design*. Retrieved from <http://hdl.handle.net/10204/1750>
- Ortlepp, W., & Swart, A. (2002). *Extended use of the Savuka dynamic test facility to improve material and analytical technology in deep-level stope support*. Retrieved from <http://hdl.handle.net/10204/1862>

- Ortlepp, W. D. (1997). *Rock fracture and rock bursts*. Retrieved from Johannesburg, South Africa:
- Ortlepp, W. D., Stacey, T. R., & Kirsten, H. A. D. (1999). *Containment support for large static and dynamic deformations in mines*. Paper presented at the International symposium; 4th, Rock support and reinforcement practice in mining, Kalgoorlie; Australia.
- Player, J., Thompson, A., & Villaescusa, E. (2008). *Dynamic testing of reinforcement system*. Paper presented at the 6th International Symposium on Ground Support in Mining and Civil and Engineering Construction, Cape Town, South Africa.
- Player, J., Thompson, A., & Villasescusa, E. (2009). Dynamic testing of threadbar used for rock reinforcement. *RockEng09, Rock Engineering in Difficult Conditions, CIM Montreal, Paper, 4030*, 12p.
- Player, J., Villaescusa, E., & Thompson, A. (2008). *An Examination of Dynamic Test Facilities*. Paper presented at the Australian Mining Technology Conference, Australia: Queensland.
- Player, J., Villaescusa, E., & Thompson, A. (2009). Dynamic testing of friction rock stabilisers. *RockEng09, Rock Engineering in Difficult Conditions, Toronto*, 9-15.
- Player, J. R., E., V., & A., T. (2004). *Dynamic Testing of Rock Reinforcement using the Momentum Transfer Concept*. Paper presented at the Fifth International Symposium on Ground Support in Mining and Underground Construction, Perth.
- Plouffe, M., Anderson, T., & Judge, K. (2008). *Rock bolts testing under dynamic conditions at CANMET-MMSL*. Paper presented at the Proc. 6th Int. Symp. on Ground Support in Mining and Civil Engineering Construction, Cape Town, S. Afr. Inst. Min. Metall. Symposium Series S.
- Potvin, Y., Wesseloo, J., & Heal, D. (2010). An interpretation of ground support capacity submitted to dynamic loading. *Mining Technology*, 119(4), 233-245. doi:10.1179/037178410X12886993781746
- Qiao, C. S., & Tian, Z. Y. (1998). Study of the possibility of rock burst in Dong-gua-shan Copper Mine. *Chinese Journal of Rock Mechanics and Engineering*, 17, 917-921.
- Roth, A., Cala, M., Brändle, R., & Rorem, E. (2014). *Analysis and numerical modelling of dynamic ground support based on instrumented full-scale tests*. Paper presented at the Proceedings of the Seventh International Conference on Deep and High Stress Mining, Sudbury. [https://papers.acg.uwa.edu.au/p/1410\\_08\\_Roth/](https://papers.acg.uwa.edu.au/p/1410_08_Roth/)
- Sandbak, L., & Rai, A. (2013). Ground support strategies at the turquoise ridge joint venture, Nevada. *Rock mechanics and rock engineering*, 46(3), 437-454.
- Scolari, F., Brandon, M., & Krekula, H. (2017). *Dynamic inflatable, friction rockbolt for deep mining*. Paper presented at the Deep Mining 2017: Eighth International Conference on Deep and High Stress Mining, Perth, Australia.

- Simser, B., & Potvin, Y. (2007). *The weakest link—ground support observations at some Canadian Shield hard rock mines*. Paper presented at the Deep Mining 07—Proceedings of the 4th international seminar on deep and high stress mining.
- Stacey, T. (2012). A philosophical view on the testing of rock support for rockburst conditions. *Journal of the Southern African Institute of Mining and Metallurgy*, 112(8), 01-08.
- Stacey, T. R., & Ortlepp, W. D. (1999). *Retainment support for dynamic events in mines*. Paper presented at the International symposium; 4th, Rock support and reinforcement practice in mining, Kalgoorlie; Australia.
- Stillborg, B. (1993). *Rockbolt tensile loading across a joint*. Paper presented at the International Mine Water Association Symposium Zambia.
- Tadolini, S. (1990). Mine roof bolt load determinations utilizing ultrasonic measurement systems. *Can. Min. Metall. Bull.*, 83(940), 49-54.
- Tannant, D. D., Brummer, R. K., & Yi, X. (1995). Rockbolt behaviour under dynamic loading: Field tests and modelling. *International Journal of Rock Mechanics and Mining Sciences & Geomechanics Abstracts*, 32(6), 537-550. doi:[http://dx.doi.org/10.1016/0148-9062\(95\)00024-B](http://dx.doi.org/10.1016/0148-9062(95)00024-B)
- Thompson, A., Villaescusa, E., & Windsor, C. (2012). Ground support terminology and classification: an update. *Geotechnical and Geological Engineering*, 30(3), 553-580.
- Villaescusa, E. (2014). *Geotechnical Design for Sublevel Open Stopping*: CRC Press.
- Wang, J. A., & Park, H. D. (2001). Comprehensive prediction of rockburst based on analysis of strain energy in rocks. *Tunnelling and Underground Space Technology*, 16(1), 49-57. doi:[http://dx.doi.org/10.1016/S0886-7798\(01\)00030-X](http://dx.doi.org/10.1016/S0886-7798(01)00030-X)
- Wang, Y. H., Li, W. D., & Li, Q. G. (1998). Fuzzy estimation method of rock burst prediction. *Chinese Journal of Rock Mechanics and Engineering*, 17, 493-501.
- Wiles, T. (2006). Reliability of numerical modelling predictions. *International Journal of Rock Mechanics and Mining Sciences*, 43(3), 454-472.
- Yi, X., & Kaiser, P. (1994). *Impact testing for rockbolt design in rockburst conditions*. Paper presented at the International Journal of Rock Mechanics and Mining Sciences & Geomechanics Abstracts.
- Zou, D. H. S. (2004). Analysis of in situ rock bolt loading status. *International Journal of Rock Mechanics and Mining Sciences*, 41(3), 509. doi:<http://dx.doi.org/10.1016/j.ijrmms.2003.12.040>



## APPENDIX A

### ATTRIBUTION TABLE FOR THE PUBLISHED PAPERS INCLUDED IN THIS THESIS

1. **Masoudi R., Sharifzadeh M. (2018).** “Reinforcement selection for deep and high-stress tunnels at preliminary design stages using ground demand and support capacity approach”. International Journal of Mining Science and Technology, Volume 28, Issue 4, July 2018, Pages 573-582. <https://doi.org/10.1016/j.ijmst.2018.01.004>, [SJR Q1, JCR Q1].

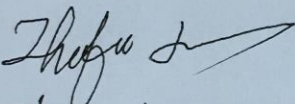
	Conception and design	Acquisition of data & method	Data conditioning & manipulation	Analysis & statistical method	Interpretation & discussion	Final Approval
<b>Reza Masoudi</b>	70%	70%	70%	70%	70%	70%
<p>I acknowledge that these represent my contribution to the above research output.</p> <p>Signed: Reza <b>MASOUDI</b></p>						
<b>Mostafa Sharifzadeh</b>	30%	30%	30%	30%	30%	30%
<p>I acknowledge that these represent my contribution to the above research output.</p> <p>Signed: Mostafa Sharifzadeh</p>						

**PPERMISSION TO USE COPYRIGHT MATERIAL AS SPECIFIED BELOW:**

[Masoudi R., Sharifzadeh M. (2018). "Reinforcement selection for deep and high-stress tunnels at preliminary design stages using ground demand and support capacity approach". *International Journal of Mining Science and Technology*, Volume 28, Issue 4, July 2018, Pages 573-582. <https://doi.org/10.1016/j.ijmst.2018.01.004>, [SJR Q1, JCR Q1]]

I hereby give permission for **Reza Masoudi** to include the above mentioned material(s) in his/her higher degree thesis for Curtin University, and to communicate this material via the espace institutional repository. This permission is granted on a non-exclusive basis and for an indefinite period.

I confirm that I am the copyright owner of the specified material.

Signed:   
Name: Zhongfu Luo  
Position: Editor-in-chief, IJMST  
Date: October 14, 2019

Please return signed form to [reza.masoudi@postgrad.curtin.edu.au](mailto:reza.masoudi@postgrad.curtin.edu.au)

2. **Masoudi R.**, Sharifzadeh M., Ghorbani M. (2019). “Partially decoupling and collar bonding of the encapsulated rebar rockbolts to improve their performance in seismic prone deep underground excavations”, International Journal of Mining Science and Technology, 29(3), 409-418.  
<https://doi.org/10.1016/j.ijmst.2018.09.001>, [SJR Q1, JCR Q1].


	Conception and design	Acquisition of data & method	Data conditioning & manipulation	Analysis & statistical method	Interpretation & discussion	Final Approval
<b>Reza Masoudi</b>	65%	65%	65%	65%	65%	65%
<p>I acknowledge that these represent my contribution to the above research output.</p> <p>Signed: Reza <b>MASOUDI</b></p>						
<b>Mostafa Sharifzadeh</b>	25%	25%	25%	25%	25%	25%
<p>I acknowledge that these represent my contribution to the above research output.</p> <p>Signed: Mostafa Sharifzadeh</p>						
<b>Masoud Ghorbani</b>	10%	10%	10%	10%	10%	10%
<p>I acknowledge that these represent my contribution to the above research output.</p> <p>Signed: Masoud Ghorbani</p>						

PERMISSION TO USE COPYRIGHT MATERIAL AS SPECIFIED BELOW:

[Masoudi R., Sharifzadeh M., Ghorbani M. (2019). "Partially decoupling and collar bonding of the encapsulated rebar rockbolts to improve their performance in seismic prone deep underground excavations", *International Journal of Mining Science and Technology*, 29(3), 409-418.  
<https://doi.org/10.1016/j.ijmst.2018.09.001>,[SJR Q1, JCR Q1]]

I hereby give permission for **Reza Masoudi** to include the abovementioned material(s) in his/her higher degree thesis for Curtin University, and to communicate this material via the espace institutional repository. This permission is granted on a non-exclusive basis and for an indefinite period.

I confirm that I am the copyright owner of the specified material.

Signed:   
Name: Luo Zhenfu  
Position: Editor-in-chief  
Date: October 22, 2019

Please return signed form to [reza.masoudi@postgrad.curtin.edu.au](mailto:reza.masoudi@postgrad.curtin.edu.au)

3. Sharifzadeh M., **Masoudi R.**, Ghorbani M. (2017) "Siah Bisheh Powerhouse Cavern Design Modification Using Observational Method and Back Analysis" Rock Mechanics And Engineering, Vol.5: Surface and Underground Projects, edited by Xia-Ting Feng, CRC press, Taylor and Francis Group, Pp.153-180.

	Conception and design	Acquisition of data & method	Data conditioning & manipulation	Analysis & statistical method	Interpretation & discussion	Final Approval
<b>Mostafa Sharifzadeh</b>	50%	50%	50%	50%	50%	50%
<p>I acknowledge that these represent my contribution to the above research output.</p> <p>Signed: Mostafa Sharifzadeh</p>						
<b>Reza Masoudi</b>	25%	25%	25%	25%	25%	25%
<p>I acknowledge that these represent my contribution to the above research output.</p> <p>Signed: Reza <b>MASOUDI</b></p>						
<b>Masoud Ghorbani</b>	25%	25%	25%	25%	25%	25%
<p>I acknowledge that these represent my contribution to the above research output.</p> <p>Signed: Masoud Ghorbani</p>						

4. Masoud Ghorbani, Kourosh Shahriar, Mostafa Sharifzadeh, **Reza Masoudi (2019)** "A critical review on the developments of rock support systems in high stress ground conditions", International Journal of Engineering Geology, Under review.

	Conception and design	Acquisition of data & method	Data conditioning & manipulation	Analysis & statistical method	Interpretation & discussion	Final Approval
<b>Masoud Ghorbani</b>	55%	55%	55%	55%	55%	
<p>I acknowledge that these represent my contribution to the above research output.</p> <p>Signed: Masoud Ghorbani</p>						
<b>Kourosh Shahriar</b>	20%	20%	20%	20%	20%	
<p>I acknowledge that these represent my contribution to the above research output.</p> <p>Signed: Kourosh Shahriar</p>						
<b>Mostafa Sharifzadeh</b>	15%	15%	15%	15%	15%	
<p>I acknowledge that these represent my contribution to the above research output.</p> <p>Signed: Mostafa Sharifzadeh</p>						
<b>Reza Masoudi</b>	10%	10%	10%	10%	10%	
<p>I acknowledge that these represent my contribution to the above research output.</p> <p>Signed: Reza <b>MASOUDI</b></p>						

5. Sharifzadeh M., **Masoudi R., (2019)**. "Selection of reinforcement at the preliminary stages of deep mining support design". EUROCK 2020, under review.

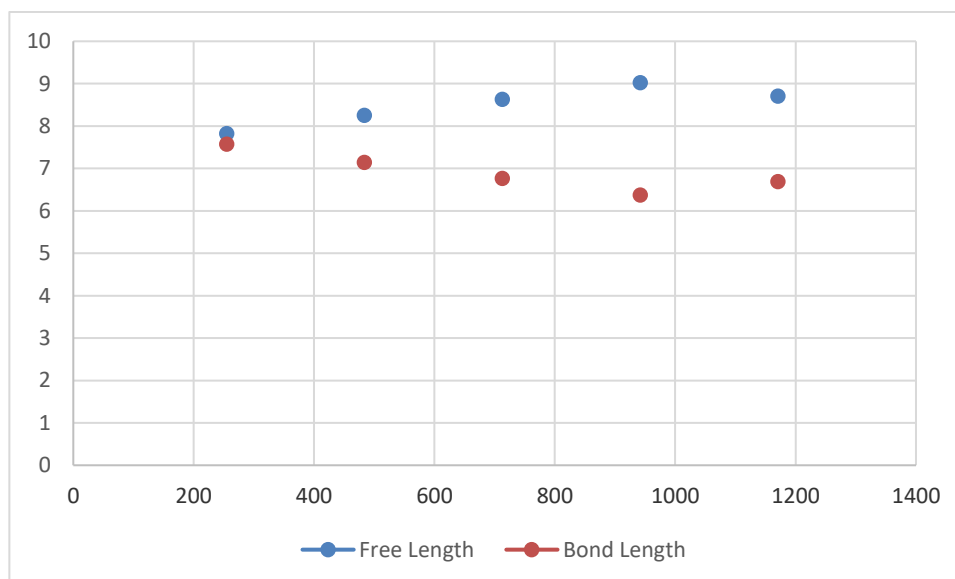
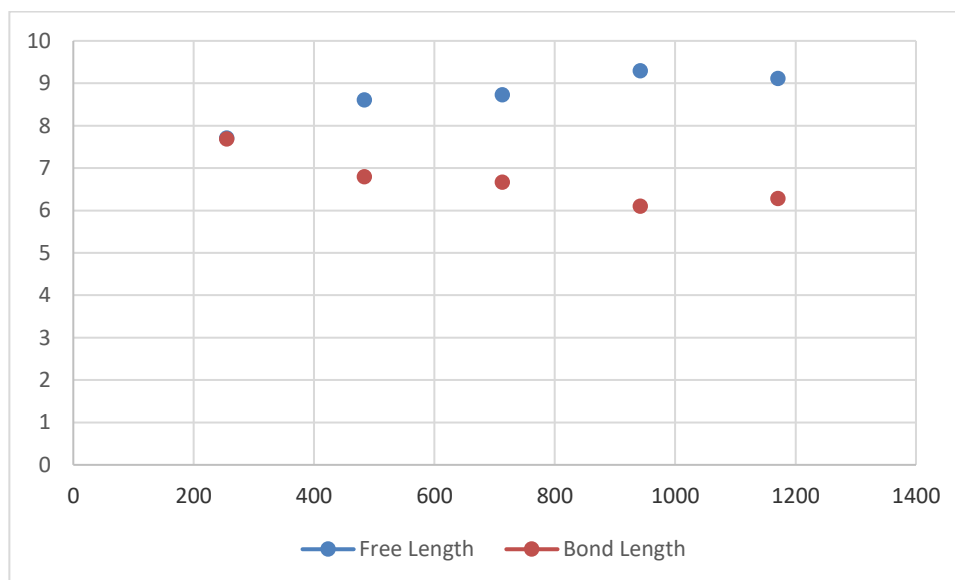
	<b>Conception and design</b>	<b>Acquisition of data &amp; method</b>	<b>Data conditioning &amp; manipulation</b>	<b>Analysis &amp; statistical method</b>	<b>Interpretation &amp; discussion</b>	<b>Final Approval</b>
<b>Mostafa Sharifzadeh</b>	50%	50%	50%	50%	50%	
<p>I acknowledge that these represent my contribution to the above research output.</p> <p>Signed: Mostafa Sharifzadeh</p>						
<b>Reza Masoudi</b>	50%	50%	50%	50%	50%	
<p>I acknowledge that these represent my contribution to the above research output.</p> <p>Signed: Reza MASOUDI</p>						

This page intentionally left blank



## APPENDIX B

### GRAPHS OF MORE RESULTS FOR FREE LENGTH VARIATION



The whole digital information of the experiments are available in Curtin University data base

This page is intentionally blank

## APPENDIX C

### MORE RESULTS OF DIT TESTS

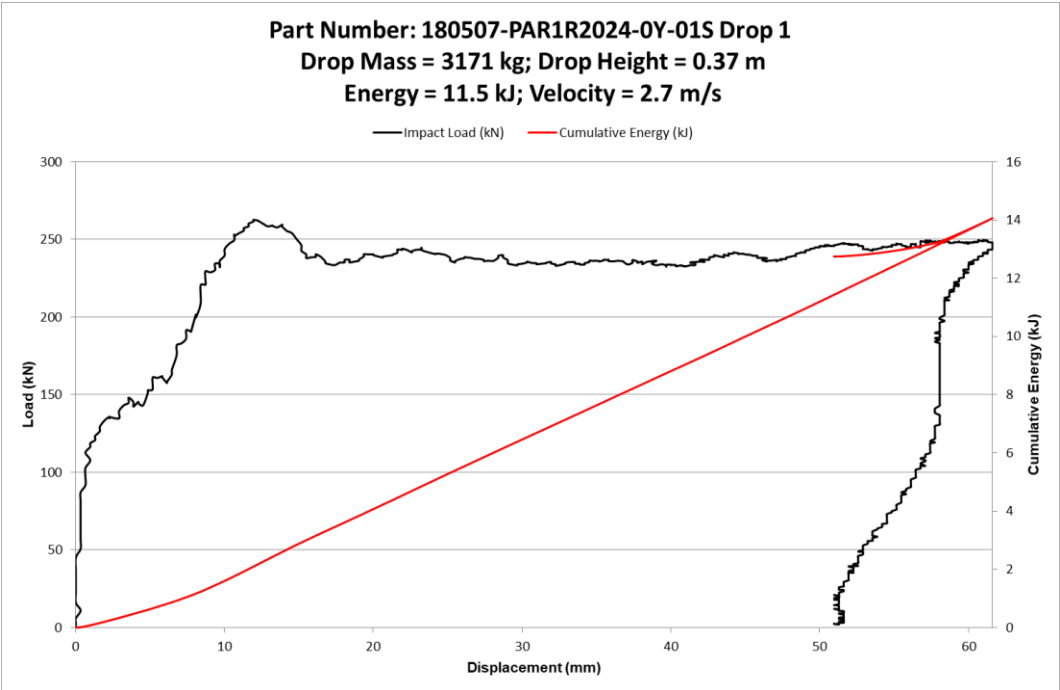
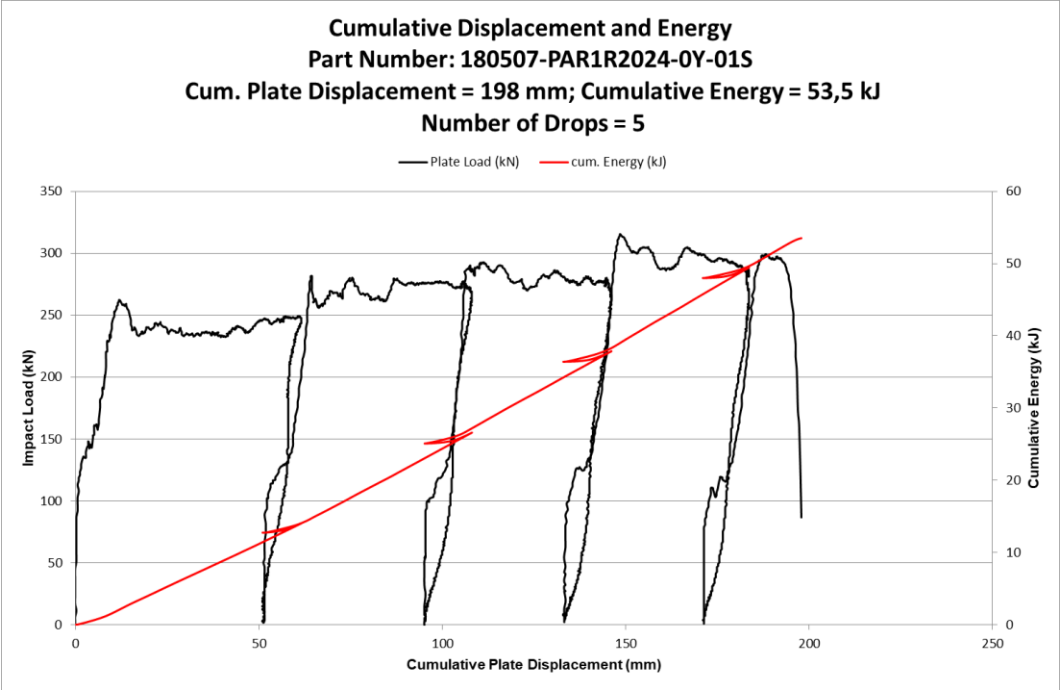
#### Test Sample Summary

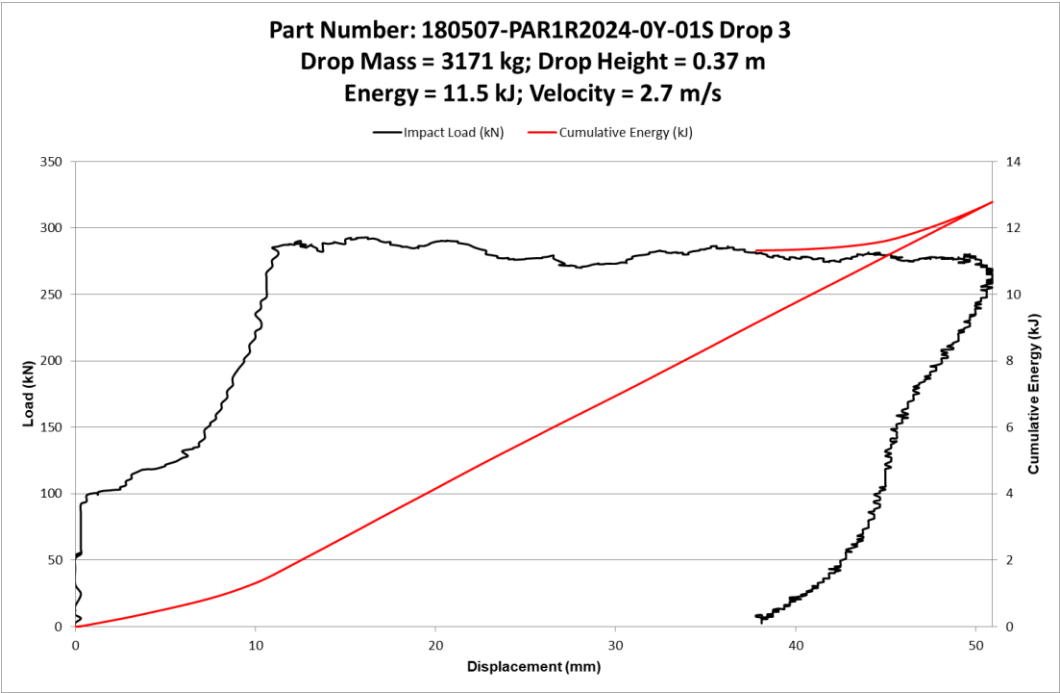
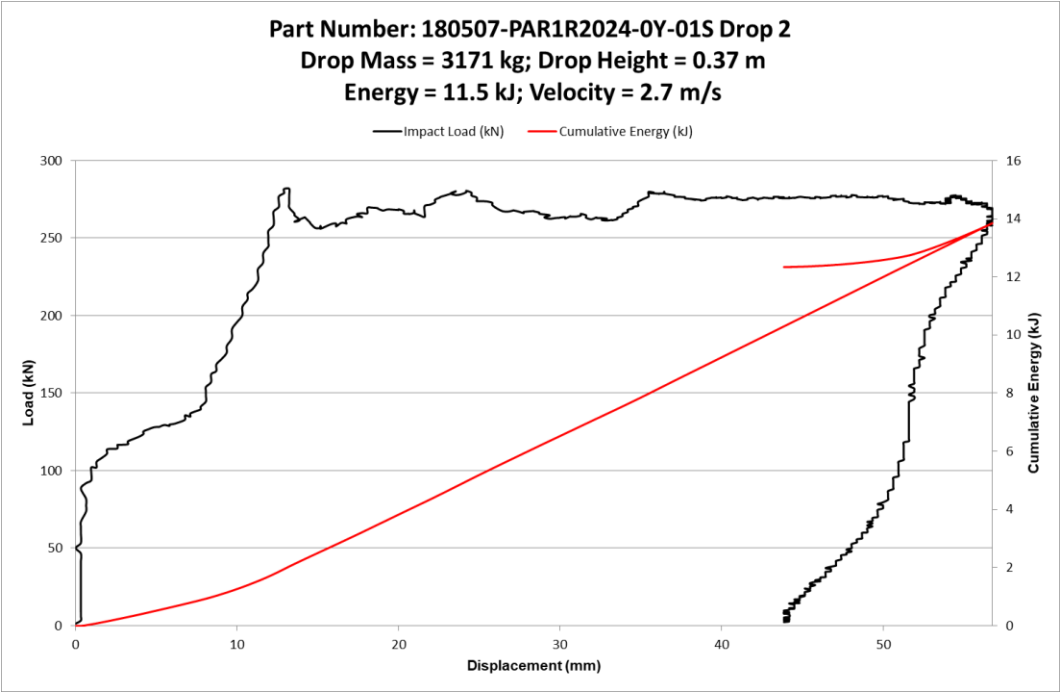
Sample Name	180507-PAR1R2024-0Y-01S	
Stock Code		
Test Date	7/05/2018	
Sample Length		
Test Type	Split Tube	
Input Energy (kJ)	12, 12, 12, 11, 11	
Number of drops	5	
Cumulative Deformation - Max. (mm)	181	
Impact Load - Max. (kN)	316	
Absorbed Energy - Max. (kJ)	59.2	
Absorbed Energy - Unit (kJ/m)		

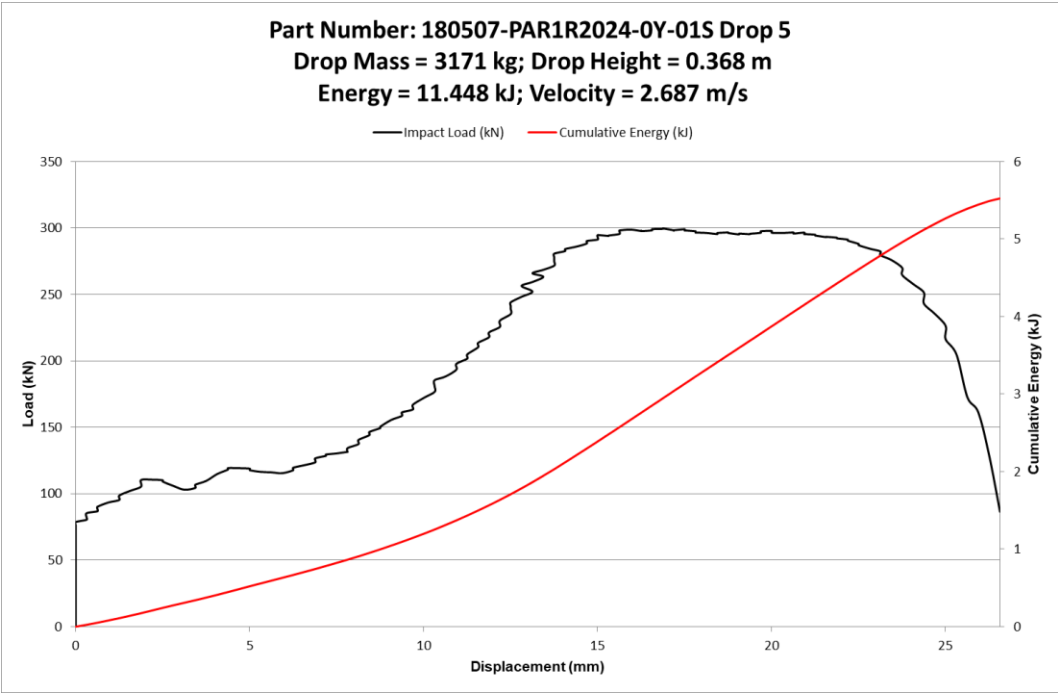
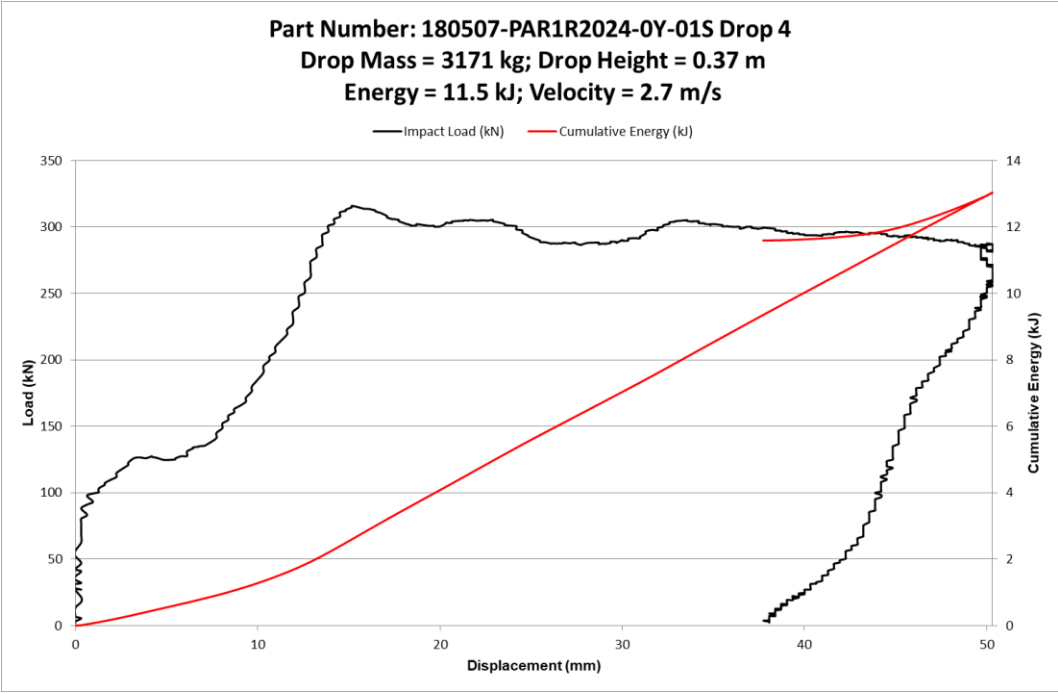
#### 180507-PAR1R2024-0Y-01S

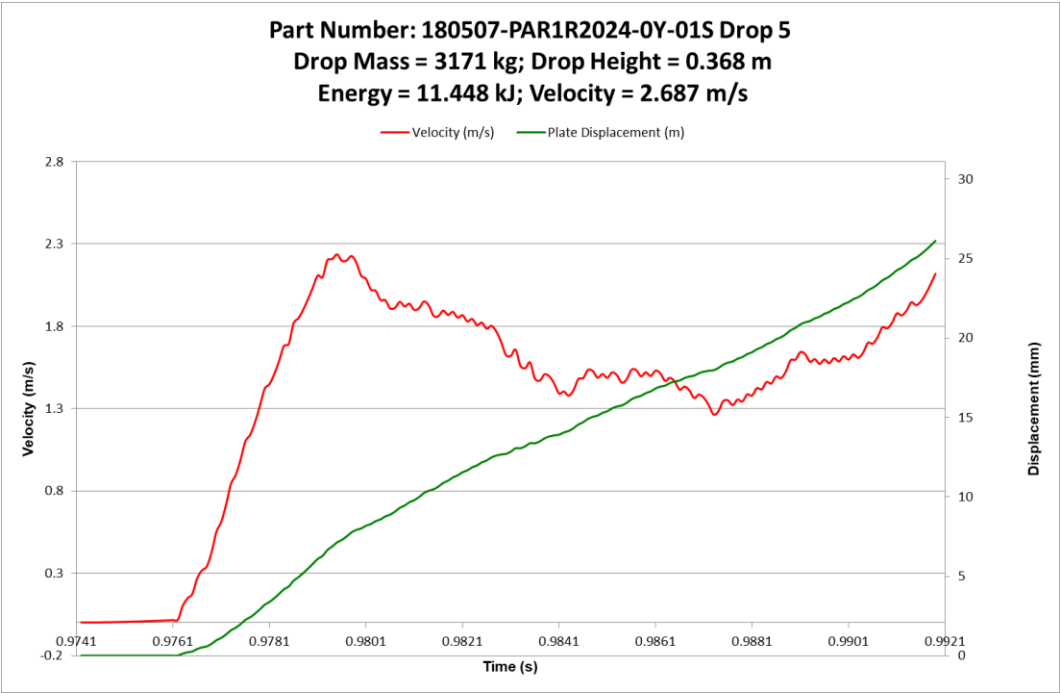
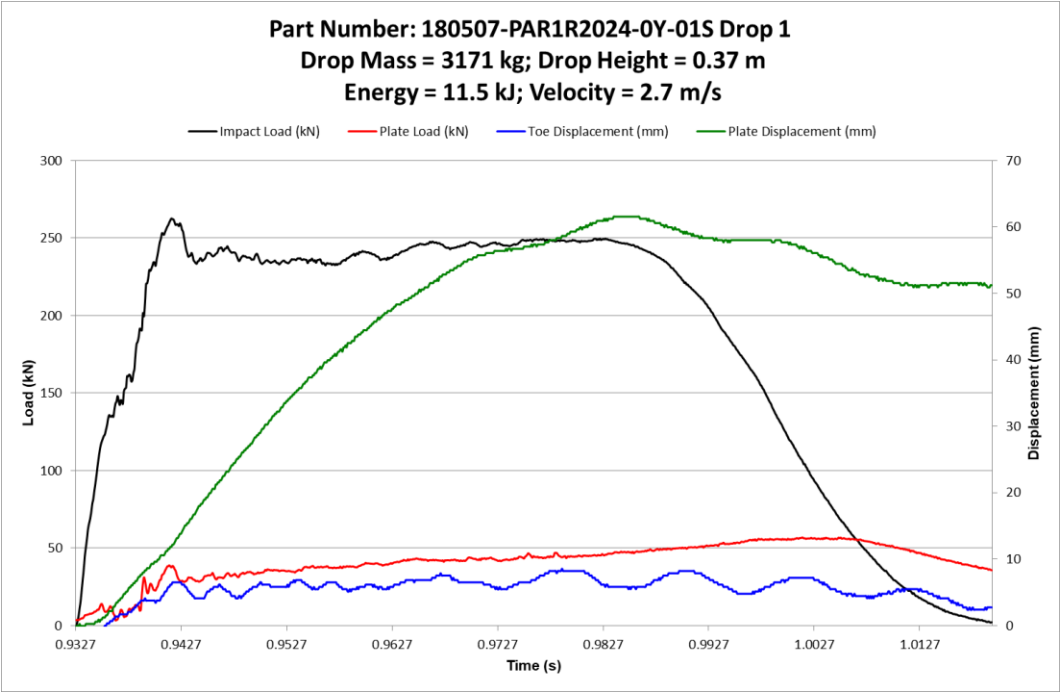
Drop Nr	Drop Mass (kg)	Drop Height (m)	Input Kinetic Energy (kJ)	Impact Velocity (m/s)	Plate Displ (m)	Toe Displ (m)	Stretch (m)	cum. Stretch (m)	Impact Load (kN)			Plate Load (kN)			Absorbed Energy(kj)
									Peak	Ultimate	Avg.	Peak	Ultimate	Avg.	
1	3171	0.37	11.5	2.7	0.051	0.003	0.048	0.048	262	263	242	14	57	41	14.1
2	3171	0.37	11.5	2.7	0.044	0.005	0.039	0.087	282	282	273	48	51	30	13.9
3	3171	0.37	11.5	2.7	0.038	0.002	0.036	0.123	292	293	279	22	57	38	12.8
4	3171	0.37	11.5	2.7	0.038	0.002	0.036	0.159	316	316	294	59	59	44	13.0
5	3171	0.37	11.4	2.7	0.027	0.005	0.022	0.181	300	300	275	53	65	32	5.5

<b>180507-PAR1R2024-0Y-01S Detailed Summary</b>						
<b>Input Data</b>	Drop Number	1	2	3	4	5
	Drop Mass (kg)	3,171	3,171	3,171	3,171	3,171
	Drop Height (mm)	0.37	0.37	0.37	0.37	0.37
	Input Kinetic Energy - Theo. (kJ)	11.51	11.51	11.51	11.48	11.45
	Input Kinetic Energy - Actual (kJ)					
	Impact Velocity - Theo. (m/s)	2.69	2.69	2.69	2.69	2.69
	Impact Velocity - Actual (m/s)					
<b>Displacement</b>	Plate Displ. - Final (mm)	51	44	38	38	27
	Plate Displ. (mm)	51	44	38	38	27
	Plate Displ. - Max. (mm)	62	57	51	50	27
	Toe Displ. - Final (mm)	3	5	1	1	5
	Toe Displ. (mm)	3	5	2	2	5
	Toe Displacement - Max. (mm)	9	9	6	6	5
	Deformation - Final (mm)	49	39	37	37	22
	Deformation (mm)	48	39	36	36	22
	Deformation - Max. (mm)	53	48	45	45	22
	Cumulative Deformation - Max. (mm)	48	87	123	159	181
<b>Load</b>	Frame Load - Max. (kN)	299.74	272.77	268.63	271.07	271.62
	Frame Load - Peak (kN)	198.02	198.06	190.40	268.44	185.48
	Frame Load - Avg. (kN)	156.10	164.41	169.19	169.37	160.29
	Plate Load - Max. (kN)	56.78	51.14	57.23	58.81	65.02
	Plate Load - Peak (kN)	13.91	48.33	22.48	58.81	53.31
	Plate Load - Avg. (kN)	41.26	30.33	38.46	43.91	31.61
	Impact Load - Max. (kN)	262.51	281.79	292.82	315.77	299.51
	Impact Load - Peak (kN)	261.96	281.79	292.10	315.77	299.51
	Impact Load - Avg. (kN)	242.34	272.58	278.68	294.39	275.00
<b>Time</b>	Time to Plate Displacement - Max. (mS)	50.90	49.20	46.70	38.70	17.80
	Time to Impact Load - Max. (mS)	9.00	9.30	12.70	11.60	12.10
	Impact Time (mS)	50.90	49.20	46.70	41.60	17.80
	Rebound Time (mS)	35.80	31.30	31.30	40.60	0.00
	Total Impact Duration (mS)	86.70	80.50	78.00	79.30	17.80
<b>Strain</b>	Peak Load Avg. Load Rate (N/s)	278.15	281.73	306.45	341.89	303.67
	Impact Avg. Strain Rate (mm/s)	1,210.47	1,153.95	1,090.74	1,209.68	1,492.28
	Rebound Avg. Strain Rate (mm/s)	-288.34	-412.24	-409.35	-301.92	NA
<b>Energy</b>	Absorbed Energy - Final (kJ)	12.75	12.34	11.32	11.59	5.52
	Absorbed Energy - Max. (kJ)	14.06	13.85	12.78	13.03	5.52
	Cumulative Absorbed Energy - Final (kJ)	12.75	25.09	36.41	48.00	53.52
	Cumulative Absorbed Energy - Max. (kJ)	14.06	27.91	40.69	53.72	59.24









The whole digital information of the experiments are available in Curtin University database